FINAL REPORT

STUDY OF TRANSITION TEMPERATURES IN SUPERCONDUCTORS

11 MARCH 1968 THROUGH 10 MARCH 1970

CONTRACT NO. NAS 8-21384

PREPARED BY

L. J. VIELAND AND R. W. COHEN

RCA LABORATORIES
PRINCETON, NEW JERSEY 08540

FOR

NATIONAL AERONAUTICS AND SPACE ADMINISTRATION
GEORGE C. MARSHALL SPACE FLIGHT CENTER
HUNTSVILLE, ALABAMA, 35812

PRECEDING PAGE BLANK NOT FILMED.

ABSTRACT

An x-ray investigation of the martensitic transformation in Nb_3Sn has been made; the Debye-Waller factor for Nb and Sn atoms has also been determined; the specific heat of non-stoichiometric Nb_3Sn has been measured at 0 and 103 kg; the effect of Sb and Al doping on the martensitic transformation in Nb_3Sn has been studied; the location of H in hydrided Nb_3Sn has been determined by neutron diffraction; rf sputtering of β-W alloys is described; the band density of states band model is given and its applicability to the normal and superconducting state discussed; the elastic constants of transforming Nb_3Sn have been determined; the effect of uniaxial strain on T_c has been measured; the growth of large crystals of Nb_3Sn from Sn has been studied.

TABLE OF CONTENTS

LIST OF ILLUSTRATIONS

LIST OF ILLUSTRATIONS (Continued)

LIST OF ILLUSTRATIONS (Continued)

LIST OF ILLUSTRATIONS (Continued)

I. INTRODUCTION

The research described in this report has had two principal long-range goals: (a) to develop a theoretical understanding of the high T_c β-W superconductors which would allow us to predict how new materials might be made with higher T_c's, and (b) to fabricate promising new materials with the hope of achieving these higher T_c's. Our method was based on the belief that a completely empirical approach to materials research in superconductivity had little chance of success. There are simply too many compounds and alloys that can be made and too many parameters that can be varied in a reasonably sized research project. From the onset, we decided that the best way to achieve better materials was to gain a working physical and chemical understanding of the most promising (β-W) class now known. We hoped that this understanding would naturally reveal how the materials scientists should attempt to elevate T_c. Over the course of this work, we have substantially accomplished the first of the above goals; however, we have not yet succeeded in producing a superconductor with a substantially higher T_c than the present maximum of about 21°K. It is nevertheless our judgement, based on the theoretical and experimental work in this project, that there is a strong possibility of producing a material which will be superconducting at liquid-neon temperatures.

At the beginning of our research, we were confronted with many unusual experimental anomalies. It was not known what relationship, if any, these anomalies had with the high T_c's of these materials. The progress we have made in our understanding since that time is highlighted below.

1. The initial success of the model-band theory in explaining the anomalies of the cubic lattice state above the lattice transformation temperature T_m gave us a physical understanding of these anomalies and identification of the microscopic material parameters that are responsible for them (this work is covered in Appendix A on page 26).
2. Using the parameter values obtained in 1, the application of the theory to the properties of Nb_3Sn below T_m met with truly astonishing success except very close to T_m, where some mysteries remain (see Appendices B through D, pages 34 to 59).
3. Considerable experimental effort has been made to discover whether the discrepancies near T_m have any bearing on the superconducting properties. These studies, reported in Appendix G on page 82 and Section III.A.1 on page 20, are continuing.

4. The applicability of the theory in both crystal phases encouraged us to apply the band theory to calculate the transition temperature in terms only of the parameters obtained in 1. The results agreed with the observed T_c's of Nb_3Sn and V_3Si (see Appendix F on page 68). Furthermore, an analytic relation was derived between the high T_c's and the existence of the lattice transformation in these materials. This was the first quantitative example of a principle which has long been believed to be true; namely, increasing the electron-phonon interaction leads to high T_c's, but also introduces lattice instabilities that tend to reduce T_c. We obtained the prediction that if T_m of Nb_3Sn could be depressed to below 30°K by the introduction of a suitable dopant which would act only to move the Fermi level in the spirit of the rigid band model, the T_c of Nb_3Sn could be enhanced as much as 10°K.

5. A straight-forward test of the theory of the superconducting state was accomplished by measuring the change of T_c with uniaxial compression. An extremely large effect was observed which was in good agreement with the prediction of the theory (see Appendix E on page 60).

6. A further successful test of the superconducting state theory was the Debye-Waller factor measurements which indicated that the major portion of the phonon spectrum was "Debye-like". This result vindicated one of the major assumptions of the theory (see Section II on page 10).

7. In order to achieve the predicted enhancement of T_c, attempts were made to introduce small amounts of Cd, Zn, In, Al, and Sb into Nb_3Sn as substitutes for Sn. Only in the cases of Al (Section III.A.1 on page 20) and Sb (Appendix G on page 82) did the dopant remain in the lattice after annealing. In both cases, only small changes in T_c were observed, although 10% Al substituted for Sn did raise T_c by about 0.6°K. It was determined that rigid band effects do not occur in the Al and Sb system. Instead, we conclude that the electronic band configuration of Nb_3Sn is inherently stable and not easily perturbed by as much as 20% Al or Sb. It thus becomes likely that the β-W phase containing the appropriate dopant is unstable when prepared by equilibrium techniques.

8. In an effort to fabricate metastable alloys of $Nb_3(SnIn)$ and other promising systems, an rf-sputtering technique was employed (Section III.B on page 23 and Appendix H on page 91). This technique had proved successful in mixing a wide variety of so-called immiscible metals. The difficulty encountered here was that dopant evaporated from the sample during the annealing which is necessary to achieve order. However, we believe that this is not a fundamental difficulty, but can be overcome by available techniques.

II. MEASUREMENTS

A. X-RAY STUDIES

1. X-Ray Investigation of the Lattice Transformation in Single Crystal Nb_3Sn

Although the elastic softening of the high T_c, β-W superconductors at low temperatures provides the basis of the band model for these materials, the details of the lattice transformation are not fully understood and do not seem to be in agreement with certain predictions of the model. Two aspects of the transformation in Nb_3Sn which are particularly problematic are the absence of an observable latent heat, and a transformation temperature some 6°K below the temperature at which the elastic restoring force for strains carrying the lattice from cubic to tetragonal (C_{11}-C_{12}) appears to vanish. These discrepancies are seen in a comparison of sound velocity, x-ray, and specific heat data for one single crystal of Nb_3Sn, as reported in (ref. 1) and Appendices C and D on pages 41 through 59. However, x-ray and thermal data are found to be strongly sample dependent, and we have, therefore, studied two crystals on which previous studies had been made. Both crystals were grown at RCA by chemical vapor deposition (ref. 2). Some comparative data are shown in Table I.

Table I

Comparative Data for Two Crystals Used in Lattice Transformation Study

Sample*	Atomic Percent Nb	a_o (95°K)	T_M (°K)	Crystallinity
I	74.7	5.2827 (5.2906 at R.T.)	51	Poly, with a few large grains
II	75.4	5.2839	44	Single

*These are the same samples and designations as reported in the specific heat study (Appendix D on page 55).

Sample II is a fragment (about one half) of the crystal on which all elastic constant measurements in Nb_3Sn have been made. A weak specific heat cusp was seen at 44°K, and previous x-ray work (ref. 1) on another piece of the same material showed a clear tetragonal splitting at 43°K. Sample I was found to exhibit a specific heat peak at 51°K with no evidence of a singularity or latent heat.

a. Experimental - Samples were prepared by lapping faces parallel to [100] planes, and cemented to the stage of a low-temperature x-ray diffraction camera with the <001> direction along the rotation axis. MoK_α radiation was used throughout. Temperature was controlled manually to about $\pm$ 0.1°K, and read with a Pt thermometer, using a Wheatstone bridge.

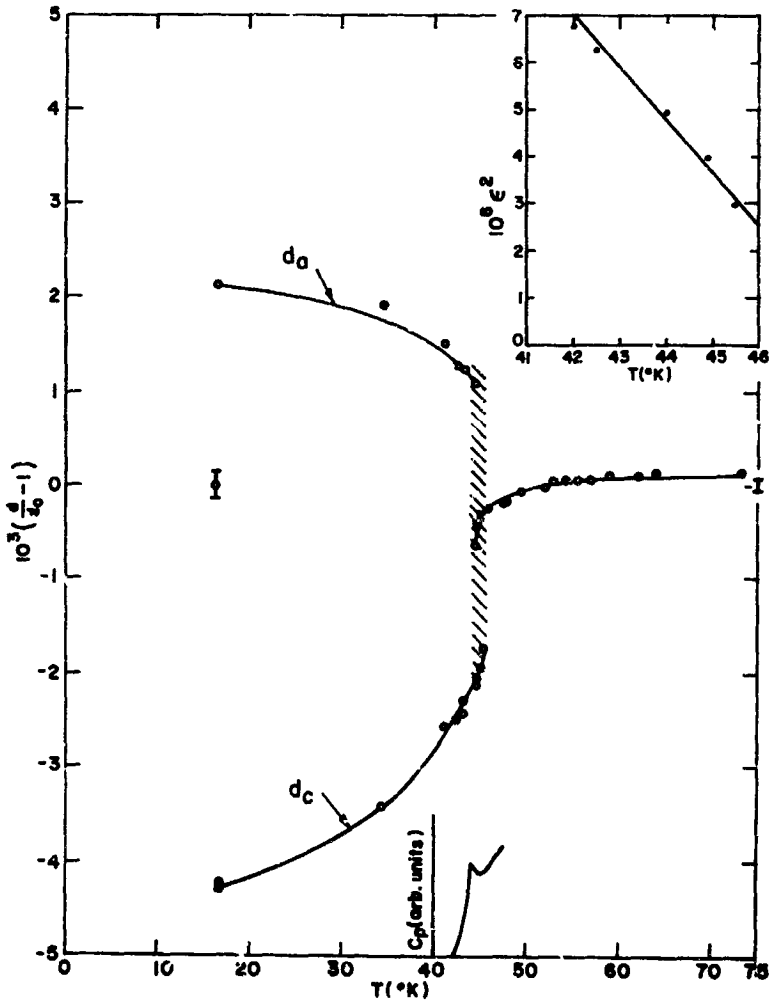

Figure 1. Tetragonal distortion and specific heat vs. temperature for Nb_3Sn, sample II.

b. Results - Since both [12,0,0] and [14,0,0] reflections were used the data shown in Figs. 1 and 2 are normalized to the extrapolated 0°K lattice spacing, d_o. The tetragonal strain $\varepsilon = \left|\frac{2}{3}(c/a-1)\right|$ is given by the lower branch of the figure, i.e., $-\varepsilon = \left(\frac{d_c}{d_o} - 1\right)$. The measured specific heats are shown schematically on the same temperature scale.

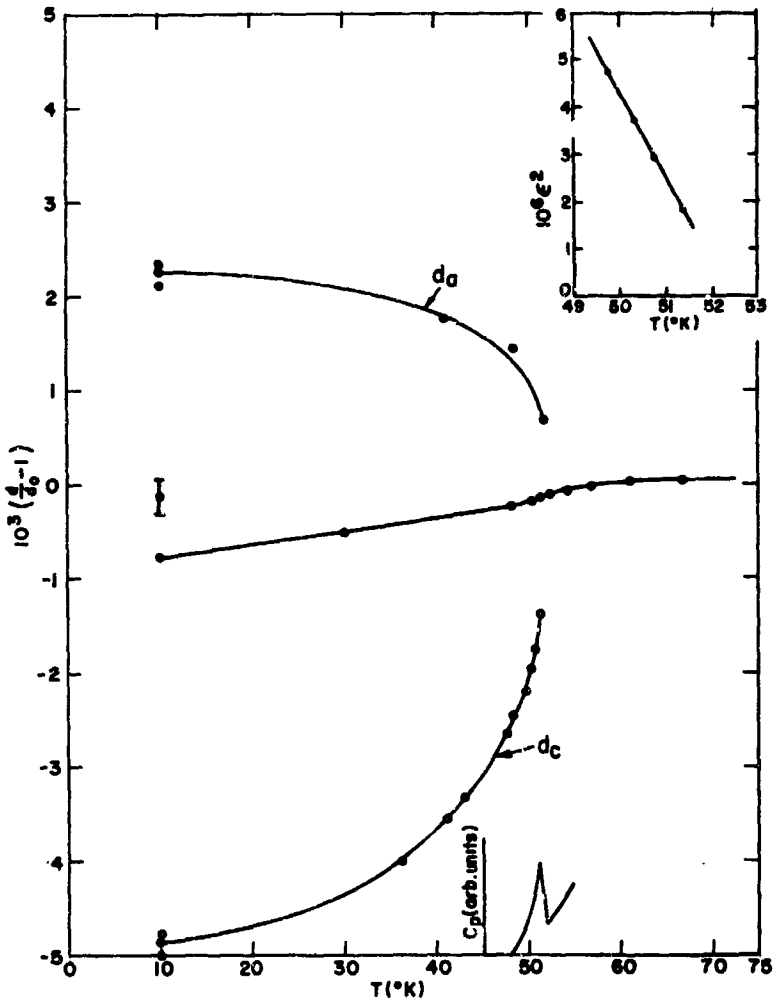

Figure 2. Tetragonal distortion and specific heat vs. temperature for Nb_3Sn, sample I.

The strain curve for sample II shown in Fig. 1 is found to be in good agreement (within 10% at all $T < T_m$) with previous measurements (ref. 1). The low-temperature point with vertical error bars is $[(2d_a+d_c)/3d_o-1]$ which is identically zero if no volume change accompanies the transformation. Above 44°K the data are quite different from that previously reported (ref. 1). There is a region extending from 44° to 45.5°K over which three peaks are seen, corresponding to the a and c axes, and in addition, a central peak representing the high temperature phase. The region of overlap is shown by the shaded area of Fig. 1. In order to ascertain the origin of the strong temperature dependence of this peak above T_m, the camera was rotated to permit the observation of internal reflections. Assuming the crystal is already tetragonal above the temperature at which splitting is observed, then the peak in question must represent the c (smaller) axis, i.e., we are looking at [00ℓ] type reflections. Rotating through 33.7° permits observation of [0,8,12] planes, and rotation through another 22.6° brings the [0,12,8] type into reflecting position. Since the changes in d spacing $\delta(2\theta)$ are proportional to $(h^2 + k^2 - 2\ell^2)\varepsilon$, the peak shifts for these two reflections are of different magnitude and opposite in sign. The progressive increase in $\delta(2\theta)$ between these two peaks, which we observe as the temperature is lowered below about 53°K, is consistent with the above interpretation.

Since the shift in peak position is not accompanied by any appreciable increase in peak width, it appears that this effect is not due to crystal inhomogenieties giving rise to a variable transformation temperature, but simply represents the development of a single tetragonal domain. The first appearance of the split peaks at about 45.5°K signals the development of a multi-domained structure, i.e., both a- and c-type reflections are observed. The course of the transformation is shown in Fig. 3. The c-axis (high-angle) contribution to the total intensity is large compared to the low-angle peak, which implies that over the irradiated region of the crystal face, most domains are oriented close to the original c-axis orientation. At low temperatures, ω-scanning (fixing 2θ at the Bragg angle and rotating θ) gives the relative intensities c:a 2:1, with domain alignments up to about $\frac{1}{2}^\circ$ off the cubic axes*.

* These data were taken before the crystal was oriented with regard to the <001> direction.

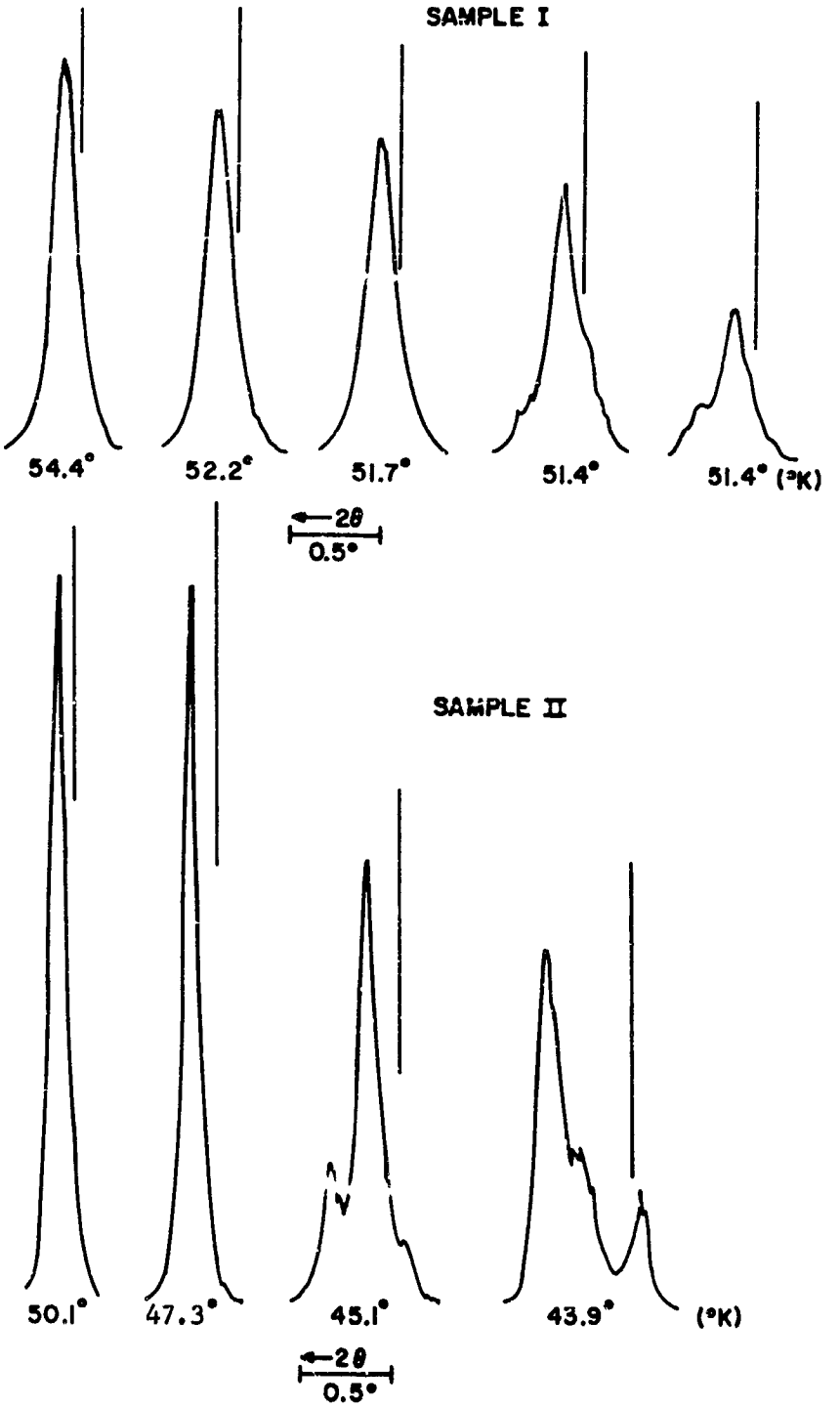

Figure 3. *[12,0,0] traces for samples I and II at various temperatures near T_M. The vertical line represents a fixed reference angle.*

Figure 2 shows the overall behavior of sample I. T_m is somewhat higher and scales with $\varepsilon(0°K)$. The tetragonal splitting appeared more like a second-order Landau transition, with only a slight distortion preceding the splitting at 51.4°K, and a strain near T_m given closely by a relation of the type $\varepsilon^2 \sim (T_m - T)$ as expected in the Landau theory. As before, the intensity contributed by the domains appears to grow with the strain near T_m, so that the situation very near T_m remains unresolved with regard to the occurence of domains of smaller ε. The splitting is shown in Fig. 3. The last trace is at the same temperature as the previous one, but with the crystal rotated 0.04° to decrease the contribution from the untilted central peak and to bring out the c-axis contribution from tilted domains. Unlike sample II, the central peak does not vanish at lower temperatures. Using ω-scanning, we find that about 10 to 20% of the total intensity is contributed by this peak. At low temperatures the peak becomes rather diffuse in both θ (orientation) and 2θ (d-spacing), but remains untilted.

c. Discussion - Since sample II is the crystal on which elastic constant measurements were made, the parameters of the band model are available for calculating the details of the tetragonal distortion. The failure to observe the latent heat predicted by the model is dealt with in Appendix D on page 55. The arguments presented there must be modified somewhat by the observation of appreciable tetragonality above what was previously taken to be T_m, which accounts for the relative weakness of the specific heat discontinuity, and the appreciable excess specific heat above T_m. The tetragonal strain below T_m is given by the theory in terms of parameters obtained from elastic constant data in the cubic state. A plot of the strain as a function of temperature for this crystal is shown in Fig. 4. There are no adjustable parameters in this plot, with the exception that T_m has been taken to be 45.5°K, the highest temperature at which the splitting is observed, instead of 49.6°K, which is where $C_{11}-C_{12}$ extrapolates to zero. The agreement between theory and experiment is remarkable*. The linear dependence of ε^2 on T near T_m, found for both samples, is not at variance with the prediction of the model.

The question of whether or not the data for sample I can be fit equally well can be answered to some extent in the following way: since $\varepsilon(0°K)$ is given by $2kT_o/U_2F_m$ and $\varepsilon(T_m) = -\frac{4}{3} kT_m/U_2$, where kT_o is the Fermi energy at 0°K, U_2 the deformation potential, and $F_m = 1-\exp(-T_o/T_m)$, we require, in order to fit the experimental strains at low T and at

---

* This is the same theoretical curve shown in Appendix B, (page 36) which was there compared with the data of (ref. 4) taken from a different piece of the same crystal.

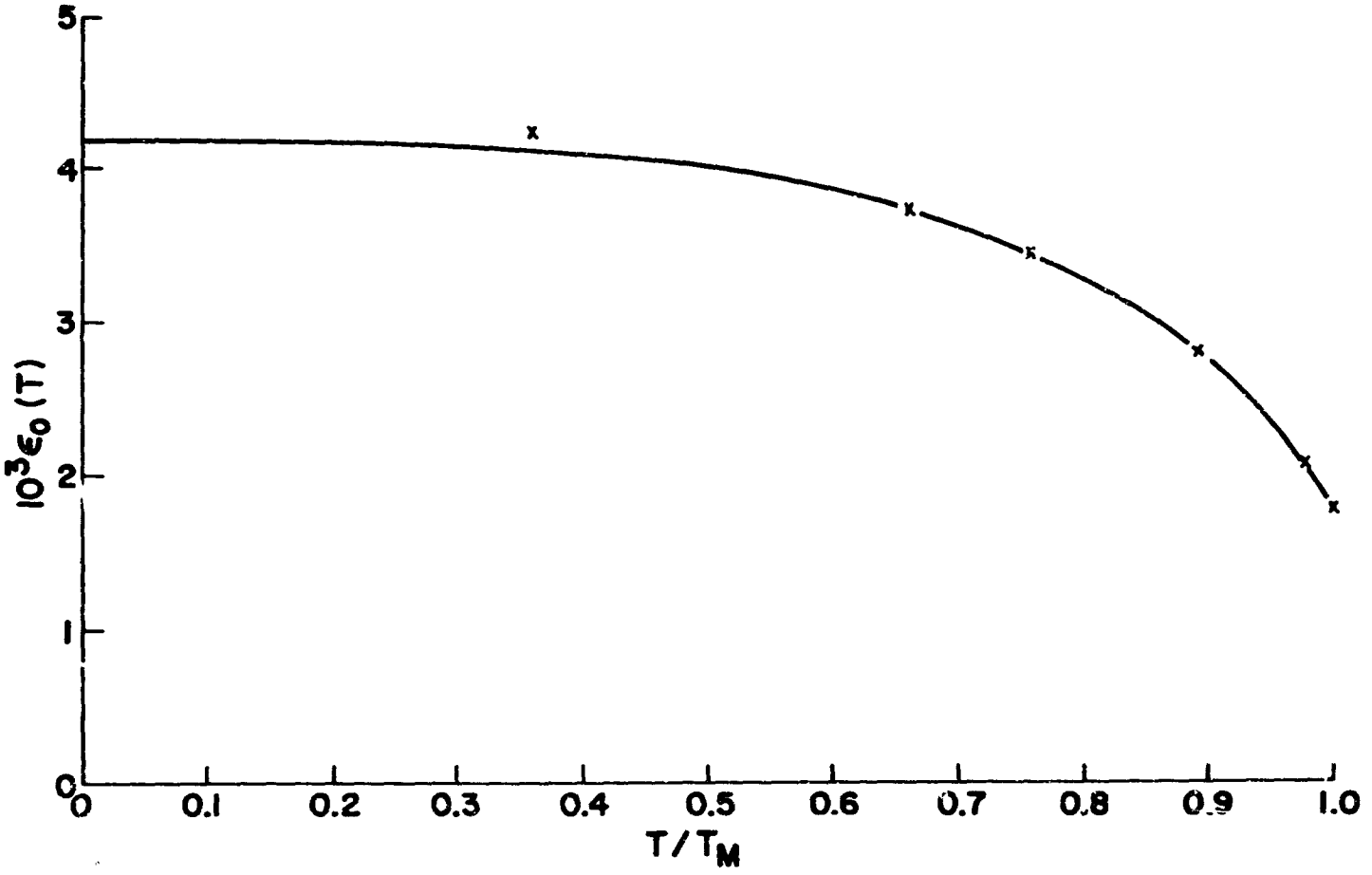

Figure 4. Theoretical (line) and experimental (crosses) strain vs. reduced temperature for sample II.

T_m, $T_o = 115°$ and $U_2 = 5.4 \times 10^{4°}$. This compares with values of 80° and $4.7 \times 10^{4°}$ for sample II. The increase in T_o appears somewhat excessive, since the temperature dependence of the resistivity of this material is consistent with $T_o = 80°$.

The discovery of a precursor effect to the martensitic transformation, together with the excellent fit of the strain below T_m, suggests the possibility that a second order parameter, besides ϵ, exerts a significant influence on the free energy of the crystal above T_m, but plays a negligible role at lower temperatures, where the strain energy is large ($C_{11} \neq C_{12}$). The small strain above T_m then arises from coupling between the strain and the second parameter, affecting the elastic constants and magnetic susceptibility above T_m, as observed, and serving to smear the latent heat of the transformation. The nature of this second parameter, if it exists, is not known.

2. Debye-Waller Measurements on Single-Crystal Nb_3Sn

Before the discovery of the lattice transformation in Nb_3Sn, Mossbauer effect studies (ref. 3) revealed a peculiar softness in the phonon spectrum at low temperatures, manifested as a very low recoil-free fraction at 4.2°K, and corresponding to a Debye temperature of about 56°K. The data could be represented as a combination of a Debye-like spectrum with reasonable $\theta_D = 290°$, and a temperature-independent optical-like mode, which was interpreted as arising from the loose (square well) binding of the Sn atoms. (Sn^{119} was the γ-ray source). This result now certainly appears to be related to the lattice softening known to occur in high T_c, β-W superconductors, and it even hints at a mechanism for the transformation by analogy to the behavior of certain ferroelectrics, where a cubic-tetragonal transformation is triggered by the interaction of a low-frequency optical mode with the acoustic branch of the phonon spectrum. However, there are difficulties in this interpretation. The most straight-forward is that just as we now know that the lattice softens appreciably at temperatures near T_m, we also know that it recovers its high-temperature stiffness at $T << T_m$ (see Appendix C on page 41). In addition, the frequency range of the spectrum affected by the softening must be very low, since no evidence of softening is seen in the specific heat near T_m, i.e., the thermal energy residing in the affected modes is negligible. This is a very important point, because the Mossbauer (and Debye-Waller) measurements average over a different moment of the frequency spectrum than the specific heat, giving more weight to low-frequency phonons, and it is this moment that appears in the electron-phonon interaction. In other words, the calculation of the superconducting transition temperature, making the usual assumption of a Debye spectrum, is only meaningful if large discrepancies between Mossbauer and specific heat results are either not observed or well understood.

The provocative Mossbauer results have led us to investigate the problem through the Debye-Waller effect. This is the reduction in x-ray peak intensities resulting from lattice aperiodicity introduced by thermal and zero-point vibrations, and it is precisely the same effect seen in Mossbauer studies as a reduction in the fraction of recoilless γ-ray emissions.

X-ray line intensities are proportional to the square of the structure factor $F_{hk\ell}$, which for Nb_3Sn can be written,

$$F_{hk\ell} = 2f_{Nb}\left\{\cos 2\pi\frac{h}{4}\cos 2\pi\frac{\ell}{2} + \cos 2\pi\frac{k}{4}\cos 2\pi\frac{h}{2} + \cos 2\pi\frac{\ell}{4} \times \cos\frac{2\pi k}{2}\right\} + f_{Sn}\left\{1 + \cos 2\pi\left(\frac{h}{2}+\frac{k}{2}+\frac{\ell}{2}\right)\right\}, \quad (1)$$

where $f = f_0 e^{-B}$, f_0 is the atomic scattering factor for an atom at rest, and B is the Debye-Waller factor for the appropriate atom. The D-W theory gives for B

$$B = \frac{6h^2}{mk\theta_B^2}\left\{\phi(x) + \frac{x}{4}\right\}\frac{\sin^2\theta}{\lambda^2} \equiv 8\pi^2\,\overline{\mu_s^2}\,\frac{\sin^2\theta}{\lambda^2}, \quad (2)$$

where h and k are the Planck and Boltzman constants, m the atomic mass, $\overline{\mu_s^2}$ the mean square displacement in the direction of the reflecting plane normal, and θ and λ the Bragg angle and x-ray wavelength ($\sin\theta/\lambda = 1/2d$). The bracketed term is the Debye integral

$$\phi(x) = \frac{1}{4}\int_0^x \frac{t\,dt}{e^t - 1} \quad (3)$$

where $x = \theta_B/T$, and the subscript indicates that the Debye temperature appropriate to x-rays is slightly different than the usual θ_D because of the different averaging procedure alluded to above.

Two types of experiments have been performed, involving small crystals ($\sim$4 mil spheres) in divergent beam geometry, and reflection off large crystal faces using powder diffractometer techniques. Two examples of the former are shown at the top of Fig. 5, where the temperature dependence of the {880} and {210} intensities (each point is an average of six equivalent reflections) are shown -- the first to give some idea of the random errors and the second to show an interesting and unexpected effect. For the {210} set, the large lattice spacing

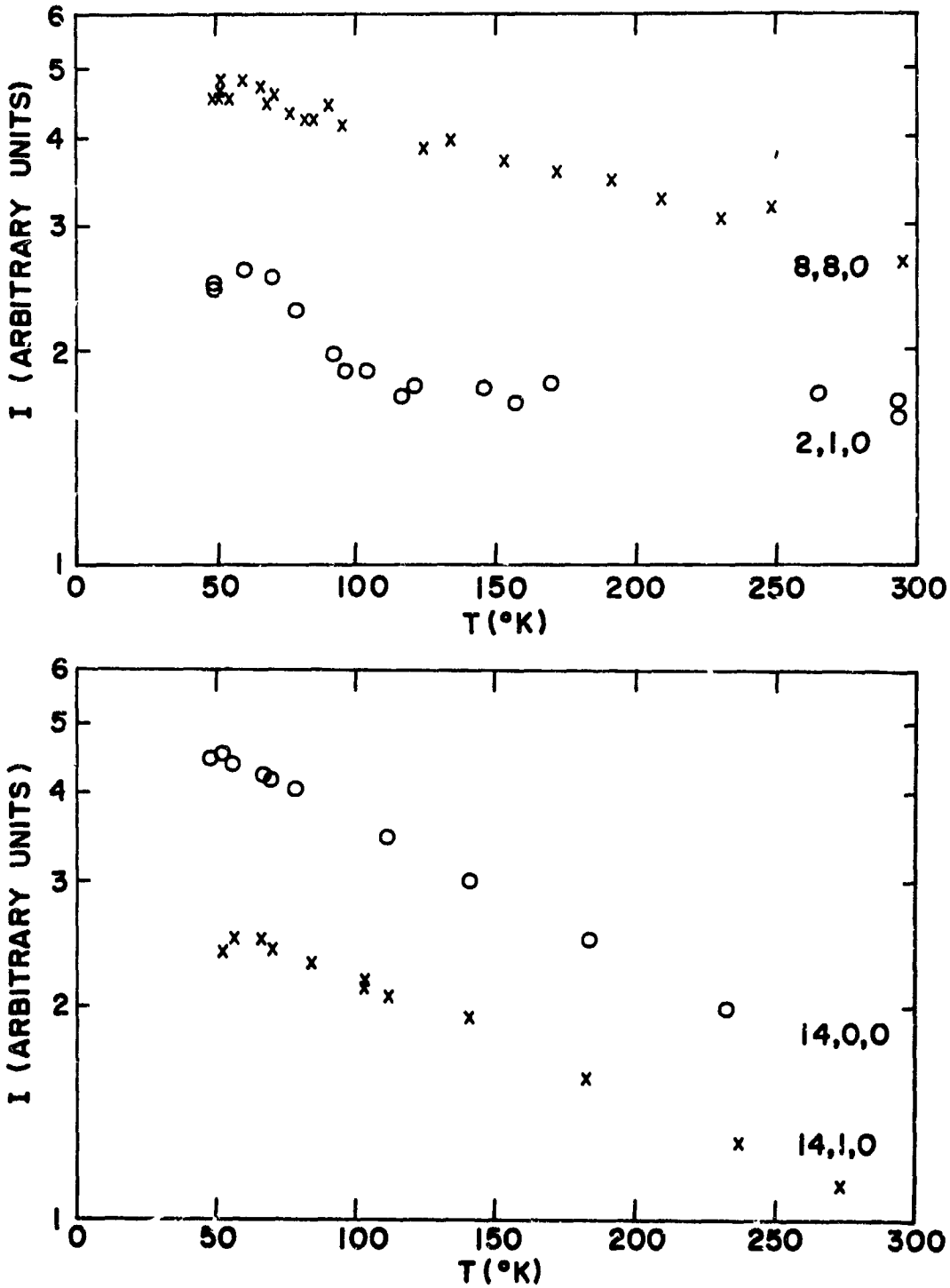

Figure 5. Integrated intensity vs. T. for four reflections. The intensity ratio of the [14,0,0]/[14,1,0] reflections are given absolutely along the ordinate.

makes B very small and practically removes the temperature dependence of the intensity. At low T, however, the sudden change in I is interpreted as arising from a decrease in crystal perfection (less extinction), presumably connected in some way with the approaching lattice transformation. The relatively high temperature, compared to T_m, at which this occurs is perplexing.

The procedure for finding the B's at any temperature is to compare the ratio of the observed to calculated intensity for a large number of peaks as a function of $(\sin\theta/\lambda)^2$; the ratios decrease for high angles and for low Debye θ_D. In spite of the availability of computer programs for handling the data, the situation is complicated by such factors as extinction corrections and/or effects such as seen for the {210} reflections, and a satisfactory, self-consistent, calculation has not yet been completed.

A somewhat simpler situation occurs in the type of experiment, using large crystals, illustrated at the bottom of Fig. 5. Here we studied the intensities of two peaks in the far-back reflection where B is maximal, and the closeness of the peaks in 2θ should minimize systematic errors. From the structure factor it is seen that the [14,1,0] reflections involve Nb atoms only, while the [14,0,0] is a mixed type, with $F = 2f_{Nb} + 2f_{Sn}$. Any anomalous scattering from tin atoms should therefore be apparent in a comparison of the two peaks, which are an optimal pair, since there are no pure tin reflections.

First we show that the data for the [14,1,0] is in agreement with the D-W theory. For temperatures not far from θ_B, it can be shown that $(d\ln I/dT)_{T\ \theta_B} = -.946(2B(\theta_B)/\theta_B)$, which is a function of θ_B only, from which we obtain $\theta_{Nb} = 318°$. In Fig. 6 the solid line for Nb is the theoretical curve for this θ_B. The experimental points are converted to B values by using the relation $\ln[I(T)/I(300°)] = 2[B(300°)-B(T)]$, where B(300°) is assigned to the curve. (We have suppressed the angular part of B on the ordinate, dividing by $(1/2d)^2 = 1.76 \times 10^{-16}\ cm^{-2}$). It is seen that reasonable agreement is obtained, with a slight positive departure of the data at T < 100°K. This might be related to the effect seen in the {210} data and appears to be quite general (cf., the absence of saturation at low T in the {880} data).

For the [14,0,0] reflection, to a very good approximation,

$$I_{14,0,0}/I_{14,1,0} = \left[\frac{f_{Nb}^{o}\exp(-B_{Nb}) + f_{Sn}^{o}\exp(-B_{Sn})}{2f_{Nb}^{o}\exp(-B_{Nb})}\right]^2$$

$$= .25\,[1+1.6\exp-(B_{Sn}-B_{Nb})]^2 \qquad (4)$$

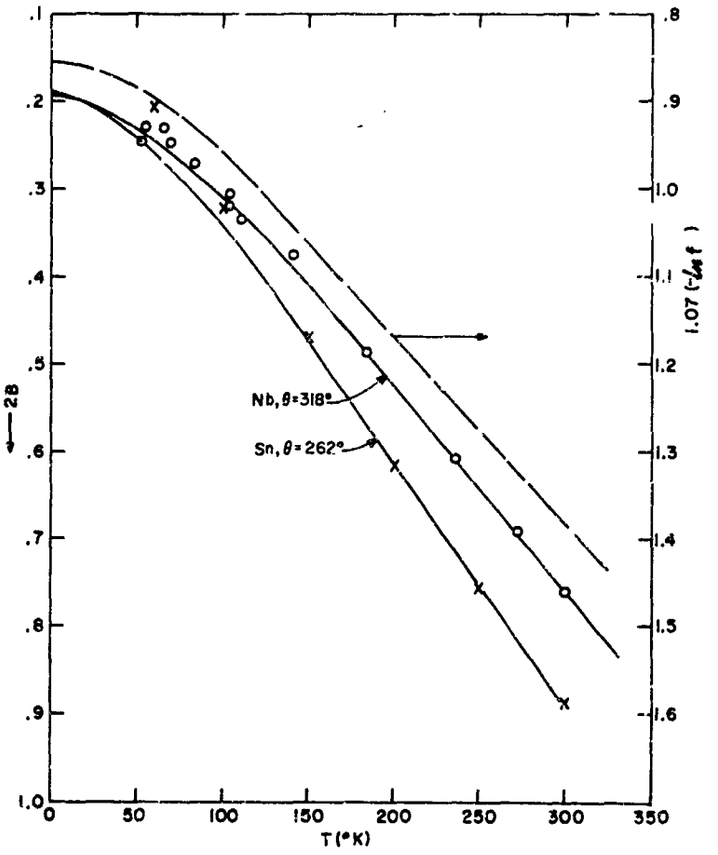

Figure 6. Debye-Waller factor 2B vs. T. o-$2B_{Nb}$, x-$2B_{Sn}$; solid lines theoretical, dashed line, Mossbauer results of ref. 3.

so that from the I ratios we can construct a B vs. T curve for the Sn atoms, represented by the crosses of Fig 6. The data are fit quite nicely over most of the temperature range by the theoretical curve with $\theta_B = 262°$. In this case, the magnitude of B and its temperature dependence are independently in agreement with theory for the appropriate θ_B. The simplest averaging of the θ_B's, $\bar{\theta}_B = (3\theta_{Nb} + \theta_{Sn})/4$ gives $\bar{\theta}_B = 304°$, while from the room temperature elastic constants (Appendix C on page 41) we get $\theta_D = 300°$.

We conclude that at least above 100°K, the data are readily interpreted in terms of an ordinary Debye solid. The theory of the Mossbauer effect gives for the recoilless fraction

$$f = e^{-\frac{2B}{4\lambda^2}}$$

so that for the Sn^{119} λ-ray, $2B = -1.07$ lnf. We have plotted the smoothed curve of Shier and Taylor as the dashed line of Fig. 6. Note that the ordinate is arbitrarily displaced by 0.7 units in order to bring the curve close to the D-W results. The T dependence of f is certainly D-W like, as discussed above, and it seems almost inescapable that the discrepancy represents an error in the *absolute* determination of the recoilless fraction, far beyond the allowance made in ref. 3.

B. SPECIFIC HEAT STUDIES

During the contract period, the facility for making specific heat studies in magnetic fields up to 105 kg was added to our previous low-field capability. The anomalous behavior observed in previous studies seemed to be resolvable only by quenching superconductivity to as low a temperature as possible, and with this end in mind, we performed a complete study of a new sample of Nb_3Sn. This material turned out to be somewhat off stoichiometry, with a mean composition $Nb_{3.3}Sn$(76.5 at.% Nb), and a broad transition at 16.4°K. Nevertheless, the results proved to be very interesting, perhaps more so than anticipated, and they are reported here in some detail.

The specific heat is shown in Fig. 7. A fortunate aspect of these results is that the entropy at T_c obtained by extrapolation of the normal state data back to 0°K, is equal to that obtained by direct integration of the superconducting state data, thereby permitting a straight-forward interpretation of the data in terms of a separable electronic density of states and lattice (Debye) term. This is not possible for ordinary Nb_3Sn (ref. 4), and the present results help to clarify some of the problems raised by the earlier work. In Table II we show some comparative properties for samples of varying stoichiometry. The quantity γ is the linear specific heat coefficient, $\Delta C/\gamma T_c$ is the relative specific heat jump, ρ_0 is the residual resistivity, κ is the Ginzburg-Landau parameter, and $H_c(0)$ is the thermodynamic critical field at T = 0°K.

The result for θ_D is of particular interest, since it was not heretofore possible to identify, with any certainity, the T^3 term above T_c with a Debye temperature. Now it appears that the identical slopes above T_c can be taken as evidence for identical Debye θ_D's and that the anomalous linear term found in the Nb_3Sn case arises from an additional contribution to the specific heat connected with the lattice transformation. The agreement between the specific heat and elastic constant θ's for Nb_3Sn is certainly not coincidental. θ_{el} is calculated on the assumption that C_{11} and C_{12} are restored below T_m to their high T values, as shown in Appendix C on page 41. However, the value of C_{44} measured at low T is

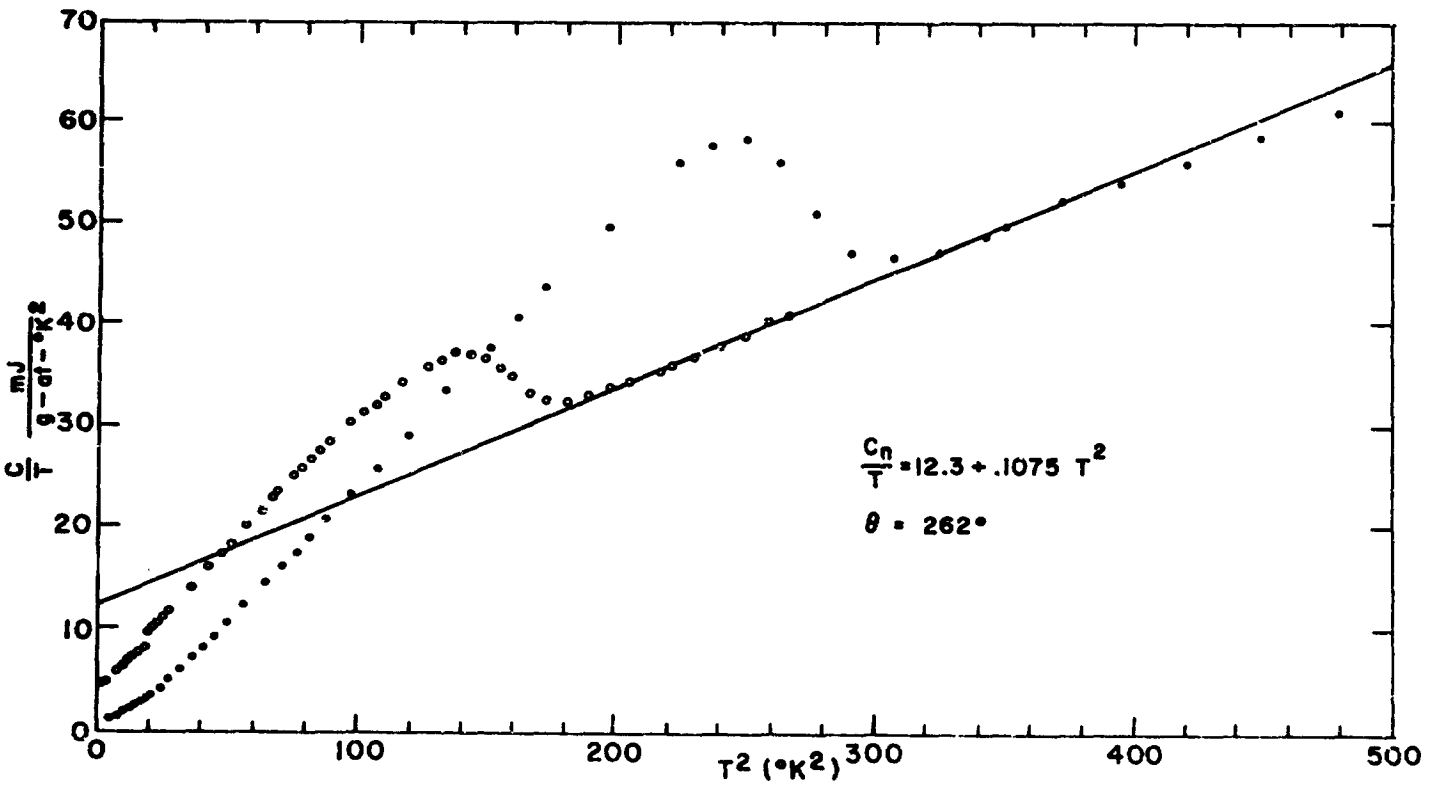

Figure 7. Specific heat of $Nb_{3.3}Sn$, C/T vs. T^2, at H = 0 and H = 103.5 kg.

Table II

Materials Parameters for Niobium Tin
of Various Stoichiometrics

Structure at T_c	Nb_3Sn Tetragonal	$Nb_{3.3}Sn$ Cubic	Nb_4Sn Cubic
T_c (°K)	18.0	16.4	8
γ(mJ/g-at.-°K^2)	13	12.3	5.8
$\Delta C/\gamma T_c$	2.4	2.1	1.4
Θ_D(sp. ht.)	262	262	307
Θ_D(elastic)	265		
ρ_o ($10^{-5}\Omega$-cm)	1	~2	
$\kappa(T_c)$	22	37	
$H_c(0)$ (Gauss)	5350	4500	

about one-half of the high T value, and it is the measured value of C_{44} that gives $\Theta = 265°$. This means that the elastic softening seen for the C_{44} shear mode at the low frequency used for the acoustic measurement extends to frequencies of the order of the Debye frequency, and is, therefore, observed in the specific heat. This is in marked contrast to the $C_{11}-C_{12}$ shear mode, where the extreme softening observed acoustically near T_m has no apparent effect on the specific heat. (It is also of interest to note that Θ_{el} calculated from the high T value of C_{44} is 300°, as found in Nb_4Sn, which is a weak coupling superconductor. There are, however, other possible explanations of this result [cf. (ref. 4)]). The softening of C_{44}, which is accelerated by the tetragonal transformation, is not predicted by the band model of the lattice transformation, and is in itself a striking result. However, its implications for the model are not clear, since this effect is not observed in V_3Si (ref. 5), which, in this respect, provides an exemplary case for the model.

The present results also shed some light on the situation regarding critical fields in Nb_3Sn. In Fig. 8 are shown some critical field data from the literature (refs. 6,7) together with the single point determined from the specific heat at 103 kg. The V_3Ga data shows the

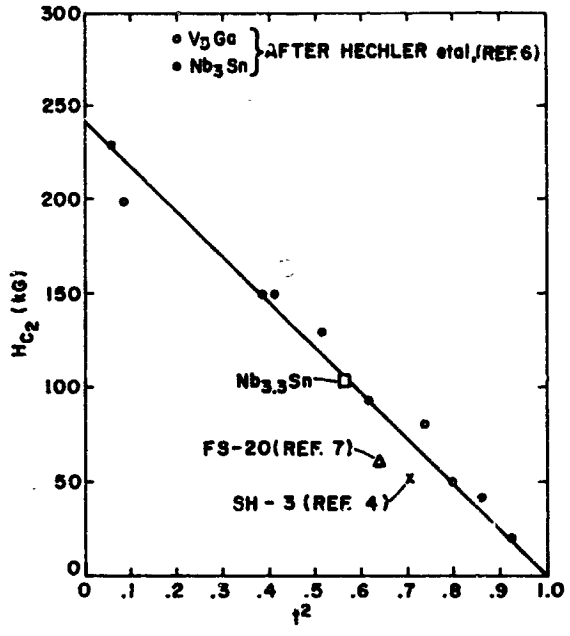

Figure 8. Upper critical field vs. $(T/T_c)^2$ for vanadium gallium and several niobium tin specimens.

effect of paramagnetic limitation of the upper critical field; at low T these data are below that of Nb_3Sn in spite of significantly higher values of $\kappa(t = 1)$ and the thermodynamic critical field $H_o(0)$. High T_c, stoichiometric Nb_3Sn, as exemplified by the previous specific heat sample SH-3, and a vapor-deposited specimen FS-20, do not appear to be limited. $H_{c2}(0)$ for #FS-20 has been estimated to be about 220 kg (ref. 7), so that with $H_{c2} = \sqrt{2}\,\kappa H_c$, we get $\kappa_1(0)/\kappa_1(1) = 1.3$. Theory gives the maximum value 1.2 for this ratio in the absence of any paramagnetic effect, the still higher value observed here probably arising from the fact that pure Nb_3Sn is largely intrinsic ($\ell > \xi_o$), and the theory is not strictly applicable. $Nb_{3.3}Sn$ represents an intermediate case. The introduction of excess Nb has resulted in a substantial increase in $\kappa_1(1)$, but only a 10% increase in $H_{c2}(0)$, with $\kappa_1(0)/\kappa(1) = 1.0$. The fact that the experimental point lies on the published curve has obvious implications about the uniformity and/or stoichiometry of the wires used in ref. 6.

In a detailed study of the specific heat data, not yet completed, we are able to show that the specific heat jump at 103 kg can be used to drive the Maki (ref. 8) parameter $\beta_o^2 = 1$, which is required by the result $\kappa_1(0)/\kappa_1(1) = 1$. The only assumption made in obtaining this result is that the relationship between κ_1 and κ_2, where κ_2 is the G-L parameter appropriate to the magnetization, is also given correctly by the theory. With reliable resistivity measurements as a function of Nb content now being pursued, the way will be open to further exploration of the microscopic parameters of this system. It appears from preliminary work that for pure Nb_3Sn, with $\kappa = \kappa_o + \kappa_\ell$ where the subscripts o and ℓ refer to intrinsic and mean free-path effects respectively, that $\kappa_o \sim 16$ and $\kappa_\ell \sim 6$, so that the behavior of Nb_3Sn is largely intrinsic (insensitive to light doping), and $Nb_{3.3}Sn$ mostly extrinsic, with $\kappa_\ell = 21$.

A. DOPING OF Nb_3Sn

The substitution of small amounts of foreign atoms for either the Nb or Sn atoms in the β-W structure provides an interesting probe of the band model. Results of a study on the effect of Sb doping are given in Appendix G on page 82.

1. The System $Nb_3Sn_{1-x}Al_x$

Samples were prepared by sintering pressed powders at 1500°C for five hours. For reasons not understood, the annealing temperature in this system is somewhat critical, since different results (for the lattice parameter, for example) are obtained at various temperatures. The alloys were found to be almost fully reacted, with little or no Al loss.

Lattice constants and inductive transition temperature midpoints are shown in Fig. 9. Although the atomic radius of Al is 10% smaller than that of Sn, a_o remains constant up to about 5% Al, and then begins to fall rapidly. At the same time T_c remains constant to several percent and then rises rapidly to a maximum of 18.58°K at about 9%. The temperature dependence of the martensitic transformation was also studied. For $x \geq 0.06$, all samples transformed with $c/a > 1$, and $\epsilon(20°K) \sim 3.6 \times 10^{-3}$. For $x > 0.08$ the samples were cubic at all T. The $x = 0.07$ sample gave somewhat ambiguous results, indicating perhaps that it underwent a partial transformation. Of particular interest is the fact that T_m for all samples except $x = 0.07$, was about the same as for undoped material, T_m 44° ± 5°. The $x = 0.07$ sample showed a clearly split [400] peak at about 33°K, while samples with $x > 0.08$ showed no splitting, but the same peak broadening observed above T_m for the lighter doped specimens. As in the case of Sb doping, the insensitivity of T_m to doping shows an unexpected rigidity in the band structure, i.e., the band filling T_o is invariant. Nevertheless, the scale of Al doping over which unusual changes in a_o and T_c take place is commensurate with the model. In fact, although the Nb-Sn-Al system had been previously investigated by others, it was the predictions of the model which led us to cover the region with $x < 0.2$ so thoroughly, thereby leading to the highest T_c yet observed in Nb_3Sn.

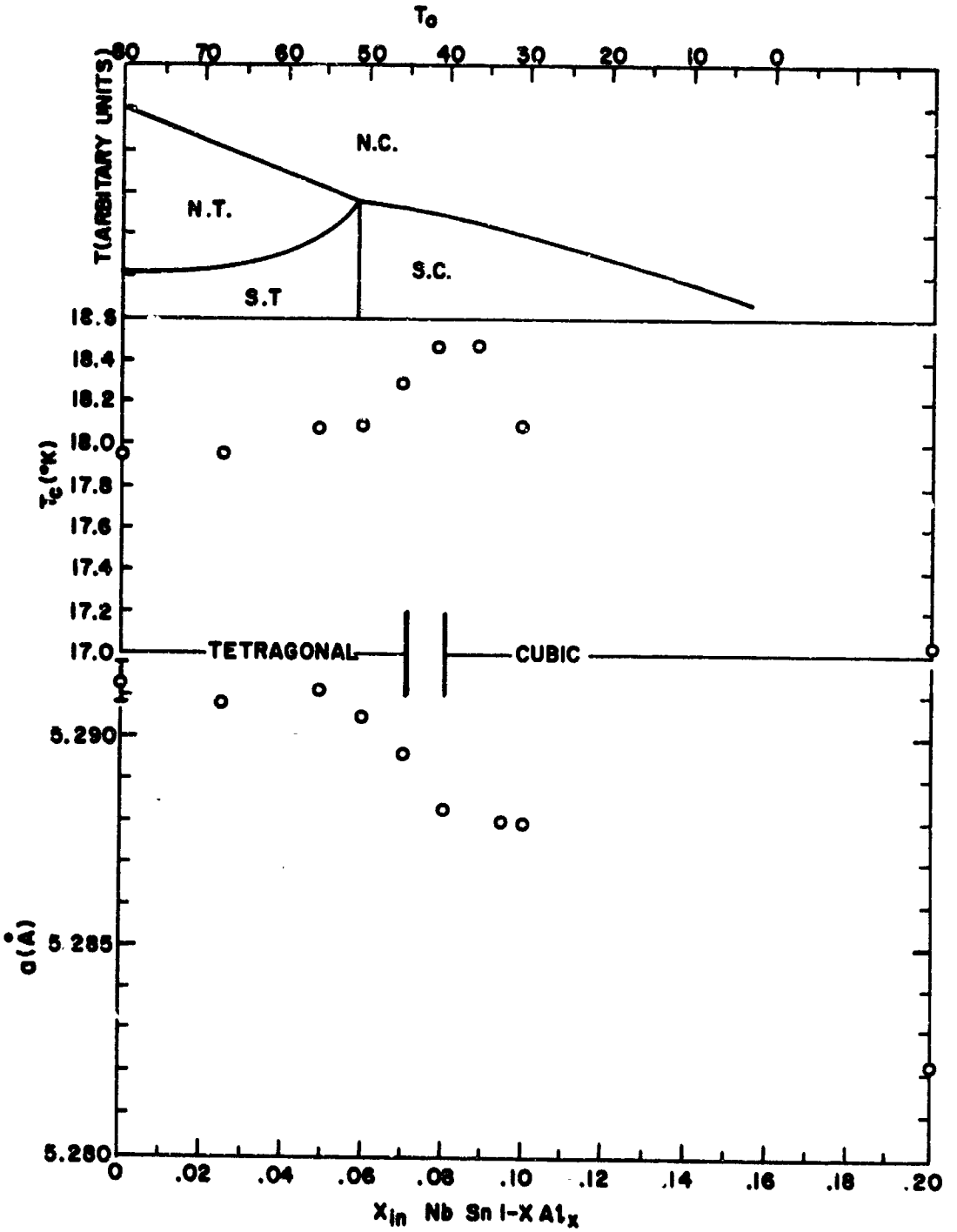

Figure 9. Effect of Al doping of Nb_3Sn on lattice constant, T_c, and martensitic transformation. The phase regions in the upper graph are N.T. ≡ normal-tetragonal, S.C. ≡ superconducting cubic, etc.

This correspondence can be seen in the phase diagram for Nb_3Sn at the top of Fig. 9, which is a plot of the phase boundaries as functions of temperature and T_o, the band filling. The scale of the abscissa is fixed by the fact that for pure Nb_3Sn, $T_o = 80°K$, and $N_o kT_o$, the total number of electrons (or holes) in the band is 0.04/atom. (The scale of the ordinate has been taken to be arbitrary, since the diagram is based on a T_c calculation using BCS theory. A more refined version of this diagram, based on the calculations of Appendix F. will not greatly change the boundaries, so that the intersection of the N.C.-N.T., and N.T.-S.T. lines with the T axes are of order 50° and 10°K respectively). This means that if Al were to introduce one hole per Al into an N-type d-band, the band would be emptied by $Nb_3Sn_{.84}Al_{.16}$, $T_o = 0°K$. The four possible phases are normal, cubic and tetragonal; and superconducting, cubic and tetragonal. For $T_o > 51$, in cooling we proceed from N.C.→S.T. As the martensitic transformation temperature falls, the N.T. - S.T. line rises to meet the higher T_c of the cubic phase. A further decrease in T_o then depresses T_c along the N.C. - S.C. line. The resemblance of this diagram to the T_c and structure measurements is unmistakable, although T_m and, presumably, T_o, seem to vary only slightly with doping. The reasons for this partial success are, of course, not apparent.

2. Hydrogen in Nb_3Sn

Work on the behavior of H in Nb_3Sn although interesting, has been held in abeyance in anticipation of N.M.R. studies recently begun at the Laboratories. We summarize here the work to date.

Nb_3Sn is not readily hydrided, even though it can be made to absorb large quantities of H. We have found the best method for preparing homogeneous samples up to Nb_3SnH is the utilization of ordinary pressing and sintering techniques with partially hydrided Nb powders as starting material. As is generally the case, the introduction of H into the lattice causes an increase in cell volume, and a decrease in T_c. As shown in Fig. 10, the A-15 structure is stable up to about Nb_3SnH, at which point a second, tetragonal phase appears. This concentration also corresponds roughly to the disappearance of superconductivity above 4.2°K. A noteworthy feature of the lattice expansion is that it is considerably more rapid than ordinarily found (in terms of H atoms per transition metal atom) and is not amenable to treatment by the usual schemes for predicting interatomic distances in the hydrides (ref. 9). The effect of H on T_c is also very pronounced, as shown in Fig. 10. This suggests that the electrons in the d-band responsible for the high density of states and/or high T_c of Nb_3Sn are few in number, coming perhaps from only one d-sub-band, unlike the situation in, say, Nb, where the effect of H is much weaker. This fact provides further verification of the band structure theory.

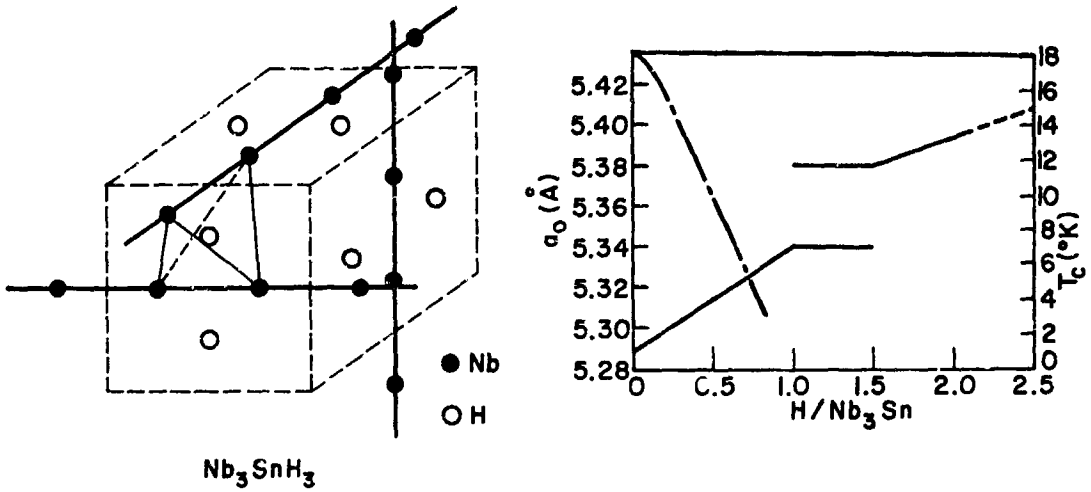

Figure 10. Location of H atoms in the Nb_3Sn unit cell. T_c and a_o vs. H/Nb_3Sn ratio.

We have determined the position of the H atoms in the unit cell by means of neutron diffraction. In Fig. 10, we show the H positions for the fully hydrided structure Nb_3SnH_3. The Sn atoms, which occupy the body center and corners, have been omitted. For the sample studied, which had slightly less than two H atoms/unit cell, the symmetry remained cubic, so that the H atoms are randomly distributed over the available sites. It is seen that the H resides on the cell faces, forming a chain system orthogonal to the Nb chains. Each H atom is tetrahedrally surrounded by four Nb atoms, and forms a cross link between a pair of Nb chains. This is a possible reason why a very small amount of H, about one atom for every 10 unit cells, is found to prevent the martensitic transformation. Another way of regarding the matter is to say that the H diminishes the electron-phonon interaction, as discussed in Appendix F on page 68.

B. RF SPUTTERING ON β-W SUPERCONDUCTORS

Simultaneous sputtering from two elemental targets has been used to deposit films with continuous composition ranges covering up to 70 at. % of non-transition metal atoms. The films, which were condensed on a liquid-nitrogen cooled substrate, were subsequently annealed below 1000°C to form β-W compounds at the appropriate composition.

Details of the experimental technique and the results are given in Appendix H on page 91. Here we give several of th latest results, starting with Nb_3Ge.

In its equilibrium form, Nb_3Ge exists off-stoichiometry and has a T_c of 6.9°K. When it is formed by rapid quenching from the melt in an arc furnace, some of the stoichiometric phase can be retained. This has a transition onset near 17°K but a width of over 10°K. We have sputtered this compound in its metastable form, annealed it, and obtained a T_c onset of close to 18°K with a width of 3°K, a significant improvement over more conventional techniques.

Stoichiometric Nb_3Al also exists only in a metastable state. It is known to have a T_c of almost 18.9°K. We have prepared sputtered films with a T_c of 18.53°K. Thus it appears that sputtering will be a useful preparation technique in the study of metastable phases.

For the last example we have recently prepared Nb_3Sn films with a T_c of 17.4°K. The transition widths were less than 0.15°K. Most importantly, the residual resistance ratios were very high for Nb_3Sn being approximately 6 to 1. We take this as strong evidence for low-specimen contamination introduced by sputtering and subsequent annealing. It is particularly important to have a reproducible and relatively clean preparation technique as we have begun third component doping studies by sputtering in order to raise T_c.

IV. SUMMARY, CONCLUSIONS, AND RECOMMENDATIONS

Our experimental effort over the past two years has tended to strengthen our belief in the power of the density-of-states band model as a phenomenological tool for approaching the problem of maximizing T_c in the β-W superconductors. The very modest success achieved in raising T_c of Nb_3Sn by Al doping may well be fortuitous. The real lesson of the doping studies lies in the apparent inapplicability of the rigid-band approximation, the reasons for which may be found in this model itself: namely, the close connection between high T_c and lattice instability.

Two principal problems compel our attention at present. The first is whether those experiments which are not explicable in terms of the present model alone (for example, the precise nature of the trarsformation at T_m) raise fundamental questions about the nature of the significant variables of a complete theory. From a theoretical point of view, every unexplained result is critical, and continuing experimental and theoretical work along these lines is clearly called for. Practically speaking, there is one experiment of utmost importance which lends credibility to that aspect of the theory of greatest interest, the calculation of T_c: that is the study of the strain dependence of T_c reported in Appendix E on page 60. The confirmation of the theory found in this very direct test stands as proof of its essential validity, which has in no way been weakened by subsequent work.

The second problem is, of course, that of finding a way to capitalize on the predictions of the model for attaining higher transition temperatures. A great deal of evidence has been accumulated in this and other laboratories over the past several years that the phases of highest T_c are often metastable, so that the high T_c, and usually stoichiometric β-W phase, is unstable with respect to non-stoichiometric alloys, other crystal structures, or distorted lattices. Work reported here demonstrates that those elements which enter the Nb_3Sn lattice readily do not change the band parameters to a significant extent, and even more striking, a great number of elements which fit the normal requirements for alloying do not enter the lattice under equilibrium conditions at all. We therefore feel that the rf-sputtering technique, the great promise of which has already been dealt with in Section III.B on page 23 and Appendix H on page 91, represents the most fruitful approach to our program of materials research in superconducitivity.

APPENDIX A*

EFFECT OF FERMI LEVEL MOTION ON NORMAL STATE PROPERTIES OF β-TUNGSTEN SUPERCONDUCTORS

R. W. Cohen, G. D. Cody, and J. J. Halloran

The β-tungsten compounds are of great interest because of their high superconducting transition temperatures T_c and the strikingly anomalous temperature dependences of a variety of characteristic properties in both normal and superconducting states (ref. 10). It is generally thought that many of these anomalies are due to extremely fine structure in the electronic density of states near the Fermi level. Labbé and Friedel (ref. 11), using the tight binding approximation for the density of states, obtained machine calculations of the elastic constant $(C_{11}-C_{12})$ as a function of temperature and were able to account for the tetragonal transformation observed (ref. 12) in V_3Si. Clogston and Jaccarino (ref. 13) found that a very narrow (~400°K) density of states anomaly at the Fermi level could explain measurements of the paramagnetic susceptibility χ of vanadium β-tungsten compounds. In this Appendix, we present a simple model of the electronic density of states which yields, with the choice of essentially one parameter for Nb_3Sn, excellent agreement with the observed temperature dependence of not only χ and $(C_{11}-C_{12})$, but the electrical resistivity ρ and the elastic constant C_{11} as well. Furthermore, the temperature dependences of χ for V_3Si and V_3Ga are correctly predicted.

The model emphasizes the crucial aspect of a sharp drop in the density of states near the Fermi level, while its particularly simple form yields simple, manageable expressions for the experimental quantities. The density of states (for both spins) N(E) as a function of energy E is assumed to have the form:

$$N(E) = N_o, \quad E > 0$$

$$= \alpha N_o, \quad E < 0, \qquad \text{(A-1)}$$

where α is a dimensionless parameter. The position of the Fermi level in the cubic state at T = 0°K is given by $E_F(0)$. Physically, the case $\alpha \ll 1$ and $E_F(0) > 0$ corresponds to a nearly empty d band overlapping an s band, while $\alpha \gg 1$ and $E_F(0) < 0$ is the case of a nearly filled d band. Since the calculations yield the same results in both cases,

---

* R. W. Cohen, G. D. Cody, and J. J. Halloran, Phys. Rev. Letters 19, 840 (1967).

we can, without loss of generality, consider the case of a nearly empty d band and set $E_F(0) = kT_o > 0$. The results are most conveniently expressed in terms of the quantity $F_\alpha(T) = [1 + \exp(-E_F(T)/kT)]^{-1}$, the value of the Fermi function at the band edge, $E = 0$. The position of the Fermi level is found by the usual technique of equating the total number of occupied states at any temperature T to that at $T = 0°K$. The result is an equation for $F_\alpha(T)$:

$$F_\alpha(T) = 1 - [F_\alpha(T)]^\alpha \exp(-T_o/T). \qquad \text{(A-2)}$$

The function $F_\alpha(T)$ is a decreasing function of T, and at low temperatures is well approximated by $F_\alpha(T) \sim F_o(T) = [1 - \exp(-T_o/T]$. For $T \leq T_o/(1-\alpha)\ln 2$, $F_\alpha \leq 1/2$, and the Fermi level has crossed the band edge and entered the low density of states region. At high temperatures, the effect of the small density of states αN_o is to slow down the movement of the Fermi level, and $F_\alpha(T)$ saturates. The rapid motion of the Fermi level gives rise to a strong temperature dependence of the effective density of states and, consequently, to all electronic properties.

We first calculate the electrical resistivity $\rho(T)$ for the model Eq. (A-1). As in the case of transition metals, we assume that the normal state current is carried by the s electrons and that the dominant contribution to the resistivity arises from s-d scattering. The treatment of the resistivity due to electron-phonon scattering departs from that of Wilson (ref. 14) in that the proximity of the Fermi level to the band edge is taken into account by limiting the range of the d band energy integration to energies $E \geq 0$. We employ a Debye phonon spectrum* with characteristic temperature θ. With these considerations, the expression for the phonon scattering contribution to the resistivity $\rho_{ph}(T)$ is

$$\rho_{ph}(T) = A\left(\frac{T}{\theta}\right)^3 \int_0^{\theta/T} dx \left(\frac{x/2}{\sinh x/2}\right)^3 \ln\left[\frac{1 + F_\alpha(T)(e^x - 1)}{1 - F_\alpha(T)(1 - e^{-x})}\right], \qquad \text{(A-3)}$$

where A is a constant. At low temperatures $T << \theta$ and $T << T_o$, $F_\alpha(T) = 1$ and Eq. (A-3) reduces to Wilson's T^3 law (ref. 14). At high temperatures

---

* Because of the rapid temperature dependence of the elastic constants in the temperature range $40°K \gtrsim T \gtrsim 300°K$, the approximation of a constant Debye Temperature would appear to be a poor one. However, according to specific heat measurements (ref. 17), the Debye Temperature actually varies quite slowly in this temperature range.

$T > \Theta$, we obtain $\rho_{ph}(T) = A(T/\Theta)F_\alpha(T)$. Thus, the usual linear increase of $\rho_{ph}(T)$ at high T is multiplied by the function $F_\alpha(T)$ which takes into account the decrease of effective number of d states participating in the scattering as the temperature is raised. The contribution to the resistivity from impurity scattering is found in the usual way (ref. 15), be we again limit the d-band integration to $E \geq 0$. Under the assumption of elastic scattering, we find*

$$\rho_{imp}(T) = \rho_{imp}(0)F_\alpha(T). \qquad (A-4)$$

Figure A-1 is a plot of the resistivity (ref. 16) of Nb_3Sn from 18°K to 850°K. The smooth curve is $[\rho_{ph}(T) + \rho_{imp}(T)]$ for $T_o = 100°K$, $\alpha = 0.04$, $\Theta = 250°K$, $A = 211\ \mu\Omega$-cm and $\rho_{imp}(0) = 11\ \mu\Omega$-cm. We have used $\Theta = 250°K$, since it is the value indicated by specific heat measurements (ref. 17). It should be pointed out that at low temperatures ($T \lesssim 250°K$) the theoretical curve is virtually independent of α, and the value $T_o = 100°K$ gave the best fit in this region. The value $\alpha = 0.04$ fixed the slope of the high temperature resistivity. The fit to the resistivity is very good over the entire temperature range. For comparison the ordinary Wilson form (ref. 14) ($F_\alpha(T) = 1$) for the resistivity is shown for $\Theta = 250°K$ and where the resistivities were matched at $T = 0°K$ and 300°K.

In order to calculate the elastic constants $C_{11}(T)$ and $C_{12}(T)$, it is necessary to compute the change in free energy $\delta F(\epsilon_{xx}, \epsilon_{yy}, \epsilon_{zz})$ when uniform strains ϵ_{ii} are applied to a cubic lattice along the crystallographic axes i. Specifically, the quantities $3(C_{11}-C_{12})/4$ and $C_{11}/2$ are the coefficients of the quadratic term in ϵ of a power series expansion about $\epsilon = 0$ of $\delta F(\epsilon,-1/2\epsilon,-1/2\epsilon)$ and $\delta F(\epsilon,0,0)$, respectively. We assume, after Labbé and Friedel (ref. 11) that the d band in the cubic state results from the superposition of three degenerate bands arising from the transition metal interactions along the three "chains" of the β-tungsten lattice. In general, the shift δE_i of the edge of the i'th band under a strain ϵ_{jj} is given by $\delta E_i = U_{ij}\epsilon_{jj}$, where U_{ij} is the deformation potential tensor. For a cubic crystal the deformation potential tensor is of the form $U_{ij} = [U_1 w_{ij} + U_2(1 = \delta_{ij})]$. It is assumed that the time dependence of any applied strain is sufficiently slow so that the electron system is always at thermal equilibrium. With the above consideration, we obtain the following expressions for the elastic constants:

---

* It should be pointed out that this "impurity" term is indistinguishable from one that would arise from the interaction of electrons with an optical mode whose frequency is vanishingly small. That such a mode may exist in these metals has been suggested by W. Rehwald (to be published).

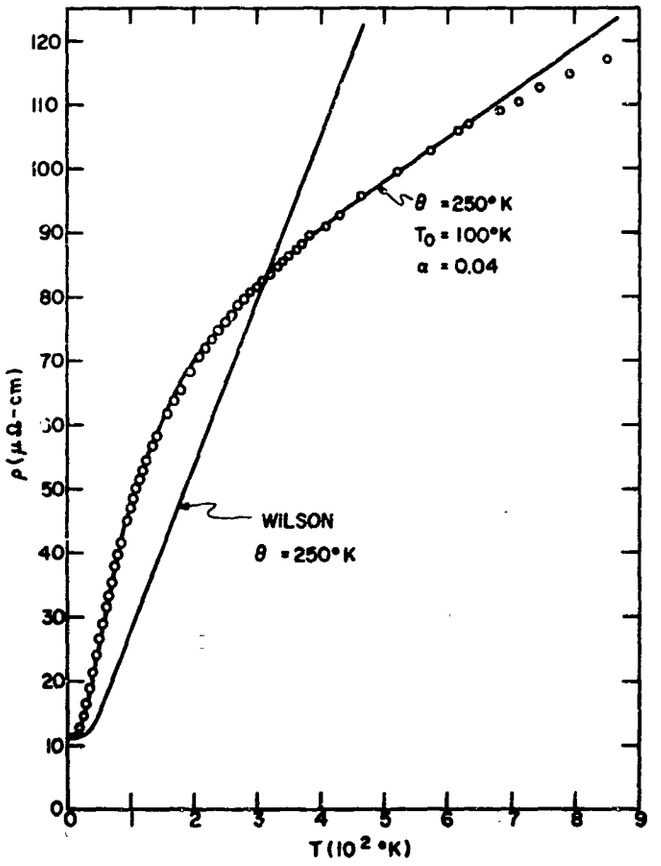

Figure A-1. The electrical resistivity of Nb_3Sn as a function of temperature. The data were taken from (ref. 16). The theoretical fit was computed from Eqs. (A-3) and (A-4) for the indicated values of the parameters. For comparision the result of the ordinary Wilson theory is shown for $\theta = 250°K$ and where the resistivities were matched at $T = 0°$ and $300°K$.

$$C_{11}(T)-C_{12}(T) = -(1/3)(1-\alpha)N_o U^2 F_\alpha(T) + A \qquad \text{(A-5a)}$$

$$C_{11}(T) = -(2/9)(1-\alpha)N_o U^2 F_\alpha(T) + A', \qquad \text{(A-5b)}$$

where $U = (U_1 - U_2)$ is the effective deformation potential and where A and A' represent lattice contributions assumed to be temperature independent. Figure A-2 shows data (ref. 18) for $C_{11}(T)$ and $[C_{11}(T)-C_{12}(T)]$ plotted as a function of $F_\alpha(T)$ where we have taken the values $T_o = 100°K$

and $\alpha = 0.04$ obtained from fitting the resistivity data. Over most of the temperature range $F_\alpha(T) \approx F_0(T)$, so that Fig. A-2 is essentially a plot of elastic constants against $[1 - \exp(-100/T)]$. The agreement between theory and experiment is excellent. Particularly satisfying is the fact that the ratio of the slopes in Fig. A-2, $[d(C_{11}-C_{12})/dF_\alpha]/[dC_{11}/dF_\alpha] = 1.55$, compares very well with the value 1.50 predicted by Eqs. A-5.

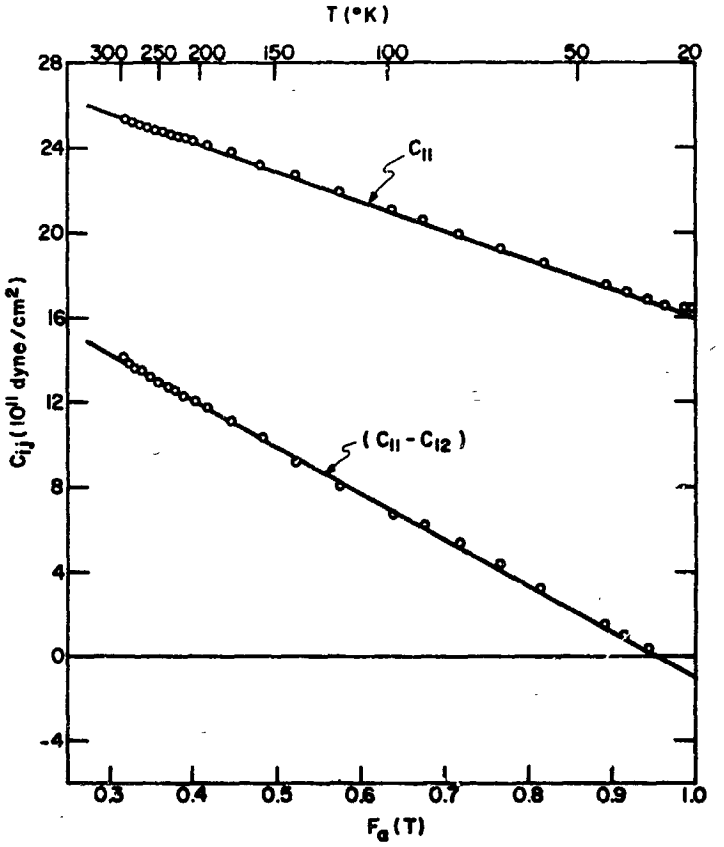

Figure A-2. The elastic constants C_{11} and $(C_{11}-C_{12})$ for Nb_3Sn as a function of $F_\alpha(T)$. The function $F_\alpha(T)$ is given by Eq. A-(2) with $T_0 = 100°K$ and $\alpha = 0.04$. The data were taken from ref. 18.

The paramagnetic susceptibility $\chi(T)$ for the density of states Eq. A-1 can be readily calculated with the result:*

$$\chi(T) = \mu_B^2(1 - \alpha)N_o F_a(T) + \chi_{orb}, \qquad (A\text{-}6)$$

where μ_B is the Bohr magneton and χ_{orb} is the orbital contribution to the susceptibility. In Fig. A-3, the theoretical susceptibility is compared with previously published experimental data (ref. 19) for V_3Si (T_o = 110°K) and V_3Ga(T_o = 95°K) and with our data for Nb_3Sn (T_o = 100°K). We have chosen α = 0.04 for all three materials, but the curves are insensitive to variations in α in this temperature range. With the exception of the deviation for Nb_3Sn below 55°K, the agreement with the theoretical temperature dependence for all three materials is very good. We find that the region below 55°K is quite sensitive to sample preparation. The Nb_3Sn sample for which data is shown was ground from a single crystal specimen which, by x-ray examination, showed a tetragonal transformation (ref. 1) at 43°K. For samples in which x-ray examinations do not reveal a lattice transformation, χ does not decrease in the temperature range T < 55°K, but is constant.

The orbital contribution to the susceptibility χ_{orb} is given by the F_a = 0 intercepts of χ. From Fig. A-3, we note that χ_{orb} does not vary appreciably from metal to metal. We further note that the quantity T_o is essentially the same for all three materials. It thus appears that T_o = 100°K is a characteristic of all β-tungsten compounds.

From the slopes of the solid lines in Fig. A-3, we find the following values of N_o for the three metals: N_o = 3.3 states/e.v.-atom for Nb_3Sn, 6.7 for V_3Si, and 6.9 for V_3Ga. Using the above value of N_o for Nb_3Sn and the slopes of the solid lines in Fig. A-2 to determine the quantity N_oU^2, we find the deformation potential for Nb_3Sn, U_2 = 4.8 e.v.

With knowledge of the deformation potential, we are able to predict the magnitude of the shift of the edges of the three sub-bands in the tetragonal state of Nb_3Sn. Below the lattice transformation temperature, the size of the unit cell along the "c" axis decreases by

---

* Actually, the first term on the right side of Eq. A-6 should be multiplied by $[1-N_oV_c(1-\alpha)F_a(T)/2]^{-1}$ to take into account the enhancement of χ due to the coulomb repulsion V_c. However, because of the scatter of experimental data, we are unable to make a definite choice of V_c (except to say that $N_oV_c/2 \lesssim 0.5$). We have, therefore, set V_c = 0; this may lead to an overestimate of N_o by as much as 30%.

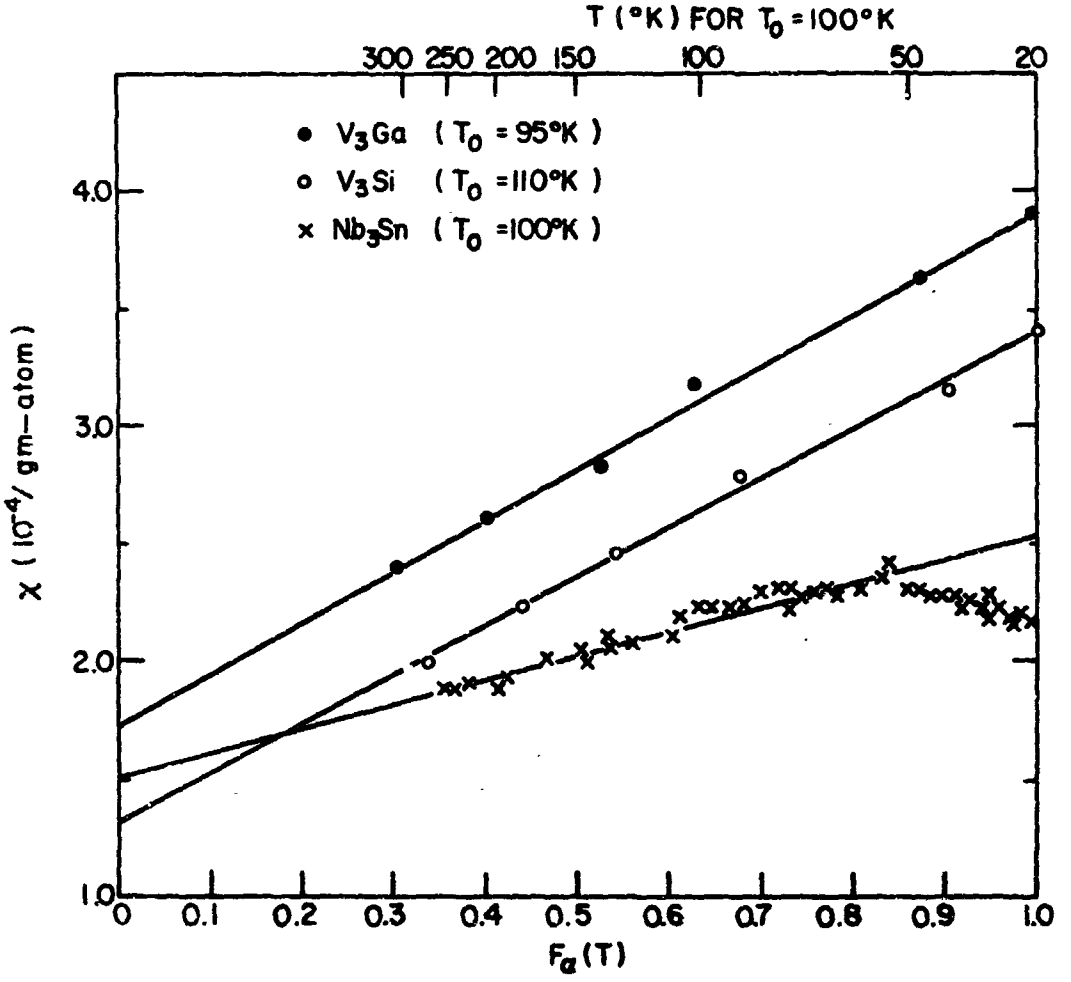

Figure A-3. The paramagnetic susceptibility χ of V_3Ga, V_3Si and Nb_3Sn as a function of $F_\alpha(T)$. The function $F_\alpha(T)$ is given by Eq. A-2 with α=0.04 and the indicated values of T_0. The data for V_3Si were taken from (ref. 19).

an amount (ref. 1) $\varepsilon = 6 \times 10^{-3}$ and increases along the "a" and "b" axes by an amount ε/2. We then compute that the edge of the "c" sub-band, initially at E = 0, moves to $E = -U\varepsilon \sim -320°K$, while the edge of the "a" and "b" sub-bands shifts to $E \sim +160°K$. The magnitude of these shifts indicates that the Fermi level at T = 0°K is in a region where the density of states is $N_0/3$. A spin susceptibility measurement (in the normal state) will then determine an effective density of states $N_0/3$ for a field parallel to the "c" axis and $N_0/9$ for a system of randomly oriented domains. Although we observe a decrease in the

effective density of states for Nb_3Sn below about 55°K, the observed decrease does not appear to be as large as predicted. Samples which do not show a tetragonal transformation and have constant χ below $\sim$ 55°K do not obey the prediction of the model for either the tetragonal or cubic states. It is believed that expansion of the free energy in terms of changes in the lattice parameter is not sufficient to describe the state below the lattice transformation temperature (refs. 20,21).

The question of the order of the transition to the tetragonal state has not been resolved. Analysis of the higher order terms in ϵ in the free energy expansion show that for the present model, the coefficient of the cubic term in ϵ is non zero, indicating a first order transtition. This result agrees with that of Labbé and Friedel (ref. 11). Analysis of the x-ray data of Mailfert et. al. (ref. 1) indicates that if the transition is of second order, $\epsilon \to 0$ as $(T_m-T)^q$ where $T_m = 43°K$ and $q \sim 1/4$. According to the theory of second-order phase transitions, (ref. 22) this would require the vanishing of all terms through ϵ (ref. 14) in the free-energy expansion, an unlikely occurrence. The susceptibility data give no evidence of a first-order transition. It is possible that domain structure in the tetragonal state washes out rapid variations in χ.

Since the model is successful in explaining such a wide variety of normal state properties of the high T_c β-tungsten superconductors, we believe that the essential feature of the model, namely the rapid variation of the electronic density of states near the Fermi level, should also be included in any analysis of the superconducting properties.

ACKNOWLEDGEMENTS

We wish to express special thanks to Dr. B. Abeles for his kind interest and help throughout this work. We are also grateful to Drs. L. Vieland and W. Rehwald for several helpful discussions.

APPENDIX B*

CHARACTERISTIC PARAMETERS OF β-W SUPERCONDUCTORS

G. D. Cody, R. W. Cohen, and L. J. Vieland

There has been considerable success in understanding the unusual properties of the high-temperature cubic phase of the high T_c β-tungsten superconductors (ref. 23). In particular, the temperature dependence of the electrical resistivity, elastic constants $C_{11}(T)$ and $C_{12}(T)$, and the magnetic susceptibility $\chi(T)$ above the lattice transformation temperature T_M have been calculated from a model of the electronic density of states. The model density of states (for both spins) has the form

$$N(E) = N_o, \qquad E > 0$$
$$= \alpha N_o, \qquad E < 0 \tag{B-1}$$

where the quantity α is assumed to be much less than unity. Physically, the model can be interpreted as a high density of states d-band overlapping a wide, low density of states s-band. The d-band is assumed to be nearly empty**; the total number of electrons in this band at T = 0 is given by $N = (1-\alpha)N_o kT_o$, where kT_o is much less than the width of the band. Furthermore, following Labbé and Friedel (ref. 11) we assume that the d-band consists of three independent equal contributions from the orthogonal chains of the β-tungsten lattice. Due to the assumed independence of the sub-bands, under a uniaxial strain ε_{11} directed along the i'th chain (i = 1,2,3), only the sub-band associated with that chain is perturbed. In that case, the shift of the edge of the particular sub-band i is given by $\delta E_i = U\varepsilon_{ii}$, where U is a deformation potential. By applying the model to the experimental quantities of the cubic state of Nb_3Sn, the parameters of the model were found to be*** N_o = 5.6 states/e.v.-atom, α = 0.04, T_o = 80°K, and U = 4.1 e.v.

---

* G. D Cody, R. W. Cohen, and L. J. Vieland, Proceedings of the Eleventh International Conference on Low Temperature Physics, 1009, (1968), St. Andrews, Scotland.

** We could, of course, consider a nearly filled d-band.

*** These values of T_o and U are slightly different than those given in (ref. 23), owing to further experimentation and more complete characterization of specimens. The value of N_o has been obtained from specific heat measurements (ref. 4).

The unusual aspects of the model are the sharp drop in the density of states, the very small number of carriers in the d-band, and the response of the d-band to lattice distortion. The sharp drop in the density of states, which greatly facilitates calculations, appears to be necessary in order to accurately reproduce the temperature dependence of experimental quantities in the cubic phase. The independent sub-band approximation has been shown to give good results for small strains in the cubic state (ref. 23). The present paper applies the band model to the tetragonal state ($T < T_M$) using the parameters obtained from the cubic state data. We calculate the magnetic susceptibility, specific heat, elastic constants, and the tetragonal distortion, and compare them with experimental data. The agreement between theory and experiment is, in some cases, excellent. However, certain discrepancies suggest that the transformed state cannot be described solely by a tetragonal strain imposed on the cubic-state model.

In order to calculate the experimental quantities in the tetragonal state, we make use of the expression for the free energy of the system in the presence of a magnetic field H, tetragonal strain ε, and uniaxial strains* η. Neglecting the small contribution of the s-electrons, the free energy is given by

$$F(T,E_F,\varepsilon,\eta,H) = NE_F + \frac{1}{2}\sum_{\ell=\pm 1}\sum_{m=\pm 1}(m+3)g\left(\tfrac{1}{4}[3m-1]U_\varepsilon + U\eta + \ell\mu_B H, T, E_F\right)$$

$$+(3/4)(A_{11}-A_{12})\varepsilon^2 + (3/2)(A_{11}+2A_{12})\eta^2 - \frac{1}{2}\chi_{orb}H^2, \qquad \text{(B-2)}$$

where

$$g(X,T,E_F) = -(N_o/6\beta)\int_X^\infty \ln\{1 + \exp - \beta(E-E_F)\}dE. \qquad \text{(B-3)}$$

In Eqs. (B-2 and B-3), A_{11} and A_{12} are temperature independent lattice contributions to C_{11} and C_{12}, respectively**, χ_{orb} is the temperature independent orbital contribution (ref. 23) to the susceptibility, E_F is the Fermi energy, N is the total number of d-band electrons, and

---

* In conventional notation, the individual strain components are $\varepsilon_{11} = (\eta-\varepsilon)$ and $\varepsilon_{22} = \varepsilon_{33} = (\eta + 1/2\varepsilon)$. We are ignoring the small differences between the elastic constants C_{11}, C_{22}, and C_{33} in the tetragonal state.

** We have neglected all higher order lattice contributions, a detailed analysis shows this to be a valid approximation in Nb_3Sn over the temperature range of interest.

$\beta=(k_B T)^{-1}$. The position of the Fermi level is established by the condition $\partial F/\partial E_F=0$.

The value of the tetragonal deformation $\varepsilon_o(T)$ is found from the condition for equilibrium (in the following, all derivations are evaluated at $\eta = H = 0$ and $\varepsilon = \varepsilon_o(T)$):

$$\partial F/\partial \varepsilon = 0. \tag{B-4}$$

Below the lattice transformation temperature T_M there are two solutions for ε_o which correspond to free-energy minima; that for which $\varepsilon_o > 0$ has the lower free energy and corresponds to the sign of the transformation for (ref. 1) Nb_3Sn. The transformation temperature T_M is given in terms of the parameters of the theory through the approximate relation

$$T_M \approx T_o\{\ln[1-3(A_{11}-A_{12})/N_o U^2]\}^{-1} \tag{B-5}$$

In Fig. B-1 is shown the theoretical curve of ε_o as a function of T/T_M. The experimental values of Mailfert et. al. (ref. 1) are given in the figure. The agreement between theory and experiment is good over most

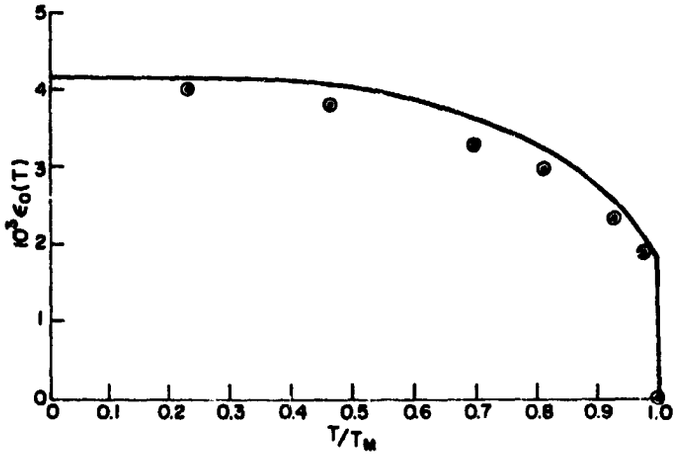

Figure B-1. Tetragonal distortion as a function of T/T_M. Curve derived from Eq. (B-4), points from (ref. 1).

of the temperature range. It is noteworthy that the value of ε_o at T = 0°K has not been fitted to the data; it is based on parameters of the model extracted from cubic-state data. At the transformation temperature,

the theory predicts a first order transformation with a large jump in ε_o. The temperature resolution in the x-ray measurements is not sufficient to detect a discontinuity in ε_o, but no hysteresis was observed (ref. 1). Furthermore, the x-ray data (ref. 1) indicate that $T_M \simeq 43°K$, whereas the elastic constant data [Eq. (B-5)] predict $T_M \approx 50°K$. At present, we do not know the origin of this difference.

The elastic constants in the tetragonal state can be derived from the free-energy function (2) according to the relations

$$\frac{3}{2}\,(C_{11}(T)-C_{12}(T)) = \partial^2 F/\partial\varepsilon^2 \qquad \text{(B-6a)}$$

$$3(C_{11}(T)+2C_{12}(T)) = \partial^2 F/\partial\eta^2. \qquad \text{(B-6b)}$$

The solution to Eqs. (B-6) indicates that the elastic constants return to the lattice values at low temperatures. Physically, this result comes about because of the fact that the stable state of the system at low temperatures is one in which all electrons are in one sub-band. Thus, there is no term in the electronic contribution to the free energy which is quadratic in ε or η. The predicted return of the elastic constants to the lattice values have been observed in Nb_3Sn by Rehwald (ref. 24), and for completeness, the author's results are reproduced in Fig. B-2.

The electronic specific heat at constant volume in the tetragonal state is obtained from the equation

$$C_V(T) = -T\partial^2 F/\partial T^2. \qquad \text{(B-7)}$$

In Fig. B-2 is shown the calculated curve of $C_V(T)$ obtained from Eqs. (B-2) to (B-4) and (B-7). Since the major contribution to the specific heat comes from the lattice modes, it is necessary to fit the curve for the cubic state near T_M by choosing an appropriate Debye temperature. Otherwise, there are no adjustable parameters. It is gratifying that the specific heat jump at T_M, and the magnitude of the energy associated with the rapidly changing strain just below T_M are in excellent agreement with theory. However, theory predicts a distinctly first-order transition at T_M, with a latent heat of 2 Joules/g-atom, which is not observed. The failure to observe a latent heat cannot be attributed to a smearing of the transition which would distribute the large latent heat over the region below T_M.

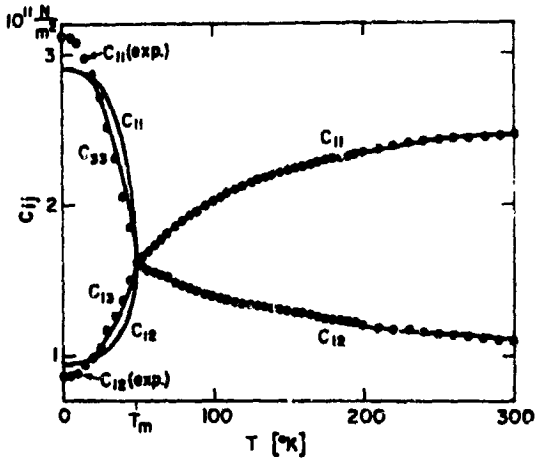

Figure B-2. Elastic constant as a function of T. Curves derived from Eq. (B-6), points from (ref. 24).

The paramagnetic susceptibility is obtained from Eqs. (B-2) and (B-3) according to the relation

$$\chi(T) = -\partial^2 F/\partial H^2. \tag{B-8}$$

The result is

$$\chi(T) = \frac{1}{3}\bar{N}_o\mu_B^2\{f(-U\varepsilon_o) + 2f(\tfrac{1}{2}U\varepsilon_o)\} + \chi_{orb}, \tag{B-9}$$

where f(E) is the Fermi function. In Eq. (B-9), the quantity $\bar{N}_o$ represents a weakly temperature dependent density of states which has been renormalized in order to take into account many-body effects (ref. 25). Analysis of cubic state data (ref. 23) shows that $\bar{N}_o = 3.3$ states/e.v.atom. Figure B-4 shows the normalized susceptibility as a function of temperature for a sample which was similar to that shown in Figs. B-1 through B-3. The theoretical curves are for the cubic state $\varepsilon_o = 0$ and the tetragonal state [Eq. (B-4)]. The unusual low temperature maximum in the susceptibility follows from the theory and arises because as the temperature is lowered all electrons spill into one sub-band with effective density of states $\bar{N}_o/3$. However, the observed decrease in the susceptibility is only about two-thirds of the expected drop. Also, the susceptibility of a crystal which shows the elastic constant (ref. 18) $(C_{11}-C_{12})$ going to zero at 32°K is roughly

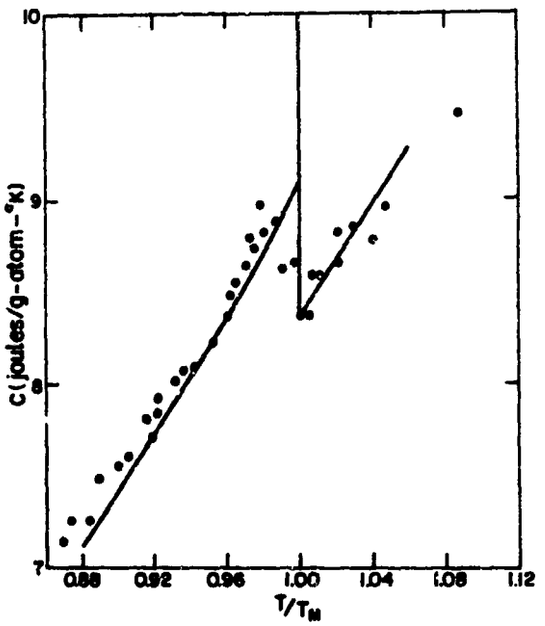

Figure B-3. Specific heat as a function of T/T_M. Curve derived from Eqs. (B-2 and B-4), and Eq. (B-7), points measured values.

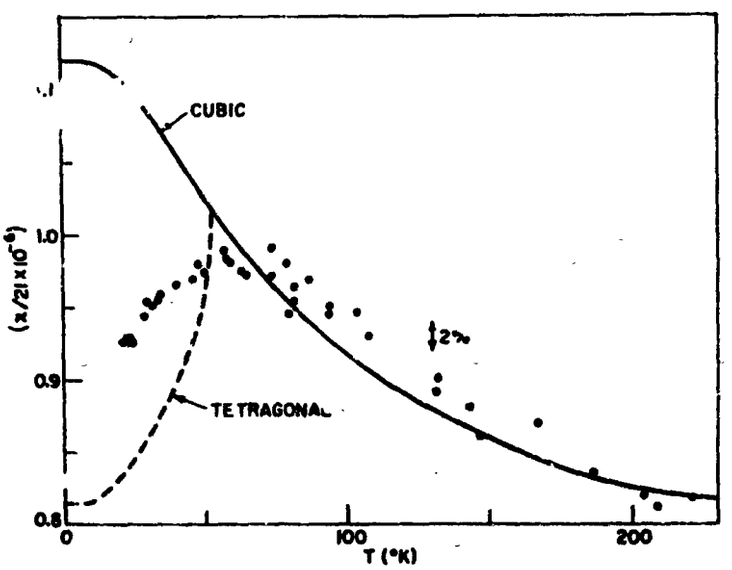

Figure B-4. Total susceptibility as a function of T. Curve derived from Eq. (B-9), points measured values.

temperature independent below approximately 60°K. Thus, the susceptibility of this crystal departs from the cubic state theory at temperatures well above the predicted T_M.

We have seen that using cubic state parameters and a simple band structure model, we are able to obtain good agreement with the overall behavior of the tetragonal state properties. In some cases, such as the value of the tetragonal deformation and the magnitude of the elastic constants, striking quantitative agreement is obtained. In spite of this success, it is felt that the discrepancies that do exist are fundamental in nature. In particular, the absence of a latent heat, the discrepancy between the values of T_M determined from various experiments, and the lack of quantitative agreement for the susceptibility suggest that the theory is incomplete. Moreover, an analysis of the observed (ref. 5) temperature variation of $[C_{11}(T)-C_{12}(T)]$ for V_3Si shows excellent agreement with Eq. (B-6a) using V_3Si parameters and indicates, in contrast to the results of x-ray experiments (ref. 12), that no tetragonal transformation should occur in this material. It is believed that the mechanism which triggers the tetragonal transformation has not been completely identified.

APPENDIX C*

ELASTIC MODULI OF SINGLE-CRYSTAL Nb_3Sn

W. Rehwald

A. INTRODUCTION

The elastic moduli of most solid materials have the tendency to increase (ref. 26) when the temperature is lowered. However, some compounds, which belong to the A-15 (β-tungsten) structure type, such as Nb_3Sn (ref. 18), V_3Si (ref. 5), Nb_3Al (ref. 27) and V_3Ga, show the opposite behavior. Sound-velocity measurements on single crystals indicated that the velocity of all measured sound modes decreased with decreasing temperature, and in particular that the velocity of the shear mode propagating in the (110)-direction and having particle motion in the $(1\bar{1}0)$-direction (called the "soft" shear mode) goes to very low values near a critical temperature T_m. This was supposed to be the transition temperature for the transformation from a cubic to a tetragonal lattice. Keller and Hanak (ref. 18) found a T_m of 32°K for a single-crystal Nb_3Sn. Although such a transformation has been observed for V_3Si by x-ray technique (ref. 12), it did not show up in the Nb_3Sn crystal used for sound-velocity measurements.

After annealing a Nb_3Sn crystal for several hours, a lattice transformation was observed by Mailfert, Batterman, and Hanak (ref. 1) at about 43°K. Since this temperature was appreciably higher than that observed for lattice softening before the annealing process, the discovery warranted sound-velocity measurements with the annealed crystal. It turned out that the critical temperature for the softening had shifted to about 49°K and that the temperature dependence of the elastic moduli below that value was markedly different from previous results.

The coincidence of the lattice softening with anomalies in the electronic behavior led Labbé (ref. 11) to the conclusion that rapid changes of the electronic density of states at the Fermi level are responsible for the lattice softening in V_3Si. A model, recently proposed by Cohen et. al., (ref. 23) uses the basic idea of Labbé and Friedel, but makes calculations of the relevant physical quantities more tractable and the physical processes more understandable. The measured elastic moduli are discussed in terms of this model.

---

* Published in part as W. Rehwald, Phys. Letters 27A, 287 (1968).

B. EXPERIMENTAL

The Nb_3Sn single crystal used for our measurements was grown by an HCl-gas transport technique (ref. 28). After a heat treatment of some 20 to 100 hours at 1000°C in vacuum the crystal had slightly reduced its room-temperature lattice constant and showed splitting of the (600) and (400) x-ray reflexes (ref. 1) below 43°K. Three different sound modes were propagated in the (110)-direction of the cubic phase with particle motion in the (110), (1$\bar{1}$0), and (001)-directions. The velocities were measured at 40 MHz by the pulse-echo method, the details of which are described elsewhere (ref. 18). The temperature was determined by a copper-constantan thermocouple, which was calibrated at 4.2° and 77°K. Using published tables (ref. 29) for the interpolation gives sufficient accuracy (better than $\pm$ 0.5 deg) in the range of interest.

Figure C-1 shows the sound velocities in (110)-direction versus temperature for the three different polarizations. There are three major differences between these results and those of Keller (ref. 18) on an unannealed crystal:

- The temperature at which the velocity of the "soft" shear mode goes to very small values is considerably higher (49°K instead of 32°K).
- The temperature coefficient of the velocity of the (001)-shear mode changes at 49°K.
- The longitudinal sound velocity goes through a minimum at 49°K and rises to approximately its room-temperature value at temperatures below.

Qualitatively, the ultrasonic attenuation increases strongly near 49°K for all three polarizations and remains high for temperatures below. In the case of the "soft" shear mode, the attenuation below the critical temperature is so high that no echoes can be observed.

From the measured sound velocities, all the elastic moduli can be calculated above 49°K. We assumed a density of 8.87 g/cm^3 and neglected its change due to thermal expansion (coefficient of thermal expansion = 7.3×10^{-6}/deg. as derived from x-ray data). Because values of $C_{11}-C_{12}$ could not be directly determined below 40°K, we tried to get C_{11} directly from a measurement of the velocity of a longitudinal sound wave in the (100)-direction. The values for the modulus C_{11}, measured in this way, coincided with those inferred from measurements in the (110)-direction at all temperatures above approximately 62°K. Below this temperature there is a discrepancy, which increases linearly with the temperature difference, the directly measured values being

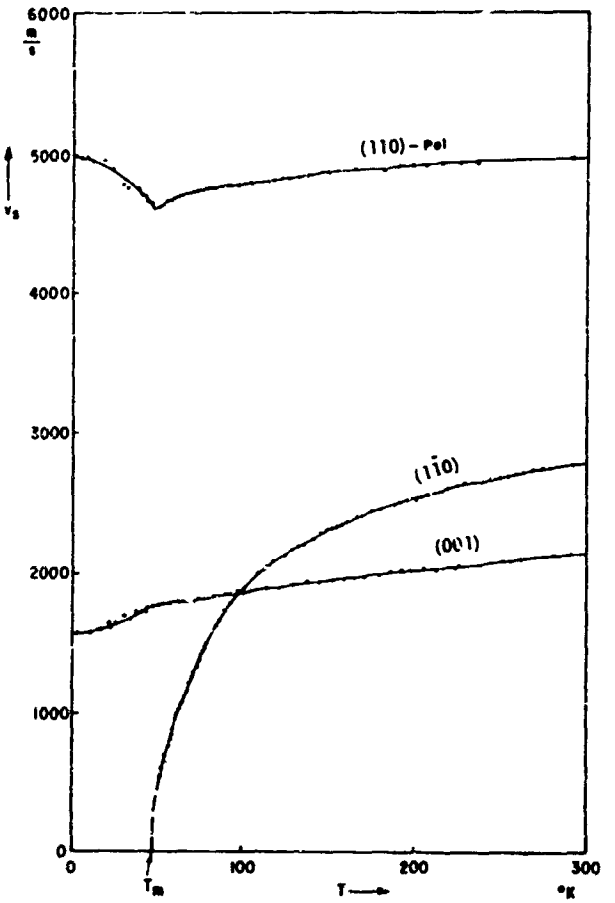

Figure C-1. Velocity of sound vs. temperature for longitudinal and two shear modes propagated along the <110> direction.

higher by 3% at the maximum deviation. Below 44°K an enormous attenuation of more than 25 dB/cm for the longitudinal wave in (100) sets in, so that no echoes could be detected. The temperature dependencies of C_{11}, C_{12} and C_{44} are compared in Fig. C-2. The directly determined values for C_{11} are indicated by circles.

It is interesting that the bulk modulus $B = (C_{11} + 2C_{12})/3$ slowly increases when lowering the temperature; its variation is of the same tendency and order of magnitude as that of most metals.

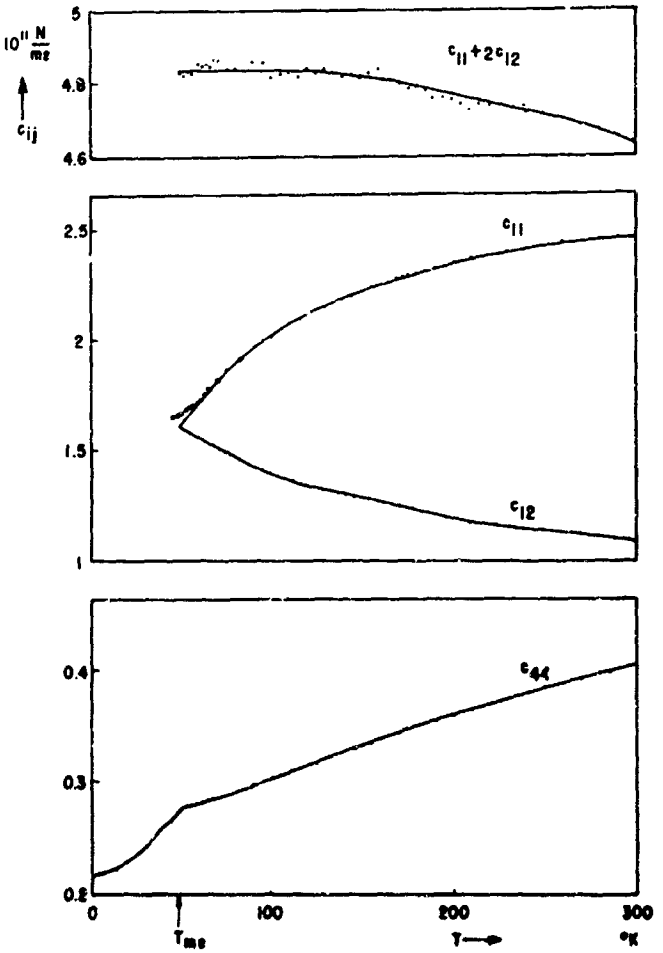

Figure C-2. Elastic constants vs. temperature. Top graph shows the bulk modulus.

C. DISCUSSION

In metals, the physical properties of the lattice are to a large extent determined by the behavior of the electron gas. For example, the Kohn-effect anomalies manifest themselves as structure in the dispersion curves (ref. 30) of lattice vibrations; so it is feasible to relate the elastic anomalies of Nb_3Sn to deviations from the usual free-electron behavior.

Labbé and Friedel (ref. 11) were the first to give an explanation of the lattice softening in V_3Si and other A15-type materials and the effects related to it (ref. 32). According to their theory the Fermi level lies in a band of high density of states very near to the band edge. In the undeformed cubic state, this band is built up of three sub-bands derived from the d-electrons of the transition metal (Nb in our case), which is arranged in three families of chains. Electronic overlap is assumed to be only within the chains. The application of external strain which changes the interatomic distances within a chain, alters the position and width of the associated sub-band. The resultant change of the occupation of the various sub-bands gives a negative contribution to the strain-dependent part of the free energy and lowers the elastic moduli connected with this strain. As a consequence of restriction to electronic overlap only within a chain, this model cannot explain the temperature variation C_{44}.

Cohen et. al. (ref. 23) use the basic ideas of Labbé and Friedel, but reduce the model to its simplest possible form. They assume a density of states in the form of a step function with the Fermi level near the jump. In their simplified model, the equations for the elastic moduli C_{11} and C_{12}, the electric resistivity and the magnetic susceptibility can be written down in explicit form and be discussed without using a computer. The basic parameters of their model are the densities of states N_o and αN_o on both sides of the jump, the distance in energy kT_o of the Fermi level from the step at $T = 0°K$ and the deformation potential coefficient U, which describes the sub-band splitting under an uniaxial tension along a cube-edge direction. The elastic moduli as derived from this model consist of a lattice contribution A_{ij} which is slowly varying with temperature, and in the case of $C_{11}-C_{12}$ also of a negative electronic contribution:

$$C_{11}(T) = A_{11} - \frac{2}{9}(1-\alpha)N_o U^2 F_\alpha(T) \qquad \text{(C-1)}$$

$$C_{11}(T) - C_{12}(T) = A_{11} - A_{12} - \frac{1}{3}(1-\alpha)N_o U^2 F_\alpha(T) \qquad \text{(C-2)}$$

$$C_{44}(T) = A_{44} \qquad \text{(C-3)}$$

The temperature dependence of the electronic part is based on the function

$$F_\alpha(T) = (1 + \exp(-E_F(T)/kT)^{-1} \qquad \text{(C-4)}$$

the value of the Fermi-function at the band edge E = 0. Considering the shift of the Fermi level with temperatures, one obtains

$$F_\alpha(T) = 1 - (F_\alpha(T))^\alpha \exp(-T_o/T). \qquad \text{(C-5)}$$

In ref. 23, the best fit to the measured temperature variation of the electric resistivity was accomplished by choosing $T_o = 100°K$ and $\alpha = 0.04$. Evaluation of the magnetic susceptibility data (ref. 31) gives a density of states of $N_o = 3.0$ states/eV atom. In Fig. C-3 our measured elastic moduli C_{11}, $C_{11}-C_{12}$ and C_{44} are plotted as

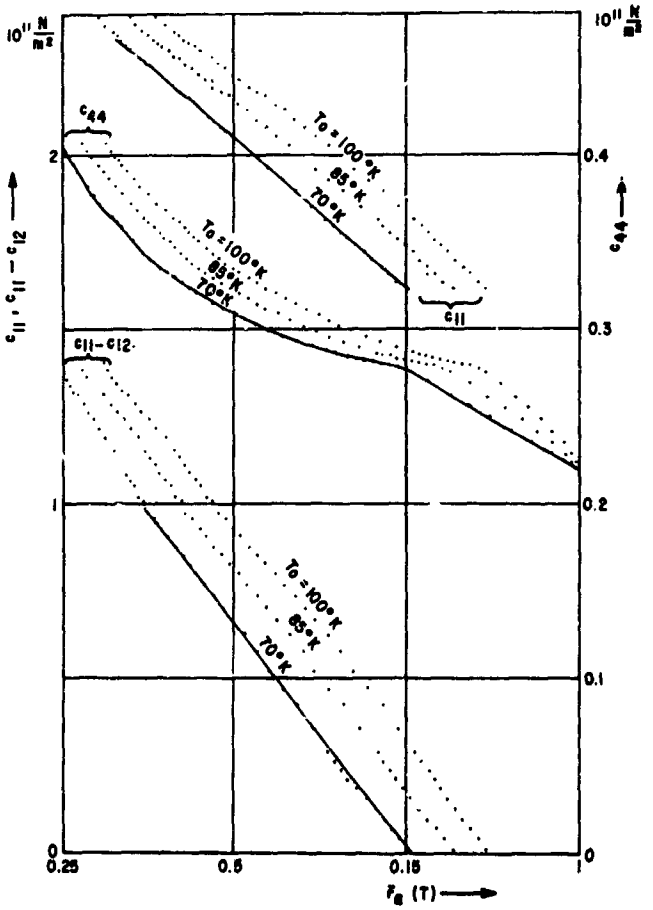

Figure C-3. Shear mode elastic constants vs. the function $F_\alpha(T)$ for various values of T_o.

as a function of $F_\alpha(T)$ with $\alpha = 0.04$ and three different Fermi-level positions: $T_o = 100°K$, $85°K$, and $70°K$. The best fit for C_{11} from the measurements in (110)-direction and $C_{11}-C_{12}$ is obtained with $T_o = 70°K$, although $T_o = 85°K$ is only slightly worse. With $70°K$ we obtain

$$A_{11} = 2.90 \times 10^{11}\ N/m^2 \quad A_{12} = 0.95 \times 10^{11}\ N/m^2$$

and

$$N_o U^2 = 8.07 \times 10^{11}\ N/m^2$$

The ratio of the slopes for C_{11} and $C_{11}-C_{12}$ is equal to 1.52, which is very close to the theoretical value of 3/2. Taking $N_o = 3$ states/eV atom we obtain a deformation potential coefficient of 5.6 eV. Extrapolating $C_{11}-C_{12}$ to zero leads to a transformation temperature $T_m = (49 \pm 0.5)°K$. Above T_m the temperature dependence of C_{11} and $C_{11}-C_{12}$ as inferred from measurements in the (110)-direction, is well described by this theory, except at temperatures above $200°K$.

An interesting quantity to discuss is the bulk modulus $B = (C_{11}+2C_{12})/3$. According to theory it should show only the faint temperature variation of the lattice contributions:

$$B = 3^{-1}(C_{11} + 2C_{12}) = 3^{-1}(A_{11} + 2A_{12}) \qquad (C-6)$$

The experimental results show this behavior at least above T_m.

Below the transformation temperature the crystal can lower its free energy by undergoing a tetragonal deformation. This splits the conduction band into a single sub-band and a pair of sub-bands and shifts the Fermi-level to a new position. Following the notation of Fig. C-4, the values of the Fermi energy E_F with respect to the band edge in the cubic state and the amount of splitting $U\varepsilon_s$ are calculable from the conditions of the minimum of free energy and the conservation of particles (ref. 34):

$$U\varepsilon_s(T) = \frac{2N_o U^2\ kT}{9(A_{11}-A_{12})} \left[\ln \left(1 + \varepsilon^{(E_F + U\varepsilon_s)/kT} \right) - \ln \left(1 + e^{(E_F - U\varepsilon_s/2)/kT} \right) \right] \qquad (C-7)$$

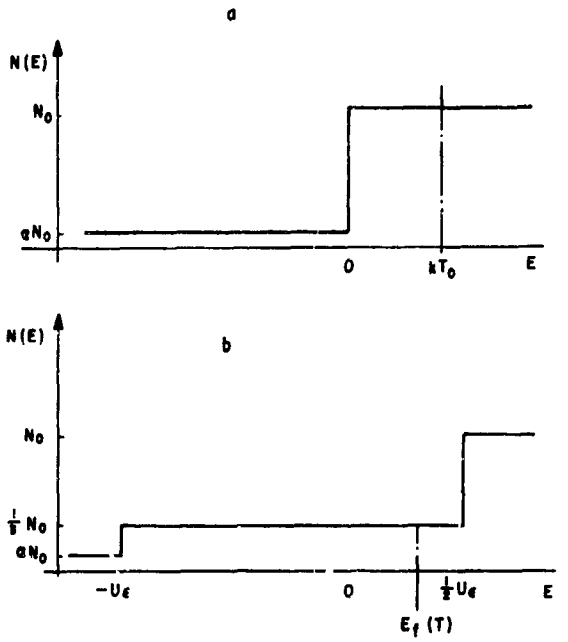

Figure C-4. Density of states as a function of energy for (a) cubic and (b) tetragonal lattice.

In Fig. C-5 the temperature variation of the Fermi level and of the band edges are plotted. At high temperatures the Fermi level lies in the band of the low density of states αN_0 with the high energy tail of the Fermi function reaching into the band with the high density of states. At lower temperatures the Fermi level moves into the high-density band and is moving towards kT_0 when the transformation takes place. Below the transformation the sub-bands split quite rapidly, and a few degrees below T_m, the Fermi level reaches a position in the single sub-band.

For calculating the elastic moduli in the tetragonal state (ref. 34), one adds a small variation ε to the spontaneous deformation ε_s and takes the second derivative of the free energy with respect to the strain component ε. Due to the tetragonal symmetry, different formulae are obtained for e.g., an uniaxial strain along the tetragonal c-axis or perpendicular to it:

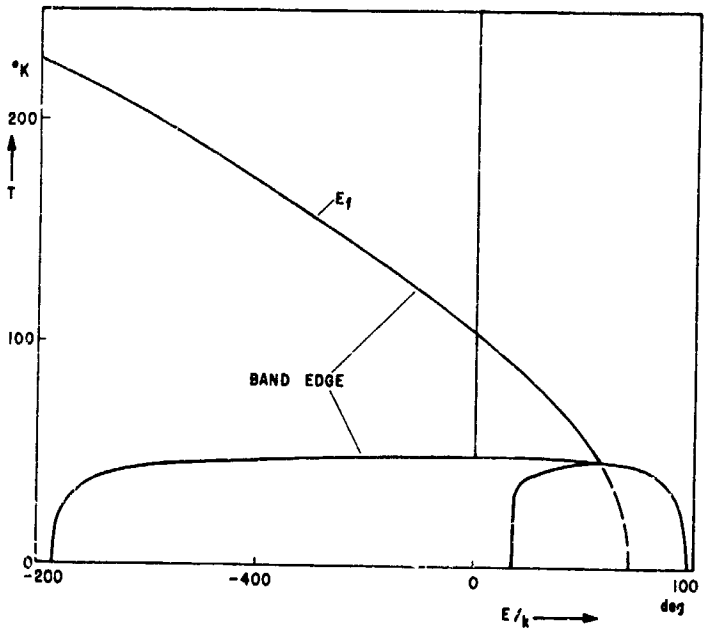

Figure C-5. Variation of the Fermi level and band edges with temperature.

$$C_{11}^{||}(T) = A_{11} - \frac{2}{3} N_o U^2 \frac{f_1 f_2}{f_1 + 2f_2} = C_{33}^{te}(T) \qquad \text{(C-9a)}$$

$$C_{11}^{\perp}(T) = A_{11} - \frac{1}{3} N_o U^2 \frac{f_2(f_1 + f_2)}{f_1 + 2f_2} = C_{11}^{te}(T) \qquad \text{(C-9b)}$$

$$C_{12}^{||}(T) = A_{12} + \frac{1}{3} N_o U^2 \frac{f_1 f_2}{f_1 + 2f_2} = C_{13}^{te}(T) \qquad \text{(C-10a)}$$

$$C_{12}^{\perp}(T) = A_{12} + \frac{1}{6} N_o U^2 \frac{f_2(f_1 + f_2)}{f_1 + 2f_2} = C_{12}^{te}(T) \qquad \text{(C-10b)}$$

Here the functions f_1 and f_2 represent the Fermi occupation number at the edges of the various sub-bands:

$$f_1 = \left[1 + \exp(-U\varepsilon_s - E_F)/kT\right]^{-1}, \quad f_2 = \left[1 + \exp(U\varepsilon_s/2 - E_F)kT\right]^{-1} \qquad \text{(C-11a,b)}$$

Fig. C-6 shows the temperature variation of the elastic moduli C_{11} and C_{12} in the tetragonal state. In the limit $\varepsilon_s \to 0$ the two functions f_1 and f_2 converge to the common value $F_\alpha(T)$, and Eqs. C-(9) and C-(10) go over into Eqs. C-(1) and C-(2), which are valid in the cubic state. Near T = 0°K, the Fermi level is located in the sub-band with a density of states equal to $N_o/3$ and the functions f_1 and f_2 have the values 1 and 0 respectively. So in the limit $T \to 0$°K, the elastic moduli are restored to the lattice contributions alone:

$$C_{11}(0) = A_{11}, \quad C_{12}(0) = A_{12} \qquad \text{(C-12a,b)}$$

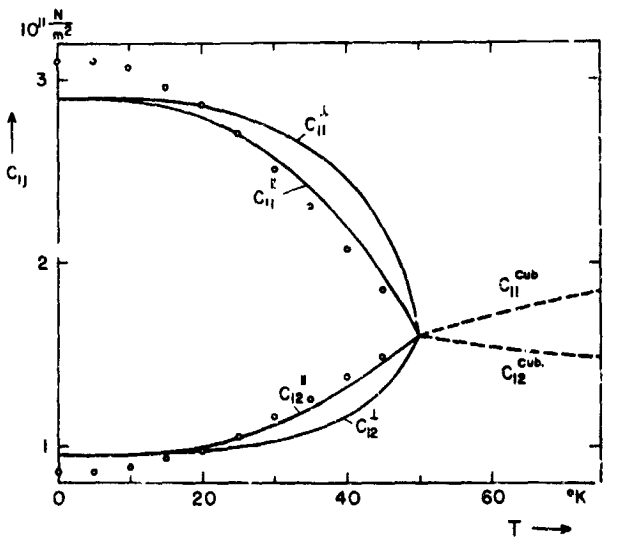

Figure C-6. Variation of elastic moduli C_{11} and C_{12} in the tetragonal state, assuming a constant bulk modulus.

It is worth mentioning that also in the tetragonal state the bulk modulus is independent of electronic contributions and equal to the lattice part $(A_{11} + 2A_{12})/3$. Assuming this relation to be valid in the whole temperature range below the transformation, we are able to calculate values for the "apparent" elastic moduli C_{11} and C_{12} from the measured velocity of a longitudinal sound wave in the (110)-direction.

2

The results are indicated in Fig. C-6. Part of the deviation from the theoretical curves is because our theory assumes a temperature invariant shear modulus C_{44}, whereas the measurements show a considerable temperature dependence of C_{44}.

The theory in its present form fails to explain the temperature variation of C_{44}. According to the models of Labbé and Friedel, and of Cohen et. al., the shear modulus C_{44} should be unaffected by the conduction electrons and exhibit only the slow increase toward lower temperatures due to the lattice alone. The reason for the failure of theory is that it assumes a one-dimensional band-model for the chains and neglects electronic interaction between different chains and between Nb- and Sn-atoms. This leads to a form of the deformation-potential tensor, in which each sub-band edge, labeled by i = 1,2,3, is shifted from E = 0 to E_i by normal strains parallel or perpendicular to the corresponding chain axis only:

$$E_1 = U_1\epsilon_1 + U_2(\epsilon_2 + \epsilon_3)$$

$$E_2 = U_1\epsilon_2 + U_2(\epsilon_1 + \epsilon_3)$$

$$E_3 = U_1\epsilon_3 + U_2(\epsilon_1 + \epsilon_2) \qquad \text{(C-13,a,b,c)}$$

In all subsequent formulae, only the difference $U = U_1 - U_2$ appears; there is no contribution from the shear strains ϵ_4, ϵ_5 and ϵ_6, however. Such a form of the deformation potential tensor is consistent with the band extrema lying along the coordinate axes in reciprocal space (as in silicon). Examining the band-structure of V_3Ga as calculated by Mattheiss (ref. 33), and putting in the correct number of electrons for Nb_3Sn, suggests the existence of band maxima near the Fermi level at either the Δ-line or the R-point $(\frac{\pi}{a}, \frac{\pi}{a}, \frac{\pi}{a})$ or the M-point $(\frac{\pi}{a}, \frac{\pi}{a}, 0)$ of the Brillouin zone. A band extremum at M would by symmetry involve a third component U_3 of the deformation potential, which could account for an electronic contribution to C44. The measured data of C_{44} versus $F_\alpha(T)$, however, do not fit a straight line. In order to explain the non-linear behavior of C_{44} (F_α) one has to introduce additional effects, such as change in the density of states by a planar shear strain.

Another difficulty lies in the discrepancy between the C_{11}-values from the two types of measurement in the temperature range between 44° and 62°K. Critical fluctuations can be excluded from the explanation since the temperature range is too big. Plotting both series of data in a $C_{11}(F_\alpha)$ diagram gives a straight line in both cases with a slope ratio of 0.68, which is close to $^2/3$. In the framework of the present theory this would indicate a spontaneous decrease in the product $N_o U^2(1-\alpha)$ for

uniaxial extension (and compression) along one of the cubic (100)-directions at a temperature of about 62°K. A careful examination of the curves of the magnetic susceptibility versus temperature (ref. 31) also shows that a deviation of the measurements from the simple $F_\alpha(T)$-dependence exists at temperatures around 62°K. It is quite feasible that already at T_{m3} 62°K some kind of transformation starts which affects the electronic band structure, but which does not lead to a measurable change in the unit cell dimensions. Perhaps shifts of atoms within the unit cell are responsible for it. At T_{m1} 43°K the transformation of the unit cell sets in, as observed by x-ray techniques (ref. 1), and also shows up as a peak in the specific heat (ref. 34). Domain formation below T_{m1} causes a high ultrasonic attenuation, as is observed for longitudinal waves in (100)-direction. The assumption of a reduction of $N_\alpha U^2(1-\alpha)$ by 32% causing a similar reduction in the elastic modulus C_{12}, leads to a vanishing of $C_{11}-C_{12}$ at about $T_{m1} = 43°K$. The question still remains as to why ultrasonic measurements in the (110)-direction lead to a different transformation temperature of $T_{m2} \approx 40°K$. A possible answer is that in the pre-transformed state between $T_{m3} = 62°K$ and $T_{m1} = 43°K$ the sample is already tetragonal and elastic theory of a tetragonal crystal has to be applied. Depending upon orientation, the value of C_{11} inferred from measurements in a cubic [110]-direction lies between the limits

$$C_{11}-C_{44}+C_{66} \text{ and } \frac{C_{11}+C_{33}}{2}+\frac{C_{44}-C_{66}}{2}$$

In the case of a measurement in the cubic (100)-direction the pressure applied by the electrodes enforces a particular orientation of the tetragonal c-axis and the measured elastic modulus is either C_{33} or C_{11}.

From the measured elastic moduli the Debye temperature was calculated, using the averaging procedure by Quimbey and Sutton (ref. 36). Results above the transformation temperature are plotted in Fig. C-7 by a solid line. Below T_m the Debye temperature was derived from calculated values of C_{11} and C_{12}.

A decrease in sound velocity on going to low temperatures has been observed in other isostructural compounds: Single crystals of V_3Si[3] and polycrystalline samples of Nb_3Al and V_3Ga (ref. 27). All these materials belong to the A15 structure type and have superconducting transition temperatures above 14°K. In the polycrystalline specimen a shear-wave velocity averaged over all orientations was measured, which decreased by 2 to 4 %. In some respects, the results on V_3Si resemble our findings for Nb_3Sn. There are, however, several salient differences: The modulus $C_{11} - C_{12}$ does not go to zero or very low values at $T_m = 20.5°K$ but stays at a constant value for several degrees and then drops again. Also C_{11} and C_{12} are not restored to their lattice part values

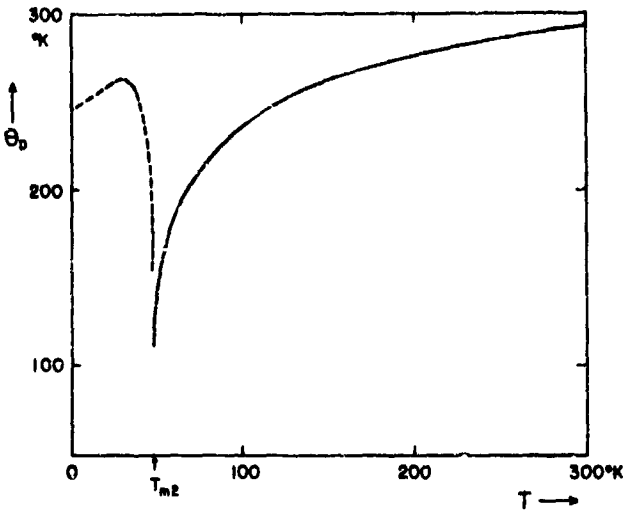

Figure C-7. Apparent Debye Θ vs. T calculated from elastic constants.

near T = 0°K. Evaluating the data of Testardi et.al. by Eqs. (C-1) and (C-2) gives a deformation potential U of about half the value of Nb_3Sn. Extrapolating the straight line to $C_{11}-C_{12} = 0$ leads to a F_α (T) ≈ 1, T ≈ 0°K, in contrast to the behavior of Nb_3Sn. The tetragonal deformation of V_3Si is of opposite sign compared to Nb_3Sn; so below T_m the pair of sub-bands with a density of states equal to $\frac{2}{3}$ N_o is lower in energy and has the Fermi level in it. Finally, the shear modulus C_{44} varies very slowly with temperature, being in better agreement with the model of noninteracting chains of transition metals.

D. SUMMARY

The temperature behavior of the elastic properties of single-crystal niobium stannide has considerably changed after annealing and making the crystal "visibly" (by means of x-rays) transforming. From all the elastic moduli, determined by sound-velocity measurements in a cubic (110)-direction, a transformation temperature of $T_m = (49 \pm 0.5)$°K is derived which is in reasonable agreement with structure observed in the temperature dependence of the magnetic susceptibility, but which disagrees with the temperature 43°K given by Mailfert et.al. (ref. 1) for the structure transformation observed by x-rays. The measured data of C_{11} and C_{12} fit well into the theory by Cohen et.al. (ref. 23) based on the fact of a jump in the electronic density of states near the Fermi level and the interaction of such a band configuration with elastic strains. The shear modulus C_{44}, however, although monotonically

decreasing toward low temperatures, does not fit quantitatively into the theory.

Because of the close connection between the elastic properties and the behavior of the conduction electrons, ultrasonic studies are a valuable tool in the investigation of the electronic structure of Nb_3Sn and similar materials and will hopefully lead to a better understanding of the superconducting properties.

ACKNOWLEDGEMENTS

The author is indebted to Drs. G. D. Cody, R. W. Cohen, and L. Vieland for valuable discussions, to Dr. B. Abeles and Mr. K. R. Keller for their permission to use their ultrasonic apparatus, and to Dr. J. Hanak for supplying the crystal and his assistance in the sample preparation.

APPENDIX D*

SPECIFIC HEAT AND THE LATTICE TRANSFORMATION IN Nb_3Sn

L. J. Vieland and A. W. Wicklund

Nb_3Sn(T_c = 18°K) belongs to the β-tungsten class of intermetallic compounds, many members of which are superconductors with transition temperatures among the highest known. Since the discovery by Batterman and Barrett (ref. 12) of a lattice transformation in V_3Si(T_c = 17°K) from a low temperature tetragonal phase to the β-tungsten (cubic) structure at $T_m \sim 25°K$, much interest has been focused on the nature of the transformation and its connection, if any, with high T_c superconductivity. Ultrasonic measurements on single crystal V_3Si (ref. 37) and Nb_3Sn (ref. 18) reveal an anomalous lattice softening with decreasing temperature, the elastic constant for the shear mode corresponding to the tetragonal distortion $[(C_{11}-C_{12})/2]$ approaching zero near T_m. However, not all samples transform, and the apparent vanishing of the soft-shear mode is not a sufficient condition for the development of the tetragonal phase. X-ray results suggest that the transformation is of second order for both V_3Si (ref. 12) and Nb_3Sn (ref. 1), there being no observable thermal hysteresis. For Nb_3Sn, T_m = 43°K, and the tetragonality (c/a-1) is 2.2 times as great, and of opposite sign, to that of V_3Si.

We have measured the specific heat of several samples of Nb_3Sn over the range 25° to 80°K, using the heat-pulse technique in a calorimeter of conventional design. Temperature was measured with a Pt resistance thermometer with calibration traceable to the National Bureau of Standards. The specific heat of the calibrated addendum amounted to 1/4-3/4 of the total specific heat for the various samples. The data are shown in Fig. D-1. The solid circles (sample I) are for a high-purity polycrystalline boule of vapor-grown material (ref. 2), with a relatively broad superconducting transition extending from 17.75° to 18.00°K, while the crosses represent data on a sample of sintered Nb_3Sn (PS-1) exhibiting a sharp transition at 18.1°K. Below 43°K and above 59°K, the results for the two specimens were indistinguishable. While the absence of a specific heat peak for PS-1 suggests that this sample does not undergo a transformation, at least over the range of the measurement, it should be borne in mine that x-ray diffraction patterns for sintered Nb_3Sn have been reported to exhibit line broadening at low temperatures (T ∿ 35°K) (ref. 12).

---

* L. J. Vieland and A. W. Wicklund, Sol. St. Comm. 7, 37 (1969).

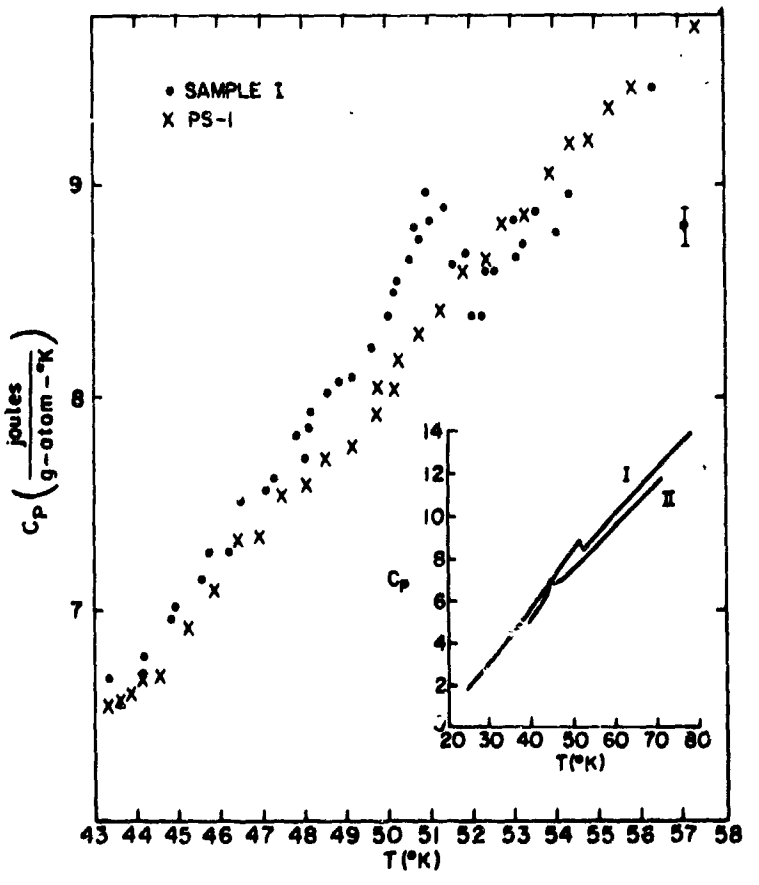

Figure D-1. Specific heat of three samples of Nb_3Sn: I, high purity vapor grown crystal; PS-1, sintered material; II, vapor-grown single crystal showing a lattice transformation by x-rays at T_m = 43°K.

The inset shows the behavior over the entire range for sample I, together with data for the annealed single crystal on which elastic constant measurements have been made* (sample II). The position of the peak for this specimen is consistent with T_m determined from x-ray data on material from the same boule. In spite of the small sample size for II, and the large addendum correction, the difference in the specific heat of samples I and II in the cubic state is thought to lie outside experimental error.

According to the theory of Labbé and Friedel (ref. 11), the transformation is of the Jahn-Teller type, in which the threefold degeneracy of the orthogonal d sub-bands, arising from interaction along the transition metal chains in the β-W structure, is removed by the strain accompanying the cubic to tetragonal transition. Cohen et.al. (ref. 23), retaining this basic idea, developed a model based on a particularly simple density of states (step function), which greatly facilitates calculation, and applied it with notable success to the temperature dependence of the elastic constants, resistivity, and magnetic susceptibility of cubic Nb_3Sn. In this model, the Fermi level in the cubic state at 0°K lies a small distance kT_o from the edge of a narrow band of constant density of states N_o, the density of states outside this band being αN_o where α is a small number [0.04]. Under the tetragonal distortion one sub-band edge shifts in energy $\Delta = U\varepsilon$, and the two sub-bands belonging to the orthogonal Nb chains shift by $-\Delta/2$, where ε is the strain, $\varepsilon = 2/3(c/a-1)$, and U the deformation potential. The elastic constants C_{11} and $(C_{11}-C_{12})/2$, are proportional to the coefficients of the leading terms in the free-energy expansion with respect to the appropriate strain, and are found to vary linearly with the value of the Fermi function at the band edge $F_\alpha(T)$, given closely at low temperatures ($T < T_m$) by $F_\alpha(T) = \left(1-e^{-T_o/T}\right)$. Higher order terms in the expansion in tetragonal strain near T_m, $\delta F = A\varepsilon^2 + B\varepsilon^3 + C\varepsilon^4$, are given by $B = (-A/6)(1-F_\alpha)(U/kT)$ and $C = (-A/16)(1-F_\alpha)(U/kT)^2$, where $A = -N_o(1-\alpha)U^2F_\alpha/4$. The strain at any temperature can be obtained from the conditions of minimum free energy,

$$\delta = (2/3F_o)\{F_o(\eta + \delta)-F_o(\eta - \tfrac{\delta}{2})\},$$

and particle conservation,

$$3T_o/T = F_o(\eta + \delta)+2F_o(\eta - \tfrac{\delta}{2}),$$

[α may be safely taken to be zero below T_m], where $\delta = |U\varepsilon/kT|$, $\eta = E_F/kT$, $F_o(x) = \ln(1+e^x)$, and F_o is the value of F_α at the temperature T' where $C_{11}=C_{12}$. The model gives the following picture of the transformation: there is a strongly first-order phase change a few degrees above T', with a spontaneous strain of $\varepsilon(T_m) = -B/2C = -4kT_m/3U$, and a latent heat $Q = -T\partial(\Delta F)/\partial T \approx (4/9)N_ok^2T_mT_o[1-F_\alpha(T_m)]$. The negative strain [$c/a < 1$, as observed for Nb_3Sn], arises from the fact that for T_o/T_m not too large, B and C are both positive and large compared to the lattice contributions. (The case of V_3Si is not clear cut, since the

lattice contribution to B is negative, and of the order of the electronic term). The strain varies approximately as $(T_m-T)^{1/4}$ over a large temperature range, saturating at $\varepsilon(0°K) = -2kT_o/\pi_o U$. At 0°K the electronic contribution to the free-energy is linear in ε, the elastic constants thereby being fully restored to their "lattice" ($T = \infty$) values, and the density of states at the Fermi level is 1/3 that in the cubic state.

Recent acoustic measurements on sample II* show the soft-shear mode vanishing linearly with F_α at $T' = 49.7°K$, and $T_o = 80°K$. Using these results, and taking $N_o = 5.6$ states/eV-atom (see below), we have calculated the specific heat for both the tetragonal and cubic states, as shown in Fig. D-2. Of particular interest is the fact that the calculated peak height at T_m is in good agreement with experiment, while the latent heat, $\sim 1.5J$, is not observed. Since the latent heat is the change in energy associated with a spontaneous strain of $\varepsilon(T_m)/\varepsilon(0°) = (2/3)(T_mF_o/T_o) = .35$, and a strain of this size is observed by x-rays very close (<1°K) to T_m (ref. 1), we conclude that the absence of a latent heat cannot be due to smearing of the transition as a result of domain formation. The phase transformation occurs at a temperature substantially lower than predicted and appears to be second order**. From the resolution of the peak for sample I, which was studied in greatest detail, we estimate that the maximum latent heat that might have escaped detection is of the order of 0.03J/g-atom, about 2% of the theoretical value.

A second difficulty arises from the fact that we failed to detect the expected change in N_o accompanying the transformation. The phonon enhanced density of states used in the calculation, ($N_o = 5.6$/eV-atom), can be obtained independently from susceptibility measurements above 60°K (ref. 31), after correction for coulomb and phonon interaction terms (ref. 38), and from specific heat measurements below 25°K on sintered material (ref. 39). If we assume that the sintered material is in the cubic state, it is difficult to explain the observation that T_c and $\Delta C/T_c$ are virtually the same as for tetragonal (ref. 39) material. If, on the other hand, we adopt the point of view that all material is in some similar non-cubic configuration near T_c, then the apparent agreement between the densities of states inferred from susceptibility and specific-heat measurements cannot be reconciled with the model.

---

* W. Rehwald, to be published. The thermometers used in the acoustic and specific heat measurements have been checked directly against each other, and found to differ by less than 1°K over the entire range of interest.

** Domain formation might, however, be responsible for the observation of a specific heat (quasi) discontinuity, rather than a singularity.

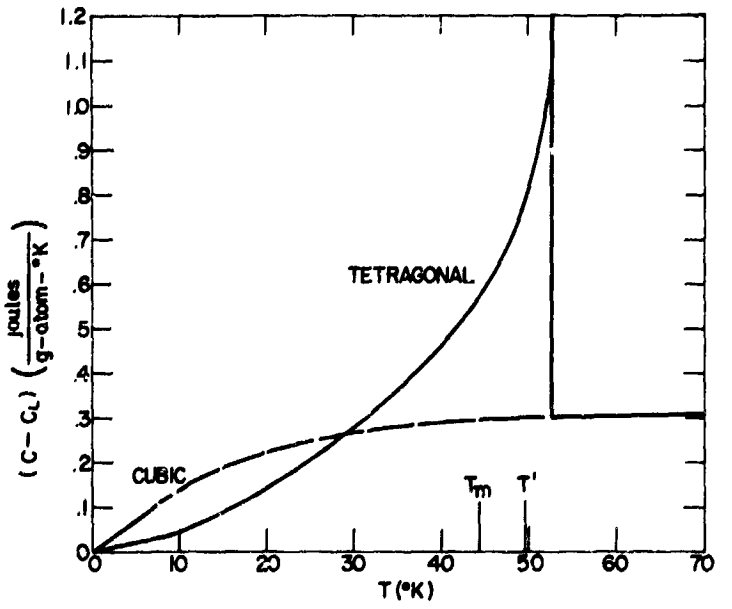

Figure D-2. Calculated excess normal state electronic specific heat of transforming Nb_3Sn based on the model of Cohen et. al. (ref. 23). C_L is the lattice specific heat in the cubic state. T' is the temperature at which $C_{11} = C_{12}$, T_m the observed transformation temperature, by both x-ray and specific heat measurements.

In spite of these problems, the calculated strain near the transformation and the temperature dependence of the strain are in good agreement with x-ray data. Using the value of $N_o(1-\alpha)U^2 = 7.86 \times 10^{12}$ dyne/cm^2 from sound velocity measurements, the deformation potential is found to be U = 4.1eV. From the result $\varepsilon(0°K) = -2\kappa T_o / F_o U$ we obtain the tetragonality $\sigma = a/c-1 = 0.0063$, in remarkable agreement with the x-ray value, $\sigma = 0.0062$.

APPENDIX E*

EFFECT OF UNIAXIAL STRESS ON THE SUPERCONDUCTING TRANSITION TEMPERATURE OF MONOCRYSTALLINE Nb_3Sn

J. P. McEvoy

A. INTRODUCTION

Recent work has shown that many normal-state properties of Nb_3Sn and other β-tungsten superconductors can be explained on the basis of a simple density of states model (refs. 23,40). These include the temperature dependencies of the electrical resistivity, paramagnetic susceptibility, and the elastic constants. In addition the model relates the tetragonal transition to observed properties of the cubic phase of Nb_3Sn-particularly the temperature at which the tetragonal transition occurs, T_m, as well as the magnitude and sign of the tetragonal distortion (refs. 40,1). The success of the model in both the cubic and tetragonal forms of the normal state of Nb_3Sn as well as V_3Si suggests that it may be applicable to the superconducting state as well. The present paper compares experimental results for the shift in the superconducting transition (T_c) under uniaxial stress to the predictions of the density of states model.

Measurements of the superconducting transition temperature have been made as a function of uniaxial stress, τ, along the (100) direction on a single crystal of Nb_3Sn that has been previously shown by x-ray analysis to undergo a tetragonal transition at 43°K (ref. 1). Large displacements of the transition temperature are observed. However, the relatively sharp zero-stress transition is broadened considerably under stress, and the results are dependent on the stress applied to the crystal as it is cooled through T_m. A systematic explanation of this hysteresis, as well as the broadening, can be made if it is assumed that: 1) in the tetragonal state the crystal is made up of domains with variable orientation of the "c" axis as well as untransformed (cubic) material in the boundaries between the domain and 2) the distribution and orientation of the domains depends on the applied stress when the crystal cools through T_m.

According to the density of states model, a uniaxial stress on a single crystal of tetragonal Nb_3Sn along the (100) direction should reduce the effective density of states and strongly depress the superconducting transition temperature (ref. 41). A preliminary calculation,

* To be published - Proceedings of Conference on Science of Superconductivity, Stanford, Cal., 1969.

based on physical parameters determined in the normal cubic state, predicts that for Nb_3Sn

$$\frac{\partial \log T_c}{\partial \tau} = -2 \times 10^{-4} \text{ at.}^{-1}$$

This result is of the order to 2000 times larger than that observed in pure transition metals such as Nb (ref. 42), and its verification should provide a crucial test of the theory. Although the broadening of the transition, as well as the hysteresis, complicates the interpretation of the present experiment, if the assumption is made that the largest shift observed corresponds to tetragonal domains properly oriented ("c" axis along the (100) direction) one obtains for the stress dependence of T_c the value

$$\frac{\partial \log T_c}{\partial \tau} = -0.5 \times 10^{-4} \text{ at.}^{-1}$$

In view of the small domains in our sample this discrepancy of only a factor of four is very persuasive. We feel that when proximity effects between domains and domain walls are properly taken into account this agreement will be much improved.

B. APPARATUS

The basic experimental problem was to determine the transition temperature of a specimen which is 4 mm in height and 10 mm^2 in area while squeezing it on two flat faces. The specimen was mechanically polished, nickel-plated and indium-soldered between 0.001 in. copper foils before being inserted between two polished-pyrex rods which transmit the applied stress. The copper foils are soldered to a small copper block which is in thermal contact with a calibrated germanium resistance thermometer and a 500-ohm manganian heater. A 0.02 in. mylar sheet was insterted between the sample and the pyrex blocks to aid in obtaining uniform pressure. The transition temperature was measured by recording the inductance of a flat coil made up of 1200 turns of #50 wire surrounding the specimen. The inductance of the coil was measured by an Anderson inductance bridge operated at 2000 Hz. At the superconducting transition the inductance change was of the order of 7%. A schematic of the sample holder is shown in Fig. E-1.

Initially, point measurements were made as the temperature was varied through the superconducting transition. A typical set of data points shown in Fig. E-2 required three to four hours to complete. Since it became apparent that the transition depends not only on the applied

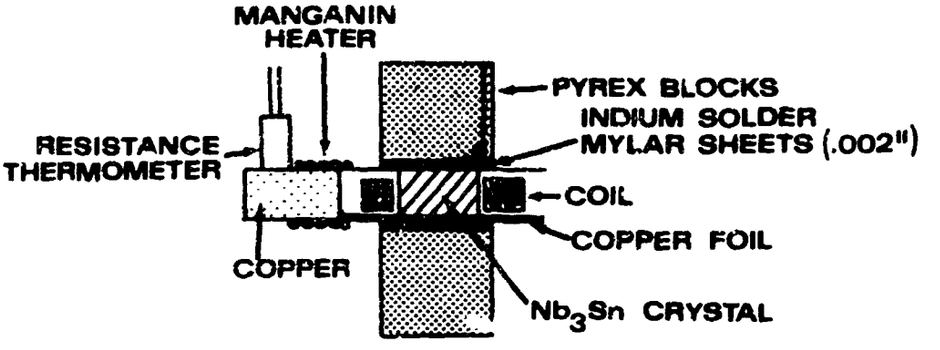

Figure E-1. Sample holder.

stress, but also on the previous history of the specimen, it was advantageous to continuously monitor the inductance change. A PAR HR-8 Lock-In Detector was used to detect the off-balance signal from the bridge and the increase change directly recorded on an x-y recorder against a voltage proportional to the temperature. A block diagram of the system is shown in Fig. E-3.

The applied stress was generated by a screw-advance device which transmits the force through a steel wire to the pyrex blocks. A spring gauge calibrated in 0.2 lb steps (0-100 lbs) was used to measure the applied force. For the area of the crystal the maximum stress was 400 atm. (1 lb $\approx$ 4 atm.). These components are shown in Fig. E-4. The sample was isolated from the bath by a vacuum can sealed by a copper-to-copper cone-and-socket joint sealed with silicone vacuum grease. All leads were heat sinked to 4.2°K as shown in Fig. E-5. Temperature control at 18°K with a resolution of one millidegree was realized with a partial pressure of two microns as measured at room-temperature.

C. EXPERIMENTAL RESULTS

Perhaps the clearest experimental results are those taken on a sample cooled through T_m under zero-applied stress as shown in Fig. E-6. As shown in the figure, different parts of the sample have different sensitivity to the applied stress. The existence of at least two-tetragonal orientations in the cubic single crystal as well as the possibility of untransformed material between the domains can account for the effective increase of the transition width under stress. From the theory (ref. 41) we expect the shift in T_c to be a maximum for that portion of the specimen which has the lowest T_c initially (i.e., aligned domains) and a minimum for the portion of the crystal with the highest

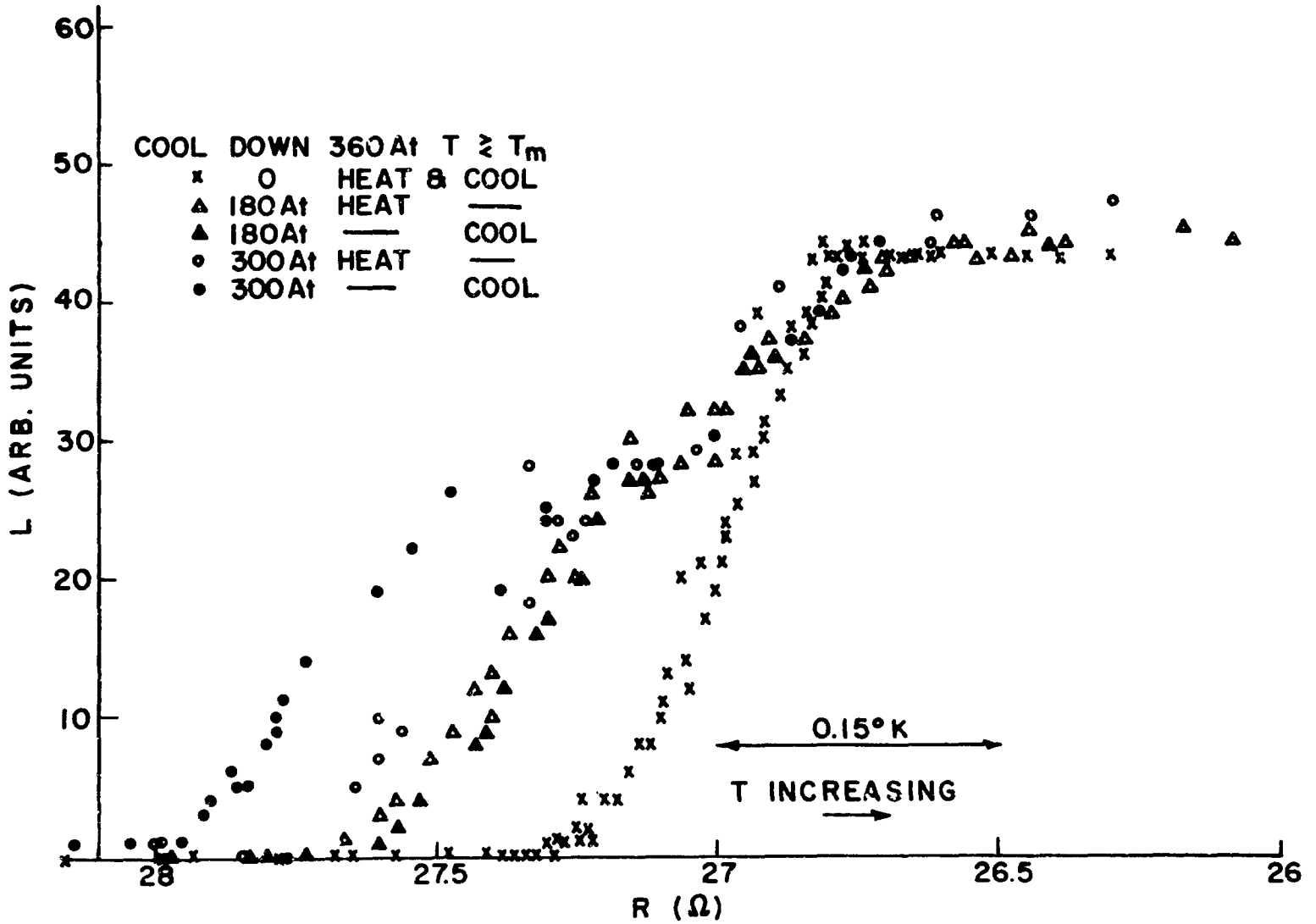

Figure E.-2. Point measurements of inductance change at superconducting transition. The temperature increases to the right.

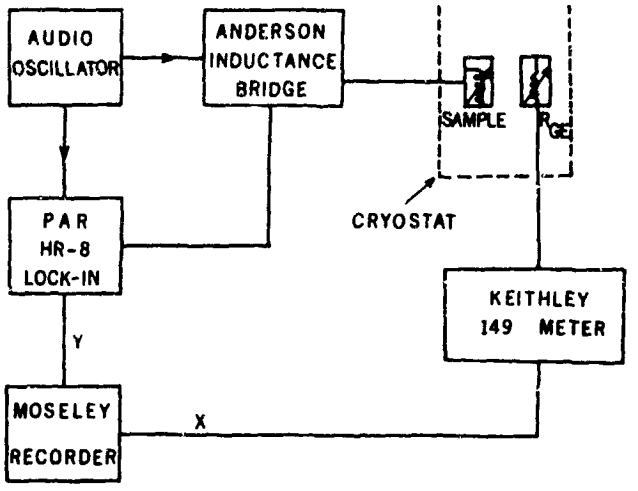

Figure E-3. Block diagram of continuous method for monitoring inductance change.

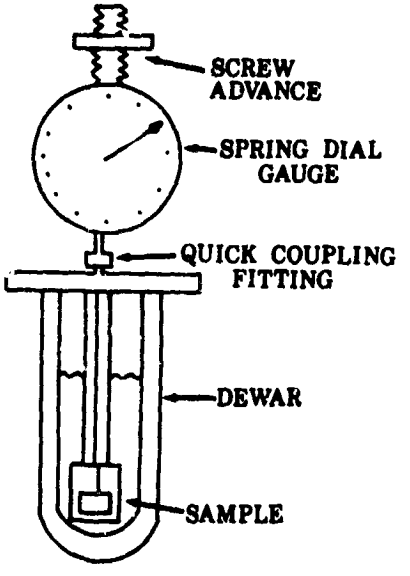

Figure E-4. Stress application and measurement.

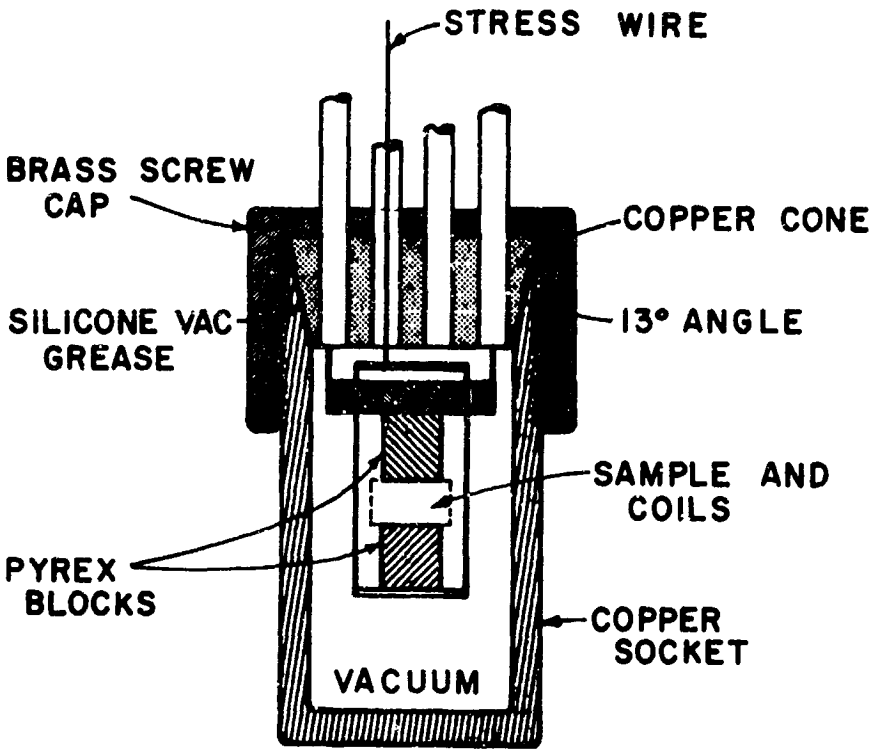

Figure E-5. Detail of vacuum can, thermal sink, and stress application.

T_c (unaligned domains or possibly cubic material). In Fig. E-6 three values of $\frac{\partial T_c}{\partial \tau}$ are shown which differ by as much as an order of magnitude. The maximum shift has been taken to represent the effect of an applied stress on material whose "c" axis is oriented in the (100) direction, and it is this value that has been compared to the theoretical prediction of the density of states model. It is interesting to note that results similar to Fig. E-6 were obtained by Weger et.al. on V_3Si (ref. 43).

A second experiment which supports the above interpretation involves heating the specimen above the temperature T_m under applied stress. It is expected from the previous discussions and simple thermodynamic arguments that the domain distribution and orientation, as

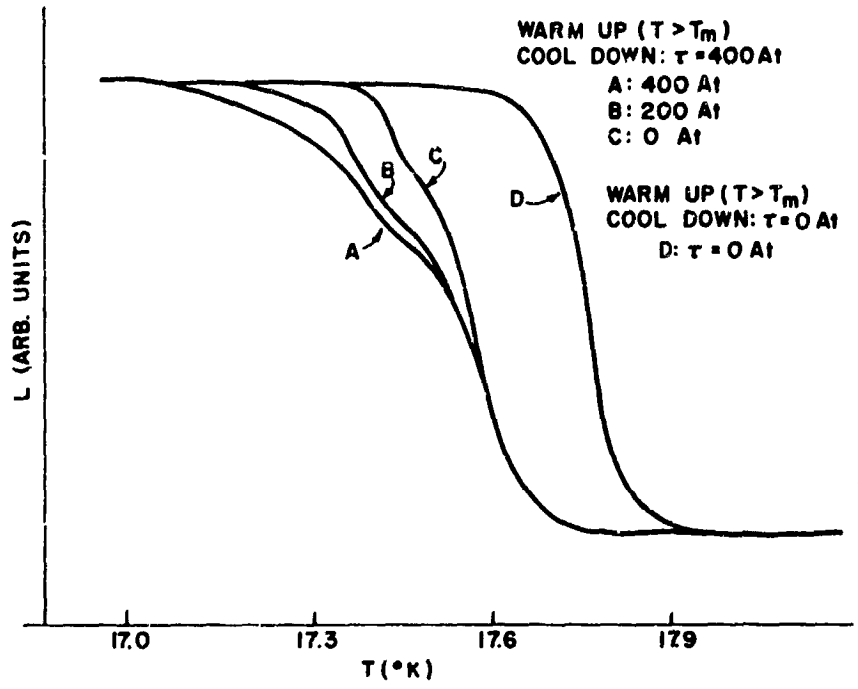

Figure E-6. Superconducting transition with applied uniaxial stress. Sample cooled through T_m in the absence of stress-stress applied at $T \gtrsim 18°K$.

well as the amount of untransformed material would be dependent on the applied stress at T_m, and hence a shift in the zero stress superconducting transition would result. This second experiment is shown in Fig. E-7. The sample was heated to approximately 100°K and the applied stress was increased to 400 atm. After cooling through T_m, plots of the superconducting transition were taken as the stress was reduced from 400 atm. (curve A) to 200 atm. (curve B) and then to zero (curve C). These results were similar to those shown in Fig. E-6 in that only a portion of the crystal was affected by the changing stress. A striking difference in this experiment is the shift in the zero stress transition temperature ($\sim 0.25°K$) from that shown in Fig. E-6. This shift is further shown by curve D of Fig. E-7, which was obtained in the same run, by heating the sample and cooling through T_m under zero stress, and which is identical and reproducible within experimental error to the similar curve shown in Fig. E-6. The theoretical work of Cohen (ref. 41) suggests that the more tetragonal the specimen is made the lower the transition temperature, and this view is strikingly confirmed by the results shown in Fig. E-7.

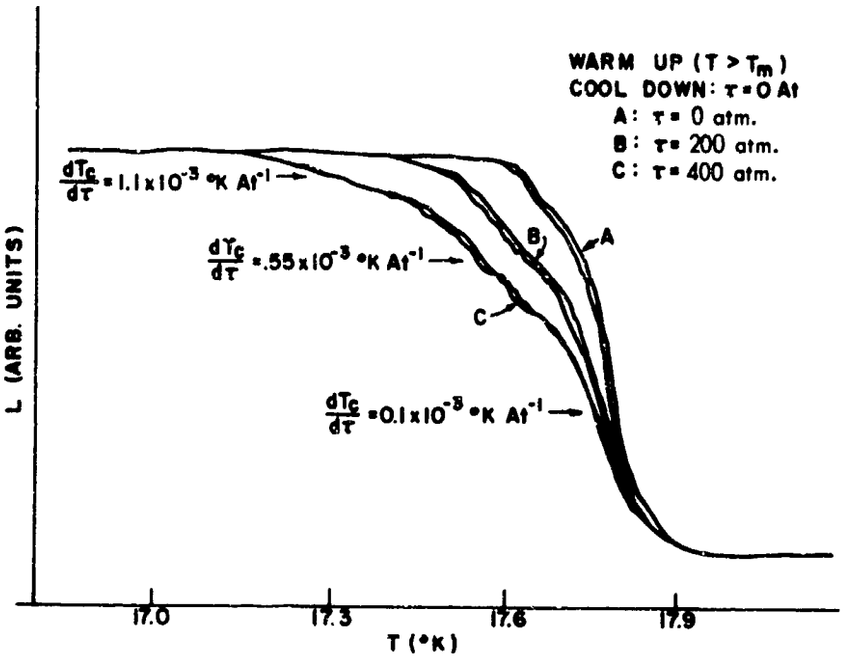

Figure E-7. Superconducting transition with applied uniaxial stress. Sample cooled down from 100°K to T>18°K with τ = 400 atm. curves A, B, and C. Curve D presents data in the same run, where the sample has been cooled through T_m to T≳18°K with τ=0 atm.

The present measurements are only partially understood at present, and require further research. It is clear that stress measurements provided a powerful tool for the investigation of superconducting properties of cubic and tetragonal Nb_3Sn.

APPENDIX F*

SUPERCONDUCTIVITY AND THE DENSITY OF STATES MODEL FOR BETA-TUNGSTEN COMPOUNDS*

R. W. Cohen, G. D. Cody, and L. J. Vieland

A. INTRODUCTION

In the field of superconductivity, it is of prime importance to determine the cause(s) of the observed high-transition temperatures in the β-tungsten compounds and to utilize this knowledge, if possible, to exceed the present maximum T_c of about 21°K. In approaching the problem of the transition temperature, it can be assumed that there is little hope unless an understanding is achieved of the anomalous normal-state properties(ref. 44) of these materials with particular attention to the cubic-tetragonal lattice transformation(refs. 12,1). Recently, attention has been focused on a unique structure in the electronic density of states for these materials as the source of their unusual normal-state properties, and models have been developed which permit the correlation of this structure with high T_c. The Labbé-Friedel-Barišić(refs. 11,45) model used a one-dimensional (3 independent degenerate sub-bands) tight-binding calculation to obtain a density of states in energy N(E) for electrons with d-like character which has singularities at the band edges and a gradually decreasing N(E) as one proceeds away from the band edge. This model can account for the tetragonal transformation in V_3Si and Nb_3Sn. The authors further proposed(ref. 45) that the high T_c's in these materials result from the same source, i.e., the placement of the Fermi level in a high density-of-states region near a band edge. It was later shown(refs. 23,24,40) that singularities in N(E) are not necessary in order to explain the anomalous normal-state properties, but that the idea of independent d-sub bands is essential.

It is possible to explain a wide variety of experimental results in both the high-temperature cubic and low-temperature tetragonal lattice phases using simple rectangular energy bands(refs. 23,24,40) with just

---

* Proceedings of the Third Materials Research Symposium on the Electronic Density of States (National Bureau of Standards, Gaithersburg, Maryland, Nov. 1969), to be published.

three important band-structure parameters obtained from experiment. The results of calculations using this simple model are often in simple analytic form and are surprisingly successful in quantitatively understanding the experimental data. Indeed the success of this model suggests its use in an attempt to calculate T_c from the basic parameters of the normal state.

The usual calculations of superconducting transition temperatures require detailed information about the phonon spectrum, the Fermi surface, and the electron-phonon coupling(ref. 46). Such information is clearly not available for the high T_c β-tungsten superconductors, so that accurate calculations of T_c are not yet possible. However, as noted above, our analyses of the normal-state properties of these materials has led to an experimentally determined set of parameters that can be used in a first-principles calculation of T_c. The primary assumption is that the predominant contribution to the electron-phonon interaction is between d-band particles and acoustic phonons via a simple deformation-potential matrix element. With this assumption, simple analytic expressions for the effective electron-electron coupling constant λ and the transition temperature can be obtained. The quantities λ and T_c can then be computed using parameters determined only from an analysis of the temperature-dependent elastic constants(refs. 23,40). Although such an approach, admittedly, is over simplified, we believe that it contains the essential ingredients of the problem of superconductivity in these materials. It enables us to establish, in a simple way, the relation between high T_c superconductivity and the cubic-tetragonal lattice transformation.

In Part B below, we sketch the important aspects of the electronic band-structure model for β-W superconductors. In the next section we derive expressions for T_c and λ and relate the magnitude of λ to the condition for the existence of the lattice transformation from the high-temperature cubic to the low-temperature tetragonal phase. The effect of the tetragonal transformation on the T_c's of V_3Si and Nb_3Sn is discussed and compared to the results of previous work. In a final section, we enumerate our conclusions.

B. THE MODEL DENSITY OF STATES

We present here the important aspects of the model electronic density of states. This model has been successful in explaining for

Nb_3Sn and V_3Si (where data are available)(refs. 23,24,40,48)* the behavior of the elastic constants and magnetic susceptibility in both the cubic and tetragonal-lattice states, the magnitude of the tetragonal-lattice distortion, the temperature dependence of the electrical resistivity, the acoustic attenuation, and the low-temperature specific heat.

As is usual in the case of transition metals, the relevant electronic-band structure is presumed to consist of a narrow, high density-of-states d band overlapping a wide low density-of-states s-band. The additional assumption is made that the d-band is almost entirely empty (or filled) so that the Fermi level at $T = 0°K$ would occupy a position $E = E_F(0) = k_B T_o \sim 10^{2}°K$, very close to the d-band edge $E = 0$. Over the energy range of interest ($< 10^{3}°K$), the density of electronic states $N(E)$ is regarded as constant both above and below the d-band edge. For the purpose of calculating the superconducting transition temperature, we shall assume that only the d-band carriers contribute to superconductivity, so that we may ignore the s-band entirely. We consider, without loss of generality, the case of a nearly empty band. The density of electronic states for electrons of one spin in the cubic-lattice state, including all interaction effects, is written in the form

$$N(E) = N_o, \quad E > 0$$
$$= 0, \quad E < 0. \qquad \text{(F-2.1)}$$

The density of states in the cubic state is shown in Fig. F-1(a). In order to deal with the effect of homogeneous uniaxial strains ε_{ii} directed along the crystallographic axes i (i = 1,2,3), we follow Labbé and Friedel(ref. 11) and assume that the d-band consists of three independent equal contributions (sub-bands) arising from the chains of the β-tungsten lattice. Because of the assumed independence of the sub-bands, under a uniaxial strain directed along a single-transition metal chain, only the sub-band associated with that chain is perturbed. The shift of the sub-band i under the strain ε_{ii} is given by

$$\delta E_i = U\varepsilon_{ii} \qquad \text{(F-2.2)}$$

*Since Nb_3Al does not display the same kind of anomalous behavior as Nb_3Sn and V_3Si (ref. 47), we do not believe the approach presented here applies to this material. On the other hand, since the magnetic susceptibility of V_3Ga is extremely temperature dependent (ref. 19), we have reason to believe that V_3Ga can be treated by the present theory.

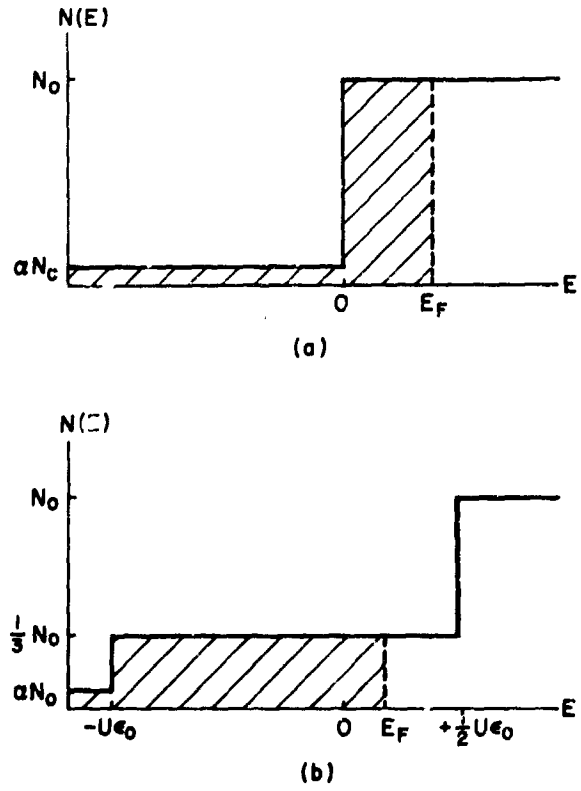

Figure F-1. The density of states configuration in (a) the cubic lattice state and (b) the tetragonal lattice phase with the sense of ε_o corresponding to that for Nb_3Sn. At $T = 0°K$, the Fermi energy $E_F = k_B T_o$ in the cubic state and $E_F = (-U\varepsilon_o + 3k_B T_o)$ in the tetragonal state. The sub-band displacement at $T = 0°K$ $U\varepsilon_o/k_B = 2T_o [1-\exp(-T_o/T_m)]^{-1}$. For Nb_3Sn, $T_o = 80°K$, $T_m = 43°K$, and $U = 4.1$ eV, so that $U\varepsilon_o/k_B = 190°K$ and $\varepsilon_o = 4.0 \times 10^{-3}$.

where U is a deformation potential. Thus, in the tetragonal-lattice state in which the spontaneous strains are $\varepsilon_{11} = -\varepsilon_o(T)$ and $\varepsilon_{22} = \varepsilon_{33} = \frac{1}{2}\varepsilon_o(T)$, the positions of the sub-band edges are

$$\delta E_1 = -U\varepsilon_o(T)$$

$$\delta E_2 = \delta E_3 = \frac{1}{2} U\varepsilon_o(T) \qquad \text{(F-2.3)}$$

The density of states in the tetragonal state is shown in Fig. F-1(b) for the case $\varepsilon_o(T) > 0$ (the case of Nb_3Sn).

The experimental quantities which will concern us in superconductivity calculations are the temperature-dependent elastic constants $C_{11}(T)$ and $C_{12}(T)$ and the sub-band displacement $U\varepsilon_o(T)$. These quantities have been calculated in previous work(refs. 23,40), and we merely state the results here. In the cubic-lattice state, which exists above a lattice-transformation temperature T_m, we have

$$C_{11}(T)-C_{12}(T) = -\frac{2}{3} N_o U^2[1-\exp(-T_o/T(] + A_{11}-A_{12} \qquad \text{(F-2.4a)}$$

$$C_{11}(T) = -\frac{4}{9} N_o U^2[1-\exp(-T_o/T)] + A_{11}, \qquad \text{(F-2.4b)}$$

where A_{11} and A_{12} are temperature-independent core contributions to C_{11} and C_{12}, respectively. The quantities N_oU^2, A_{11}, A_{12} and T_o can be determined by fitting the above expressions to experimental data. As can be seen from Eq. (F-2.4a), the quantity $[C_{11}(T) - C_{12}(T)]$ decreases with decreasing temperature. If the condition

$$\frac{2}{3} N_o U^2 > (A_{11} - A_{12}) \qquad \text{(F-2.5)}$$

is obeyed, the quantity $(C_{11}-C_{12})$, which represents the restoring force against a tetragonal transformation, will vanish at a finite temperature. The lattice then transforms to a stable tetragonal phase, the sense of the transformation (the sign of ε_o) being determined by the higher order elastic constants. The transformation is predicted to be first order, occurring at a temperature T_m which is slightly higher than the temperature at which $(C_{11}-C_{12})$ extrapolates to zero. We shall ignore this small temperature difference (about 2°K for Nb_3Sn [$T_m \approx 43$°K]) and define T_m by setting the right side of Eq. F-2.4a) equal to zero:

$$1-\exp(-T_o/T_m) = 3(A_{11}-A_{12})/2N_oU^2. \qquad \text{(F-2.6)}$$

At temperatures below T_m, the spontaneous tetragonal distortion $\varepsilon_o(T)$ grows rapidly, and the elastic constants C_{ij} are soon restored to their lattice values A_{ij} (refs. 24,48). The values of the sub-band displacement at T = 0°K for $\varepsilon_o > 0$ (Nb_3Sn) and $\varepsilon_o < 0$ (V_3Si) are given by the expressions

$$U\varepsilon_o(0) = 2k_B T_o [1-\exp(-T_o/T_m)]^{-1}, \quad (Nb_3Sn) \tag{F-2.7a}$$

$$= -k_B T_o [1-\exp(-T_o/T_m)]^{-1}. \quad (V_3Si) \tag{F-2.7b}$$

Even for fairly large reduced temperatures $T/T_m \lesssim 0.7$, the results (F-2.7) are good approximations for the spontaneous strains. Thus, given the expressions (F-2.3) for the various sub-band displacements and the result (F-2.7), we can determine the Fermi level position in relation to the various sub-band edges. This is shown in Fig. F-1b. The various energies at T = 0°K are given in the figure caption. It is noteworthy that at sufficiently low temperatures the final density of states is $\frac{1}{3} N_o$ for Nb_3Sn ($\frac{2}{3} N_o$ for V_3Si).

C. CALCULATION OF T_c FOR β-W SUPERCONDUCTORS

1. Formalism and Assumptions

In order to treat superconductivity in these materials, we shall make certain reasonable simplifying assumptions that will allow us to give estimates of T_c from the elastic properties alone and to pinpoint the parameters which control T_c. First, we shall assume that the first order process for virtual phonon exchange is the essential interaction for superconductivity*. We shall also assume that the d-electrons are

---

*If the effective Fermi energy T_o is actually of the order of or smaller than the important phonon energies, it is possible that the first order process may not be sufficiently accurate for strong coupling superconductors (ref. 49). However, it is possible to treat (ref. 50) the effect of higher order processes involving strong attractive interactions whose range in momentum space is greater than the Fermi momentum. It is found that the effect of these processes, in the t matrix approximation, is only to renormalize the pre-exponential factor in the expression for T_c. We shall ignore this effect.

primarily responsible for superconductivity. The large penetration depths(ref. 51) and small coherence lengths* in these materials are justifications for this assumption. We treat each sub-band separately; each sub-band has its own energy-gap parameter and density-of-states function. In the Nambu(ref. 52) formalism, the self energy Σ_i of an electron in sub-band i is

$$\Sigma_i(k) = -\int \frac{d\vec{k}'}{(2\pi)^3} T \sum_{n,j} \tau_3 g_j(k') \tau_3 \sum_{\lambda} |M_{ij}(q,\lambda)|^2 d(q,\lambda) \qquad \text{(F-3.1)}$$

In the above equation, $g_j(k')$ is the temperature dependent propagator for quasi-particles of 4-momentum $k' = (\vec{k}', i\omega')$ in sub-band j, and $d(q,\lambda)$ is the propagator for phonons of 4 momentum $q \equiv (\vec{q},, i\omega - i\omega')$. The matrix element $M_{ij}(q,\lambda)$ is the electron-phonon coupling for transferring a quasi-particle from sub-band i to j using a phonon (q,λ). The τ_i are the Pauli spin matrices (with τ_o the unit matrix), and all frequencies have the discrete values $\omega = \pi T(2n + 1)$ with n integral (we use units where $\hbar = k_B = 1$). We have, temporarily, ignored the Coulomb repulsion. Nambu's ansatz for the self energy is

$$\Sigma_i(k) = i\omega(1-Z_i(k)\tau_o + \chi_i(k)\tau_3 + \phi_i(k)\tau_1. \qquad \text{(F-3.2)}$$

Here $\chi_i(k)/Z_i(k)$ is the contribution of Eq. (F-3.1) to the quasi-particle energy and $\phi_i(k)/Z_i(k)$ is the energy-gap parameter. The quasi-particle Green's function at T_c is given by

$$g_i(k) = \frac{i\omega Z_i(k)\tau_o + \bar{\varepsilon}_i(k)\tau_3 + \phi_i(k)\tau_1}{(i\omega Z_i(k))^2 - \bar{\varepsilon}^2(k)} , \qquad \text{(F-3.3)}$$

where the energy $\bar{\varepsilon}_i(k)$ is written in the form

$$\bar{\varepsilon}_i(k) = \varepsilon(k) + \chi_i(k). \qquad \text{(F-3.4)}$$

In Eq. (F-3.4), $\varepsilon(k)$ is the quasi-particle energy without including renormalization effects, measured from the unrenormalized Fermi energy.

the phonon propagator, we use that of bare phonons of frequency ω_q:

*The coherence length is estimated to be approximately 130 Å. This estimate is arrived at using the penetration depth given in (ref. 51) and the Ginzburg-Landau parameter K = 21.7 (ref. 4).

$$d(q,\lambda) = \frac{2\omega_q}{(i\omega - i\omega')^2 - \omega_q^2} \quad . \tag{F-3.5}$$

In order to evaluate the functions Z, χ and ϕ, we employ the method of Koonce and Cohen(ref. 53), valid for the case where the Fermi energy is larger or of the order of the important phonon energies. We first perform the sum on n' in Eq. (F-3.1) where the functions $Z_j(k')$, $\chi_j(k')$ and $\phi_j(k')$ are considered to be independent of ω'. Performing the sum using the Poisson summation formula and requiring the self-consistent condition that the τ_3 and τ_1 components of $\Sigma_i(k)$ be independent of ω and τ_o component be proportional to ω [16], we find

$$1 - Z_i = \sum_\lambda \int \frac{d\vec{k}'}{(2\pi)^3} \frac{|M_{ij}(q,\lambda)|^2}{Z_j'} \operatorname{sgn} \xi_j' \frac{d}{d\xi_j'} \frac{1}{\omega_q + |\xi_j'|} \tag{F-3.6a}$$

$$\chi_i = - \sum_\lambda \int \frac{d\vec{k}'}{(2\pi)^3} \frac{|M_{ij}(q,\lambda)|^2}{Z_j'} \frac{\operatorname{sgn} \xi_j'}{\omega_q + |\xi_j'|} \tag{F-3.6b}$$

$$\Delta_i = (Z_i)^{-1} \sum_\lambda \int \frac{d\vec{k}'}{(2\pi)^3} \frac{|M_{ij}(q,\lambda)|^2}{Z_j'} \left\{ \frac{\Delta_j'}{\xi_j'} \frac{f(-\xi_j')}{\omega_q' + \xi_j'} - \frac{f(\xi_j')}{\omega_q - \xi_j'} \right\} \quad . \tag{F-3.6c}$$

In Eqs. (F-3.6), $Z_i \equiv Z_i(k)$, $Z_j' \equiv Z_j(k')$, etc., $\Delta_i = \phi_i/Z_i$, $\beta_c = T_c^{-1}$, $f(\xi_j')$ is the Fermi function, and

$$\xi_j = \bar{\epsilon}_j/Z_j = E_j - E_F(T_c) \tag{F-3.7}$$

is the quasi-particle energy; the observed density of states refers to the energies E_j. Thus, the functions χ_i do not appear explicity in Eqs. (F-3.6a) and (F-3.6c) for Z_i and Δ_i, so that for the purposes of calculating T_c, it is not necessary to calculate the χ_i. In deriving Eqs. (F-3.6), we have ignored the effect of real phonons, which are not expected to be important at low temperatures $T_c << \omega_q$. We have also replaced Z_i and χ_i by their T = 0°K values since these quantities do not vary significantly in the temperature range $T \lesssim T_c$.

It is now necessary to make some statement about the matrix element $M_{ij}(q,\lambda)$. We shall employ a deformation-potential matrix element for longitudinal phonons(ref. 15):

$$|M_{ij}(q,\lambda)|^2 = q^2U^2/2\rho\omega_{qL} \text{ for longitudinal phonons}$$
$$= 0 \text{ for transverse phonons,} \qquad \text{(F-3.8)}$$

where U is the deformation potential defined in Part B on page 69 and ρ is the atomic-mass density. The actual matrix element is undoubtedly reduced by screening(ref. 15), but Umklapp processes and a non-spherical Fermi surface may bring in transverse phonons(ref. 15) and thereby increase the effective interaction. Therefore, the errors involved in using Eq. (F-3.8) tend to cancel and may permit Eq. (F-3.8) to give us a rough picture of magnitude of the interaction. We shall also assume that this matrix element applies to both inter and intra-sub-band transitions, a crucial assumption in considering the effect of the lattice transformation on T_c. Next, for ω_{qL} we employ a Debye spectrum:

$$\omega_{qL} = s_L q, \qquad \text{(F-3.9)}$$

where s_L is the longitudinal sound velocity which, at low temperatures, is given approximately by(refs. 24, 8):

$$s_L = (A_{11}/\rho)^{\frac{1}{2}} \qquad \text{(F3-10)}$$

Finally, we replace the denominator $D = (\omega_q + |\xi_j'|)^{-1}$ in Eqs. (F-3.6) by the BSC-like model

$$D = (\omega_{qL})^{-1} \text{ for } |\xi_j'| < \theta_D$$
$$= 0 \qquad \text{for } |\xi_j'| > \theta_D, \qquad \text{(F-3.11)}$$

where θ_D is the Debye temperature. The choice of θ_D as a cut-off energy is reasonable since θ_D is approximately equal to the average longitudinal phonon energy. Using Eqs. (F-3.8) to (F-3.11) in Eqs. (F-3.6a) and (F-3.6c) we find that Z_i and Δ_i are constant and are given by

$$Z_i = 1 + \tfrac{1}{2}(U^2/A_{11}) \int d\xi_j' \, N_b(\xi_j')\left[\delta(\xi_j' - \theta_D) + \delta(\xi_j' + \theta_D)\right] \qquad \text{(F-3.12a)}$$

$$\Delta_i = (\Delta_j U^2/A_{11}Z_i) \int_{|\xi_j'| < \theta_D} d\xi_j' \, N_b(\xi_j')(1/2\xi_j') \tanh \tfrac{1}{2} \beta_c \xi_j'. \quad \text{(F-3.12b)}$$

Here $N_b(\xi_j)$ is the "bare" density of states of sub-band j. The renormalized density of states $N(\xi_j)$, which was given in Part B above is related to $N_b(\xi_j)$ through the formula

$$N(\xi_j) = Z_j N_b(\xi_j). \quad \text{(F-3.13)}$$

2. T_c in the Cubic State

We first solve Eqs. (F-3.12) for the cubic state which will exist at the lowest temperature if the inequality (F-2.5) does not hold. Here the Δ_i and $Z_i = Z$ are the same for all sub-bands, and we easily obtain

$$Z = 1 + \tfrac{1}{2} \lambda \quad \text{(F-3.14)}$$

$$T_c = 1.13 \, (\theta_D T_o)^{\frac{1}{2}} \exp \left\{ - \frac{1 + \frac{1}{2}\lambda}{\lambda - \mu^*} \right\}, \quad \text{(F-3.15)}$$

where the effective electron-phonon coupling constant λ is given by

$$\lambda(1 + \tfrac{1}{2}\lambda) = N_o U^2/A_{11}. \quad \text{(F-3.16)}$$

In Eq. (F-3.15), we have included the term μ^*, which represents the Coulomb repulsion(ref. 54). In deriving Eq. (F-3.15) for T_c, we have assumed T_c is sufficiently low so that $E_F(T_c) \tilde{=} T_o >> T_c$.

Equations (F-3.14) and (F-3.15) are our equations for Z and T_c for high T_c β-W superconductors which are analogous to those of McMillan (ref. 55) for ordinary superconductors. The reduction of (Z-1) by a factor of two from the expression of McMillan results from the fact that the band edge cuts off phonon interactions at energies below the Fermi level. The factor $T_o^{\frac{1}{2}}$ in the pre-exponential in Eq. (F-3.15) results for the same reason. Note the predicted isotope effect $T_c \propto M^{-\frac{1}{4}}$ instead of the usual $M^{-\frac{1}{2}}$ dependence. Equations (F-3.14) and (F-3.15) would be of little use were it not for the fact that we can use Eq.

(F-3.16) to estimate λ from quantities determined from the cubic state elastic constants (Part B, page 69). For example, if we apply our equations to transforming Nb_3Sn and V_3Si, we find, respectively*, $\lambda = 0.92$, $T_c = 28°K$ and $\lambda = 0.72$, $T_c = 21°K$. Our values of λ, calculated from Eq. (F-3.16) are quite close to those given by McMillan(ref. 55) from his equation for T_c. However, because of the difference between our Eq. (F-3.15) for T_c and that of McMillan, there is only an approximate relation between them. Our calculated value of T_c for V_3Si is close to the observed value of 17°K, whereas the computed value is about 10°K too large for Nb_3Sn. The significance of this discrepancy will be discussed below when we calculate T_c for the tetragonal lattice configuration.

3. Relation of λ to the Tetragonal Transformation

Using the foregoing results, we can easily relate the magnitude of the electron-phonon coupling λ to the condition for the existence of the cubic-tetragonal lattice transformation. From Eqs. (F-2.5) and (F-3.16), and noting the empirical relation* $A_{12} \tilde{=} \frac{1}{3} A_{11}$ which holds for Nb_3Sn and V_3Si, we have immediately,

$$\lambda \gtrsim 0.7 \qquad \text{(F-3.17)}$$

for a tetragonal transformation. Equation (F-3.17) illustrates the intimate relation between high T_c's and the lattice transformation; large λ's favor high T_c's but lead to the lattice instabilities.

4. T_c in the Tetragonal State

Let us now solve Eqs. (F-3.12) for the tetragonal lattice state of V_3Si and Nb_3Sn and compare the results with those for the cubic state.

---

*For transforming Nb_3Sn, we use the value $\theta_D = 300°K$ (ref. 4). The parameters obtained from elastic constant measurements (refs. 24, 48) are $T_o = 80°K$, and in units of 10^{12} erg-cm^{-3}, $N_oU^2 = 7.86$, $A_{11} = 2.94$ and $A_{12} = 0.84$. For transforming V_3Si, we use the values $\theta_D = 500°K$, $T_o = 75°K$, and, in units of 10^{12} erg-cm^{-3}, $N_oU^2 = 6.33$, $A_{11} = 3.22$ and $A_{12} = 1.05$. These parameters were obtained from an analysis of the elastic constant data of (ref. 5). For both materials, we use the value $\mu^* = 0.13$ for the Coulomb pseudo-potential (ref. 55).

For Nb_3Sn the relevant density of states configuration is shown in Fig. F-1b. For our purposes, the T = 0°K values of the various energies shown in the figure are sufficiently accurate. We find once again the result

$$Z = 1 + \frac{1}{2}\lambda$$

for all sub-bands. However, there are now two values of the energy gap, i.e., the gap Δ_1 for the single widened sub-band and the gap Δ_2 for the two narrowed sub-bands. Equation (F-3.12b) is then actually two coupled homogeneous algebraic equations for Δ_1 and Δ_2. The transition temperature is obtained by setting the determinant of the coefficients equal to zero. If the energy difference $(\frac{1}{2}U\varepsilon_o - E_F) = 3T_o(\exp(T_o/T_m)-1)^{-1} >> T_c$, we find

$$T_c = 1.13\ (\theta_D/3T_o)^{\frac{1}{2}}\ \theta_D[\exp(T_o/T_m)-1]\exp\left\{-\frac{1+\frac{1}{2}\lambda}{\frac{1}{3}(\lambda-\mu^*)}\right\}. \qquad \text{(F-3.18)}$$

The factor $\frac{1}{3}$ occurs in the denominator of the argument of the exponential in Eq. (F-3.18) because the final density of states in the tetragonal state of Nb_3Sn is reduced to $\frac{1}{3}$ of the cubic state value. Note the large predicted isotope effect in the tetragonal state $T_c \propto M^{-\frac{3}{4}}$. Substituting our values of the parameters for Nb_3Sn, we compute $T_c = 8°K$, and the energy-gap parameters Δ_1 and Δ_2 differ by less than 1%. A similar calculation for V_3Si yields $T_c = 20°K$, close to the cubic state value. The small difference in the cubic and tetragonal T_c's for V_3Si results primarily from its low(ref. 12) $T_m \tilde{=} 22°K$; at T_c, the effective density of states at the Fermi level is still large, so that the interaction extends over roughly the same energy range in all sub-bands as it would if the material were cubic.

Thus, we have the result that the approximations we have made work well for V_3Si; we calculate T_c's close to the observed value and predict little difference between the cubic and tetragonal T_c's. On the other hand, Nb_3Sn is predicted to have a high T_c (28°K) in the cubic state and a relatively low one (8°K) in the tetragonal state. This is surprising because we would expect our approximations to be either uniformly good or uniformly bad for these materials. We believe that we have considerably underestimated the tetragonal T_c for Nb_3Sn. Evidence for this exists in the low temperature susceptibility data which indicates a fall-off of the final density of states to about 0.5 N_o rather than $\frac{1}{3}$ N_o. The value 0.5 N_o is very close to the value predicted from the band model if we employ the effective mass approximation(ref. 48)

($N(E) \propto E^{\frac{1}{2}}$) rather than rectangular energy bands. The final density of states is critical in determining T_c, since it occurs in the exponential, so that close agreement with the observed value of T_c is obtained if we employ this modification to our model. On the other hand, we believe that the figure of 28°K for cubic Nb_3Sn may actually represent the T_c that this compound would have if it did not first undergo a lattice transformation. There is some experimental(ref. 56) and other theoretical(ref. 57) evidence that Nb_3Sn ought to have a much higher T_c than the observed 18°K. If we are correct, it is then a simple matter to show by a calculation similar to that of McMillan(ref. 55) that the maximum T_c occurs for $\lambda \approx 4$ and is 45°K for Nb_3Sn and 40°K for V_3Si. Thus, in contrast to McMillan, we find that Nb_3Sn has an intrinsically higher T_c than that of V_3Si. Of course, our result rests on the assumptions we have made in obtaining our equations for T_c and λ; of particular importance is the assumption of equal intra and inter-sub-band coupling in our model. Labbé, Barišić, and Friedel(ref. 45) did not calculate the difference in T_c in the two lattice states but felt that the difference between them ought to be small because T_c in the cubic phase varies only slowly with N_o in their model. The experimental situation with regard to the effect of the lattice transformation on T_c is not clear. A Nb_3Sn crystal* which showed lattice softening(ref. 18) but did not transform according to x-ray measurements had a T_c only 0.2°K larger than that for a transforming crystal(ref. 1). However, analysis of the elastic constants** to obtain the quantities in Eqs. (F-3.15) and (F-3.16) yields the smaller computed values of $\lambda = 0.78$ and $T_c = 20$°K, so that the failure to realize a significantly higher T_c in this particular non-transforming crystal is understood. The situation is further complicated by the fact that the tetragonal crystals of Nb_3Sn are heavily twinned (refs. 58,59), and the effect of the attendant internal strains is not known.

D. CONCLUSIONS

The results presented here and in previous papers show that a simple electronic density of states model can account for many properties

*This crystal was found to contain 1.5% interstitial H.

**For this crystal, analysis of the elastic constants reported in (ref. 18) yields $T_o = 100$°K, and, in units of 10^{12} erg-cm^{-3}, $N_oU^2 = 6.46$, $A_{11} = 2.96$, and $A_{12} = 0.90$.

of the normal tetragonal and cubic phases and the high T_c's of these materials. Our approach to the density of states differs only in detail from that of Labbé-Friedel-Barišić(refs. 11,45), although our model gives better numerical agreement with most of the experimental data(ref. 23). The present treatment of superconductivity differs considerably from that of other authors(refs. 45,55,57) in that (a) we specifically treat the effect of the tetragonal transformation and (b) attempt to estimate the magnitude of the electron-phonon interaction from the elastic properties of the material.

Despite the success of the model, certain important questions remain to be answered. First, and perhaps most important, is it true that transforming Nb_3Sn would have a T_c of substantially higher than 18°K were it not for the lattice transformation? This question can only be answered experimentally. The question which is most relevant to this conference is the relation of the model density of states to the actual band structure in the vicinity of the Fermi surface. This question is very difficult to answer because ordinary band calculations overlook structure on the energy scale that we have considered. If our success in explaining the properties of these materials has a physical basis, then the essential features of our model must result from a fundamental treatment of the β-W compounds. The early pioneering calculation of Mattheiss(ref. 33) and the insights of Weger(ref. 60) and the Orsay group(refs. 11,45) provide the foundation for such a study. The technical and theoretical importance of understanding the source of high T_c's should provide sufficient motivation.

ACKNOWLEDGEMENTS

The authors acknowledge Drs. J. Gittleman, G. Webb, and A. Rothwarf for many helpful discussions.

APPENDIX G*

THE SYSTEM $Nb_3Sn_{1-x}Sb_x$ AND THE DENSITY OF STATES MODEL FOR Nb_3Sn

L. J. Vieland

A. INTRODUCTION

Labbé and Friedel have shown(ref. 11) that much of the anomalous behavior of the high T_c, β-tungsten superconductors can be understood in terms of a band model comprising two main features; a strongly energy-dependent density of states within a few hundred degrees of the Fermi level at 0°K, and a threefold degeneracy of the relevant d-band which is removed by a low-temperature distortion from cubic to tetragonal symmetry. Cohen et. al.(ref. 23) proposed a particularly simple density of states representation (square band) which leads to striking agreement between theory and experiment for most of the properties of these unusual metals(refs. 23,40). However, the model is phenomenological, and although some experimental observations remain unexplained (ref. 40), its limitations are not clearly defined. The necessary fine structure in the density of states is not derivable from band structure calculations, which are made on a relatively coarse energy scale. Similarly, direct observation of this structure by a technique such as soft x-ray emission appears to be out of the question. One simple line of attack which remains open is the classic method of effecting small changes in electron concentration by means of doping, and correlating these changes with suitable physical properties. The major premise of the method is the validity of the rigid band approximation.

A convenient system to look at is the Nb_3Sn-Nb_3Sb pseudo-binary, about which some useful information is already at hand(refs. 61-63). The replacement of Sn by neighboring Sb in the periodic table should introduce minimum perturbations other than the desired change in electron concentration.

---

*To be published, J. Phys. Chem. Sol., 1970.

B. THEORY

The parameters of the square-band density of states model (ignoring the small overlapping s-band contribution) are No, U_2 and T_o, where N_o is the d-band density of states in the cubic state, U_2 is the deformation potential relating the shift in the band edge with uniaxial strain along the <100> direction, and T_o, which is the distance from the Fermi level at 0°K to the near band edge, is the quantity adjustable by alloying. The number of electrons (holes) in the nearly empty (full) band for $Nb_3Sn_{1-x}Sb_x$ alloys is

$$N_o kT_o' = N_o kT_o \pm x\Delta v/4$$

where Δv, the difference in valence between Sb and Sn, is probably, but not necessarily(ref. 64), + 1. Since $N_o kT_o$ is about .04 states/atom for Nb_3Sn(ref. 40), and since the d-band carriers are thought to be holes, the model suggests a maximum solubility of $x \approx .16$.

T_o is a characteristic temperature which enters exponentially into the temperature dependence of many physical properties of Nb_3Sn. A particularly useful one for our purpose is the martensitic (cubic → tetragonal) transformation temperature T_m. According to the model, T_m is [nearly] the temperature at which the negative contributions of the d-band carriers to the free-energy difference between the cubic and tetragonal states just balances the contribution from all other sources to the binding energy. This is given by ref. 23 where $A_{1i} - A_{12}$ is

$$\frac{1}{3}N_o U_2^2 \left(1-e^{-T_o/T_m}\right) = A_{11} - A_{12}.$$

where $A_{11} - A_{12}$ is the lattice contribution to the elastic constant for the shear strain carrying the lattice from cubic to tetragonal. Since for Nb_3Sn $T_o/T_m \sim 1.6$(ref. 40), we have

$$\delta T_m = \pm \frac{x}{4N_o k(1.6)} \sim 300x \text{ °K},$$

so that changes in T_m accompanying small additions of Sb should be readily detected.

C. EXPERIMENTAL

Samples were prepared by cold pressing - 325 mesh powders at 30 t.s.i. into 1/4-in. thick by 1/2-in. diameter pellets, and sintering in a nearly static helium atmosphere for 16 hours. A series having x = 0, .05, .10, .15 was made at 1250°C, and one sample with x = .20 was prepared at 1100°C. The latter showed some unreacted Nb and Sn (Sb) by anodization and microscopic examination(ref. 65) in addition to the usual (∿ 2%) NbO and other unidentified phases, while x-ray powder patterns showed only β-W phases. Lattice constants were determined with CuK_α radiation on a $36/\pi$ cm camera by the extrapolation method of Cohen, with a precision of ± .0002 Å. The low temperature x-ray work was carried out in a liquid-helium cryostat fitted with Be windows, using ordinary diffractometer and detector techniques. Powdered samples were sprinkled on to a lightly greased flat-copper stage suspended from the He bath by a stainless-steel tube. Temperatures were measured with a Au-2.1% Co versus Cu thermocouple with the cold junction attached to the He bath, allowing the temperature to be read to ± 0.1°K with a portable potentimeter. A Pt resistance thermometer was used to calibrate the thermocouple. Superconducting transition temperatures were determined inductively.

D. RESULTS

Both T_c and a_o are found to decrease linearly with temperature, the data being in good agreement with that of earlier work. In Fig. G-1, the circles represent transition midpoints, the bars transition extremities. The sample designated by the triangle (x = .2) showed two β-W phases, with a_o = 5.277 for the minor phase, estimated to be 10 to 20% of the sample volume from x-ray intensities. A second phase was also seen in the T_c measurement, with a broad transition between 7.5° and 10°K accounting for 20% of the total inductance change. Extrapolating the lattice constant data gives x = .56 for the minor phase. A materials balance then gives 18% for the proportion of this phase. The high T_c phase showed a transition much like that of the other doped samples but with a small tail (5%) extending up to 17.4°K. Annealing for 66 hr at 980°C resulted in no change in either T_c or the diffraction pattern for this specimen. A miscibility gap extending from .3 < x < . 7 at 1200°C has been reported(ref. 62), so that this unusual behavior appears to be strongly temperature dependent.

Transformation temperatures are shown at the top of Fig. G-1. The squares represent the temperature at which an observable shift in position of the intensity maximum was noted, while the rectangles indicate

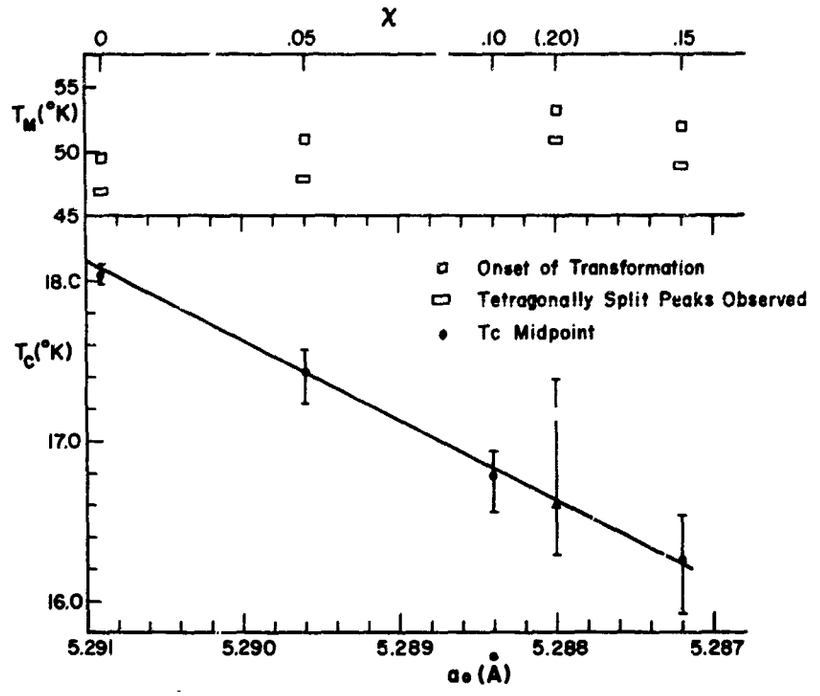

Figure G-1. T_c and T_m for $Nb_3Sn_{1-x}Sb_x$. Compositions of samples of various lattice constants are shown at the top. The sample designated by Δ had a second β-W phase, not shown, richer in Sb.

the temperature at which the transformation is evident in an unambiguous way (appreciable line splitting). Within the framework of the theory discussed above, T_m is found to be invariant.

The course of the transformation is shown in Fig. G-2 for the two samples of extreme lattice constant, x = 0 and x = .15. The {400} peak proved to be the simplest to study, by virtue of its reasonable intensity, absence of degeneracy in $\Sigma(h^2 + k^2 + \ell^2)$, and sufficient resolution of the tetragonal splitting. As seen in the figure, there is a decrease in resolution of the K_{α_1}-K_{α_2} lines above T_m, and a reduction of intensity of the main (K_{α_1}) peak. Presumably this is due to an increase in thermal diffuse scattering and/or fluctuations accompanying the vanishing of the elastic constant C_{11}-C_{12} at T_m. For both samples,

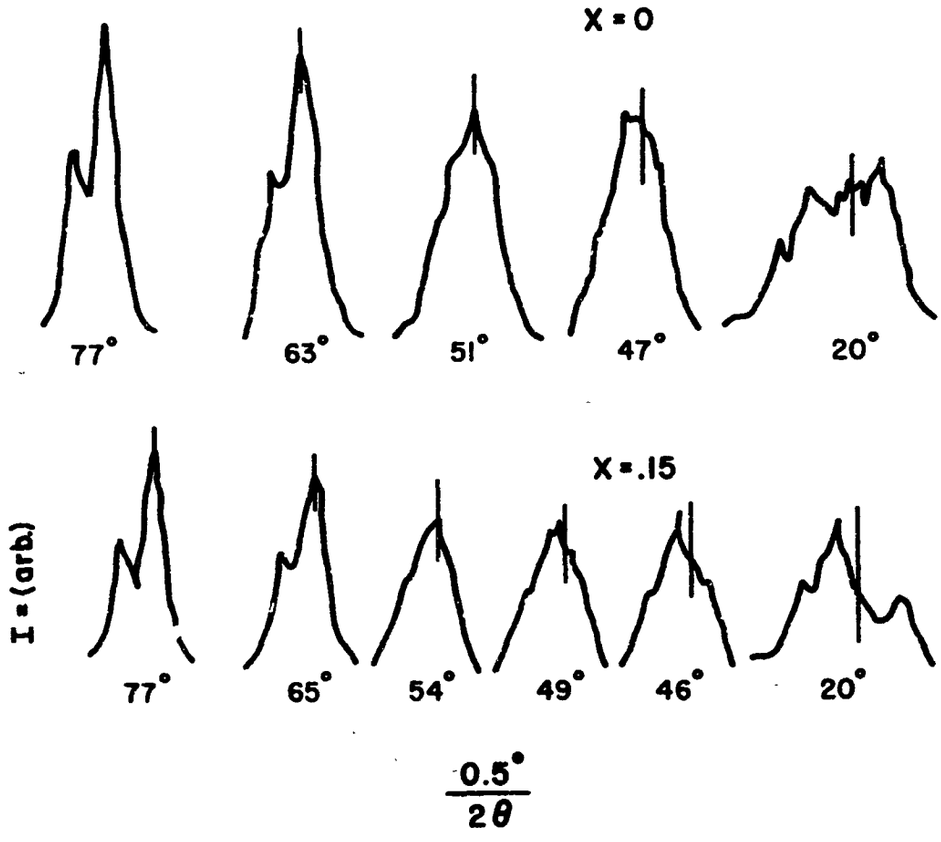

Figure G-2. {400} x-ray intensities as a function of temperature for the two extremal compositions. The vertical lines mark the position of the K_{α_1} peak maximum in the cubic state.

the onset of the transformation is marked by a shift of the peak maximum to higher angle. The d spacing in the tetragonal state is given by

$$d = d_{\text{cubic}} \left\{1 + \left(\frac{\varepsilon}{2}\right) \frac{h^2 + k^2 - 2\ell^2}{h^2 + k^2 + \ell^2}\right\},$$

where $\varepsilon = \frac{2}{3}(a/c - 1)$. For the {400} set we have $d_2 = d_c\,(1 + \varepsilon/2)$ and

$d_1 = d_c\ (1 - \varepsilon)$, where the subscripts 1, 2 indicate the relative intensities. For positive ε the shift near T_m should be to lower angle. At low temperatures, where $\varepsilon > 2 \times 10^{-3}$, four peaks should be observed (two for each wavelength radiation), with the main peak double the intensity of any other peak and the splitting $\delta\theta(d_2) = \frac{1}{2}\,\delta\theta(d_1)$. For x = 0 we find $\varepsilon = +(3.5 \pm .5) \times 10^{-3}$, although the intensity distribution, which was found to be weakly dependent on sample mounting, is not strictly consistent with a simple tetragonal splitting. Other workers have reported tetragonalities between 2.4×10^{-3} and 4.1×10^{-3}(refs. 1,66,67). The shift to higher angles near T_m could be the result of a decrease in volume of the unit cell, but analysis of the shift in centroid for several peaks reveals no consistent pattern. The transformation is volumeless, within experimental error.

For the x = .15 sample we find the remarkable result that the splitting is of the same magnitude, but of opposite sign, with $\varepsilon = -(3.2 \pm .5) \times 10^{-3}$. In this case the peak intensities are entirely consistent with the splitting.

Figure G-3 shows the {400} and {440} diffraction patterns for the single-phase samples at 20°K. The {440} peaks arise from planes having $d_2 = d_c\ (1 - \varepsilon/4)$ and $d_1 = d_c\ (1 + \varepsilon/2)$, the increased dispersion at higher angle leading to a $\delta\theta$ virtually the same as for the {400} reflections. The x = .05 sample appears to have both ε^+ and ε^- components, while for x = .10, although the intensities are not well behaved, the splitting appears to be similar to the x = .15 sample. Again for the latter, the {440} reflection allows us to assert that for this sample there is essentially no material remaining which is either cubic, or transformed but of opposite sign.

E. DISCUSSION

It is clear that the relationship between T_o and x predicted on the basis of the rigid-band model is not borne out by the data. The invariance of T_m suggests that in order to approach the data from the point of view of the density of states model, the band parameters should be taken as unaffected by the addition of Sb. The question of why the band filling (T_o) is not variable can be set aside, and the interesting implications of the change of sign of the tetragonality examined in terms of a fixed band.

The sign and magnitude of the spontaneous strain below T_m are given by the usual condition of minimum free energy. Near T_m, it is useful to write the free energy difference between the cubic and tetragonal

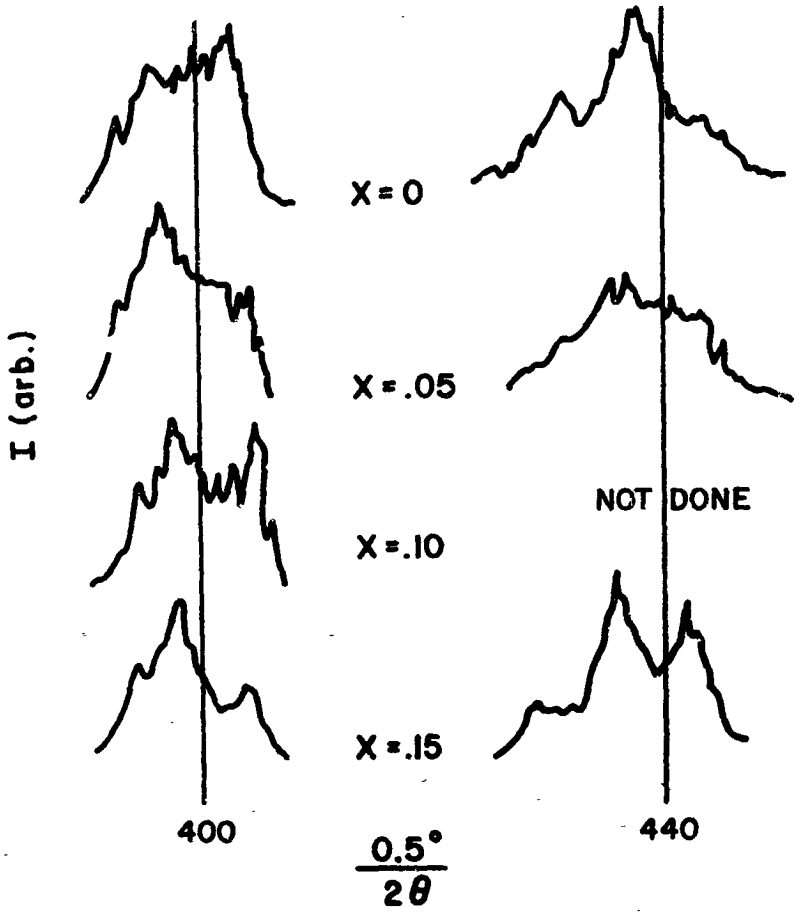

Figure G-3. {400} and {440} reflections at 20°K. Vertical lines mark the position of the K_{α_1} peak maximum in the cubic state.

states as a power series in the strain (cf. ref. 11); $\delta F \approx A\epsilon^2 + B\epsilon^3 + C\epsilon^4$, where each coefficient is the sum of both the electronic terms, calculable exactly in terms of the parameters of the model, and lattice terms representing all other contributions. Setting $\delta F = 0$ at T_m, and requiring that $\partial \delta F/\partial \epsilon|_T = 0$, the spontaneous strain is seen to be $\epsilon(T_m) \approx - B/2C$; that is, ϵ depends solely on the higher order elastic constants. Now, one of the outstanding successes of the square band representation for Nb_3Sn is the correct prediction of the strain near T_m, based on the electronic terms alone, and using parameters determined from cubic state data. We may, therefore, ignore the lattice

contributions, and assert that in the absence of a changing electronic contribution, the model does not readily admit a change in the sign of ε. The presumably small perturbation found necessary to alter the sense of the transformation implies the smallness of terms of odd order in ε in a proper free-energy expansion near T_m (ref. 68). This supports the conclusion drawn from specific heat measurements that the transformation is second order, or near second order ($B(T_m) \approx 0$), and that the expansion must contain terms other than those given by the band model if it is to properly account for the details of the behavior near T_m (ref. 69).

The strain at low temperatures is equally problematic. A general result of the band theory of the transformation is that the predicted strain at 0°K is a factor of two smaller when c > a, regardless of the form assumed for the density of states as a function of energy. Instead, we find the magnitude of the strain to be independent of sign.

Finally, we have the interesting result that T_c varies smoothly with x, which can be interpreted as indicating that the density of states is little affected by the change in sign of ε^*. This is borne out by magnetic susceptibility measurements, which show no difference in the decrease in susceptibility that accompanies the transformation for pure Nb_3Sn and for $Nb_3Sn_{.85}Sb_{.15}$**. T_c is known, however, to be a strong function of uniaxial stress applied in the <100> direction(ref. 59), this effect being several orders of magnitude larger than for ordinary superconductors, and in semi-quantitative agreement with the band model. If the density of states interpretation of this result is correct, then it is necessary to suppose that the band structure in the tetragonal state depends on the magnitude of the strain, but not the sign, suggesting that the band splitting below T_m is symmetric about the cubic band edge.

---

*At 0°K the model gives for the ratio of the density of states at the Fermi level for ε^+ splitting (a > c, Fermi level in one sub-band), to that for ε^- splitting, $N_o^+/N_o^- = (\frac{1}{2})^{1/n+1}$ where $N(E) \alpha E^n$, and $n = -\frac{1}{2}, 0, \frac{1}{2}$ are the exponents for the L'Abbe-Friedel band, square band, and free-electron band respectively,

**M. Rayl and G. D. Cody, private communication.

F. CONCLUSIONS

Significant modifications of the band model of the lattice transformation in β-W superconductors will have to be made in order to account for the data presented here. The question of the level at which the theory requires amendment is not resolved, but the difficulties encountered are certainly not dependent on the particular form chosen to represent the density of states. A possible modification of the theory clearly suggested by the data lies in the direction of postulating a band splitting independent of the sign of ε. However, the failure of Sb doping to alter the band filling represents an unexpected rigidity in the model, and raises some doubts about its fundamental validity. Before credible alteration of the theory can be made, it would appear desirable to investigate other dopants and band-structure sensitive properties in an attempt to find evidence for the model of the sort originally sought in this study.

ACKNOWLEDGEMENTS

The generous assistance of R. Paff in helping with the x-ray measurements is gratefully acknowledged, as are the efforts of R. Miller, who made the T_c measurements. The author is indebted to Drs. R. W. Cohen and G. D. Cody for helpful criticism of the manuscript.

APPENDIX H*

RF-SPUTTERED FILMS OF β-TUNGSTEN STRUCTURE COMPOUNDS

J. J. Hanak, J. I. Gittleman, J. P. Pellicane, and S. Bozowski

A. INTRODUCTION

The superconducting compounds crystallizing in the β-tungsten structure show considerable differences as well as similarities in behavior. These compounds have the nominal formula A_3B, where the A atom is a transition element and the B atom a non-transition, or group VIII element. At least one compound, V_3Si, appears to be what is usually called a stoichiometric, or line compound. In other cases, where detailed phase-diagram studies have been done, β-tungsten compounds exist as solid solutions over a composition range of several percent. Depending on the temperature and the system, the region of existence of the A_3B phase has been found to range over several percent from rich in A to rich in B, rich in A to stoichiometric, and rich in A to less rich in A (deficient in B). Stoichiometry has been found to have a pronounced effect on the superconducting properties, especially the transition temperature (T_c).

In the few compounds most intensely studied (high T_c materials), T_c maxima have been observed at or within about 2 at. % of the stoichiometric A_3B composition. Usually very small differences in maximum T_c (tenths of °K) of a given material have been observed by different experimentalists in cases where the stoichiometric compound can be prepared by synthesis methods under equilibrium conditions, as, for instance, in the case of Nb_3Sn and V_3Si. In cases where the stoichiometric composition is not formed under such conditions, the T_c values first reported for nominal A_3B compositions were much lower than subsequent ones. The higher values of T_c were obtained with materials having improved stoichiometry obtained by the use of synthesis methods capable of yielding metastable compositions. The most vivid example in this category is the compound Nb_3Ge, which had a T_c of only 6°K or less when prepared under equilibrium conditions(ref. 61) and about 17°K when prepared by splat cooling and followed by annealing below 1000°C(ref. 70). The material with the highest T_c, $Nb_3Al_xGe_{1-x}$, has been obtained

*To be published, J. App. Phys. 1970.

by the same method(ref. 71). Most of the known superconducting β-tungsten compounds have not yet been studied thoroughly from the standpoint of composition and its effect on T_c. The present work is preliminary to a thorough investigation of several such systems in order to optimize the superconducting properties of these compounds. Although splat cooling had been used with success, one serious drawback of this technique is the fact that in most cases the non-transition elements B are rather volatile, while the transition elements A are high melting; this results in unpredictable final compositions and sporadic variations in composition within a given specimen. Moreover, this technique does not lend itself to producing materials in a useful form. A more promising technique appeared to be rf sputtering. Films of three β-tungsten structure compounds, V_3Ga, V_3Ge, and V_3Si obtained by dc-getter sputtering onto heated substrates have been reported(ref. 72) and in the case of V_3Si, a value of T_c equal to that reported for bulk specimens was obtained (ref. 73). Instead of sputtering from targets of the desired final composition, as done above, we have chosen in the present work to co-sputter from two separate elemental targets(ref. 74). In this manner it is possible to deposit wide, continuous ranges of composition in one run and to measure the properties of an entire composition range of interest with a single-film sample. Previously we have used this technique with success in studying the superconductive properties of cermets and of mixtures of immiscible metals(ref. 75). In contrast to the preceding work(refs. 72,73) the films in the present study were condensed onto substrates cooled to 77°K in order to obtain maximum physical mixing of the elements; subsequently, the specimens were annealed at desired temperatures and times to effect compound formation. The main purpose of the first phase of this work was to synthesize continuous composition ranges of several such binary systems and, by measuring T_c at close composition intervals, to observe the effectiveness of this approach in optimizing the superconducting properties of these materials.

B. EXPERIMENTAL

The rf-sputtering arrangement consisted of a disk target 15 cm in diameter usually composed of two half disks of two desired constituent elements. In cases where the relative sputtering rates were very different the target area was divided unequally. Both of the targets were placed side by side on the same metal electrode powered by one rf power supply. The substrates were made of dense alumina plates. They were placed horizontally above the targets and at right angles to the interface of the two targets so as to obtain maximum composition range. Films with thicknesses ranging from 3,000 to 10,000 Å were sputtered at 5×10^{-3} torr pressure of argon along the entire substrate length through

a 2-mm wide mask. The films were then annealed in quartz tubes dynamically evacuated to 1 x 10^{-8} torr by an ion pump at temperatures to be indicated. The annealing temperatures were chosen either from literature or from estimates. After annealing, fifty regularly spaced gold contacts were evaporated across the sample film. In this manner dc resistance and T_c measurements could be made for the entire specimen at compositional intervals of approximately 1.5%. The chemical analysis was based on x-ray fluorescence measurements; its absolute accuracy was estimated to be about 5 at. %, whereas the accuracy of the compositional variation for adjacent samples was estimated to be a few tenths of a percent.

X-ray diffraction by means of the Debye-Scherrer technique was used to determine the structure. Structure analysis has been thus far possible only for the thickest films ($\sim$ 10,000 Å). Previous work with lanthanum and molybdenum films(ref. 75) has established that the sputtering method used was capable of producing films with purity satisfactory for this work and the present results so indicate. Binary systems studied in the present work included V-Si, Nb-Al, Nb-Au, Nb-Ge, Nb-Sn, Nb-Pt and Ta-Ge.

C. RESULTS AND DISCUSSION

The compositional ranges of the binary sputtered films were as much as 70 at. % wide and in each case included the composition range at which the β-tungsten structure would be expected to exist. The T_c and resistivity ratio data as a function of composition were plotted for each system except Nb-Au and they are shown in Figs. H-1 to H-6, inclusive. The T_c results are presented as vertical lines representing the transition width. The resistivity ratio was taken as the ratio of resistivities at room temperature and at a temperature just above T_c. The remarkably smooth variation in the resistivity ratio and T_c reflects the uniformity in background conditions in a given run as well as a smooth and continuous variation of composition. In several instances pronounced maxima in the resistivity ratio accompanied by narrow transition widths are indicative of compound formation and possibly of an approach to a single phase. Large transition widths and low resistivity ratio on the other hand appear to be indicative of mixtures of two or more crystalline phases. The above mentioned signs of compound formation are most evident in the case of the V-Si system (Fig. H-1) for which chemical analysis was not available and for which ascending sample numbers signify an increasing silicon concentration. Sample number 17 appears to be the compound V_3Si, which is known to be a "line" compound which had been made(ref. 12) with a resistivity ratio as high as 20.

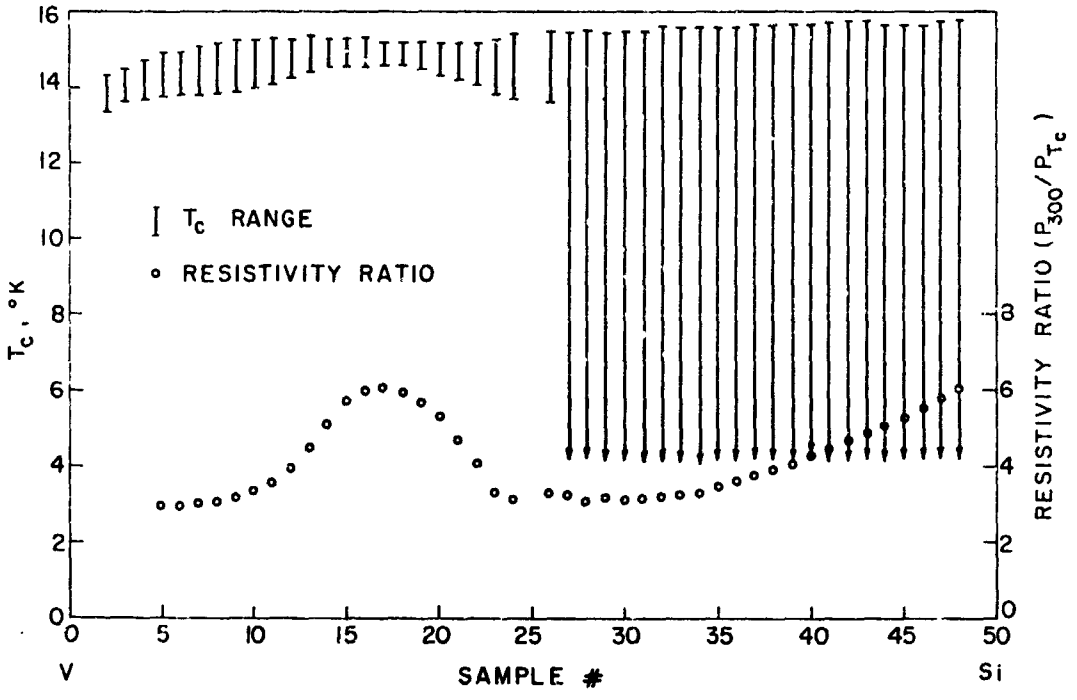

Figure H-1. Superconducting transition temperature and resistivity ratio vs. sample number of sputtered V-Si films annealed at 1000°C. (The silicon content increases continuously with sample number.)

In the Nb-Sn system (Fig. H-2) a broad maximum in the resistivity ratio is shown over a range of tin content from 12 to 24 at. %. The Nb_3Sn phase has been shown to exist in chemically vapor-deposited material from about 18 to 25% of tin(ref. 76), however, unlike in the present material the T_c decreased drastically from 18.1° to 8°K over this composition range with decreasing tin content. The constant value of maximum T_c for samples with tin content greater than 25% is consistent with the absence of other compounds in this system at a temperature of 950°C at which this material was annealed.

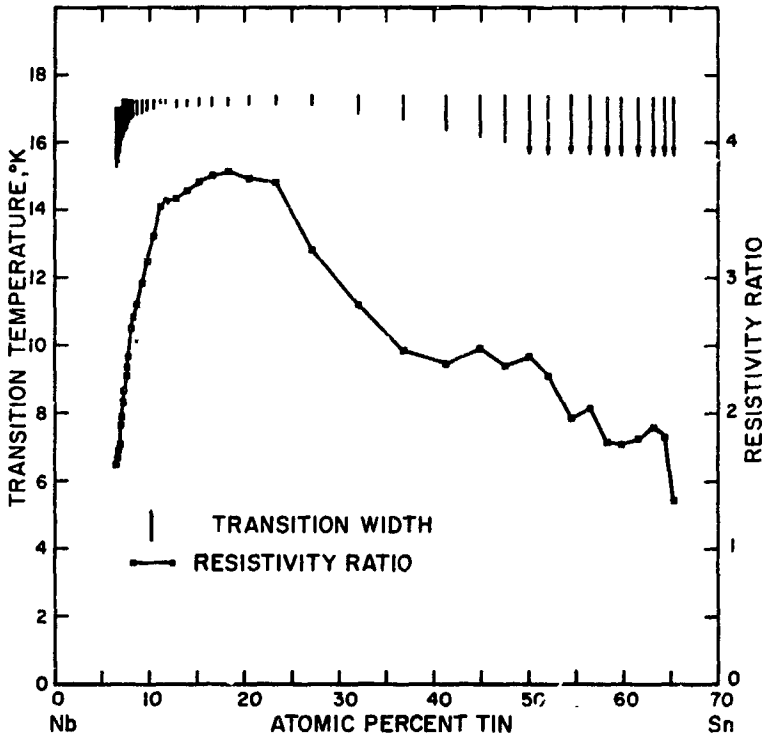

Figure H-2. Superconducting transition temperature and resistivity ratio vs. composition for sputtered films of Nb-Sn annealed at 950°C.

The system Nb-Pt (Fig. H-3) shows two maxima in the resistivity ratio. One maximum at 19% platinum accompanied by a T_c maximum of 11.0°K belongs to a β-W phase which is apparently off-stoichiometric. Preliminary x-ray data have shown that this phase was present at least over the range of compositions from 19 to 44% platinum, and in this range it underwent a continuous change of lattice constant from 5.187 to 5.153 Å respectively as compared with the nominal value of 5.155 Å reported for arc-melted Nb_3Pt(ref. 77). The compound corresponding to the second maximum has not been identified.

For the Nb-Au system a T_c maximum of 10.6°K has been obtained with a β-W structure having a lattice constant of 5.202 Å, compared with the

reported value of 5.203 Å(ref. 77). The data are not given in a graphical form because considerable evaporation of gold had taken place during the annealing which rendered the analytical results made on an unannealed sample invalid.

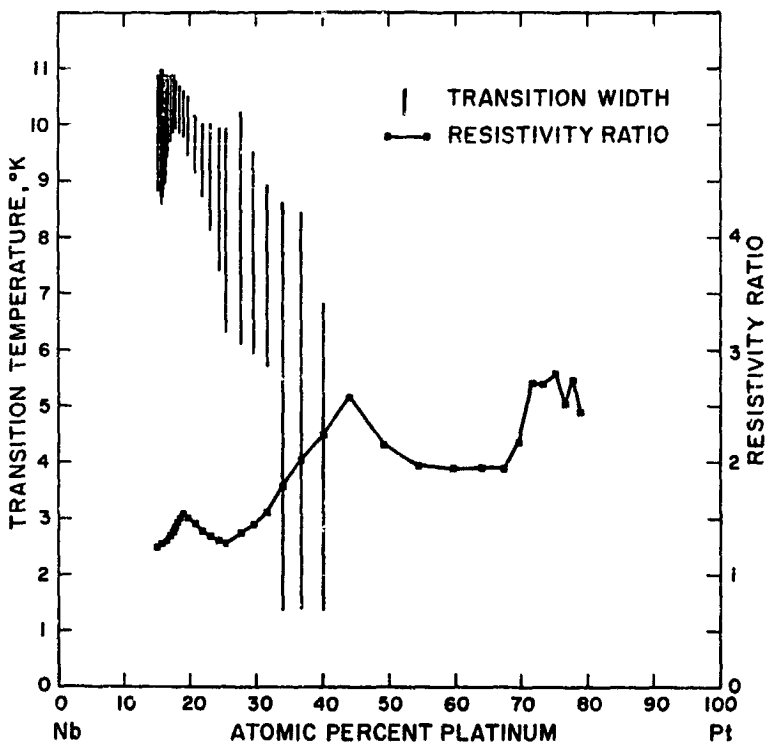

Figure H-3. Superconducting transition temperature and resistivity ratio vs. composition for sputtered films of Nb-Pt annealed at 1000°C.

A surprisingly small increase in the resistivity ratio was found in the case of the Nb-Al system (Fig. H-4) although relatively narrow transition widths and high T_c values were observed on the aluminum-rich side of the Nb_3Al composition. In this system the position of the maximum T_c as well as its value was found to be considerably dependent on the annealing temperature and time.

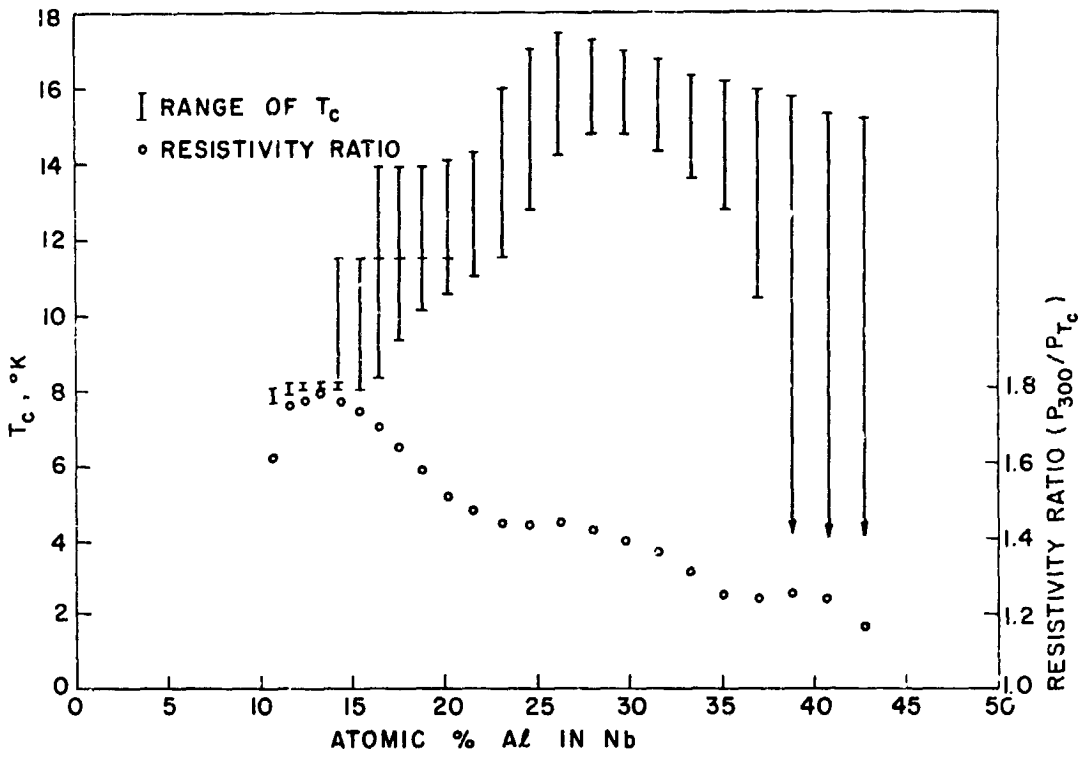

Figure H-4. Superconducting transition temperature and resistivity ratio vs. composition for sputtered films of Nb-Al annealed at 750°C.

The data for Nb-Ge (Fig. H-5) are perhaps the most significant in this work because the maximum T_c obtained was equal to the highest T_c reported thus far which was 17°K obtained by splat cooling(ref. 70). Moreover, the transition width was the narrowest obtained to date. This result indicates that a metastable phase has been formed more effectively than by splat cooling. The rise in the resistivity ratio in this system was barely observable, indicating that the compound obtained was probably still not well formed from the standpoint of homogeneity, crystallinity, and ordering. A sharp maximum in the resistivity ratio at approximately 63% germanium is indicative of the formation of the compound Nb_3Ge_5 which has been confirmed by x-ray diffraction. As in the case of Nb_3Al considerable dependence of T_c on annealing temperature and time has been observed neither of which has been exhaustively studied.

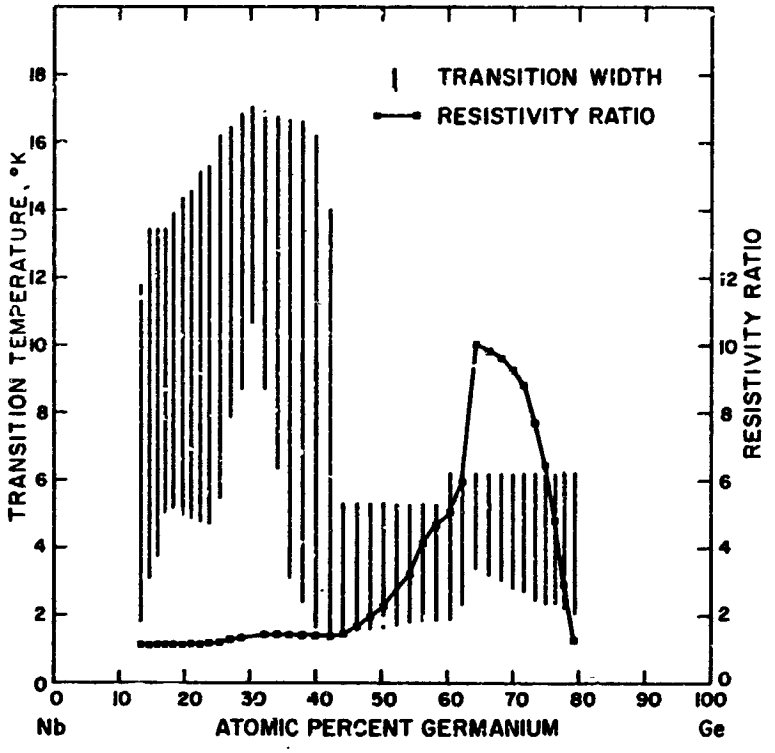

Figure H-5. Superconducting transition temperature and resistivity ratio vs. composition for sputtered films of Nb-Ge annealed at 750°C.

The data on the Ta-Ge (Fig. H-6) system represent an attempt at finding the β-W phase in a new system. In the absence of x-ray results all that can be said thus far is that a maximum in T_c of 8°K near the Ta_3Ge composition has been observed which is higher than the T_c of elemental tantalum a . . . t the dependence of the T_c and the resistivity ratio data is analogous to the Nb-Ge system. It is apparent that further annealing studies in this system are necessary.

A summary of the maximum T_c results for the sputtered β-W phases and their comparison to the previously reported values appears in Table H-I along with the annealing temperatures used and film thicknesses.

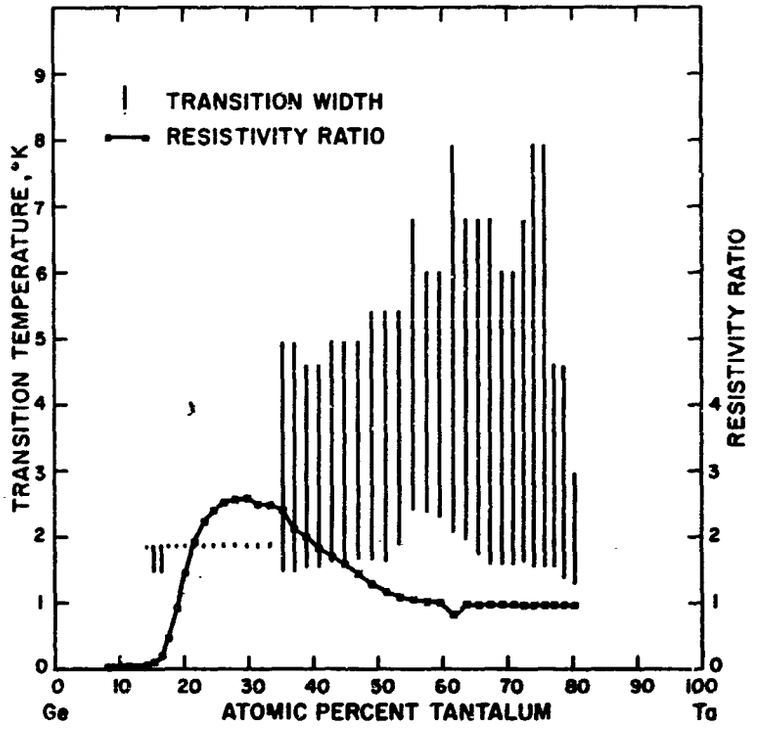

Figure H-6. Superconducting transition temperature and resistivity ratio vs. composition for sputtered films of Ta-Ge annealed at 750°C.

D. SUMMARY AND CONCLUSIONS

A technique of rf co-sputtering of binary intermetallic systems from two elemental targets has been used successfully in depositing films with continuous compositions ranges up to 70 at. % wide. Films deposited on cold substrates were subsequently annealed to yield superconducting β-W structure compounds.

The first general observation regarding the results is that in all systems studied the β-tungsten phases were readily obtained judging from the T_c results and, in the case of Nb_3Au and Nb_3Pt, also on the x-ray results. Transition temperatures were the same as, or within about, one degree of the highest T_c reported for bulk materials even though the sputtered films ranged in thickness from 3,000 to 10,000 Å and their T_c could have been easily lowered by reaction with the substrate. This approach proved to be capable of obtaining metastable compositions and,

TABLE H-I

Superconducting Transition Temperature of RF-Sputtered β-W Structure Compounds

Compound	Annealing Temperature °C	Film Thickness Å	T_c (°K)	
			Sputtered	Bulk*
V_3Si	1,000	3,000	15.4	17.1
Nb_3Sn	950	3,000	17.4	18.1
Nb_3Pt	1,000	10,000	11.0	11
Nb_3Au	1,000	10,000	10.6	11
Nb_3Al	750	4,000	17.4	18.8**
Nb_3Ge	750	4,000	17.0	17***
Ta_3Ge	750	4,000	8	---

*Ref. 77

**Ref. 47

***Ref. 70

at the same time, controlled compositions. Preparing the entire range of compositions in one run has the advantage of eliminating changes in the properties of the specimens due to random variations of the environment. Thus, even small variations in properties gain significance, as for instance, indication of the compound formation from the resistivity ratios.

A comment should be made regarding the composition at which optimum T_c occurred and the region of existence of the β-W phase in each system. The graphical data indeed show differences in the position of the maximum

T_c also in several instances the breadth of the T_c maximum and resistivity ratio maximum would suggest increased composition ranges for the existence of the β-W phases. All quantitative conclusions regarding these two items, however, must be reserved until more accurate chemical analysis and detailed x-ray diffraction data are obtained.

The primary significance of the results is that of establishing the validity of this synthesis approach. The results justify the undertaking of the more tedious part of the optimization, namely, the temperature time annealing studies, to be followed by detailed structure determination.

ACKNOWLEDGEMENTS

The authors express their thanks to Mrs. D. Hoffman for work connected with substrate preparation and Mr. R. Paff for x-ray crystallograph. We also thank Dr. G. W. Webb for valuable discussions.

APPENDIX I

SOLUTION GROWTH OF Nb_3Sn FROM LIQUID TIN

by
J. J. Hanak and D. E. Johnson

A. GENERAL

This paper is a status report on the development of a method for the growth of large single crystals of the superconducting compound Nb_3Sn. This compound is presently of commercial interest for the construction of powerful superconducting magnets, and, in the future it may be of use for superconducting electrical power lines. Scientific interest in Nb_3Sn centers on its high superconducting transition temperature (T_c), and the T_c dependence on the electronic properties of the normal state. Crucial to many measurements is the availability of single crystals, which have been thus far prepared solely by a chemical transport technique (ref. 2) using HCl gas. This technique yielded crystals weighing up to one gram, which have been used in the determination of the normal-state and superconducting properties including the x-ray examination of the martensitic transformation (ref. 1), the temperature variation of the elastic constants (ref. 24), magnetization (ref. 78), paramagnetic susceptibility (ref. 70), specific heat (ref. 69), and the superconducting energy gap(ref. 80). Several intended measurements (e.g., neutron diffraction)require much larger crystals than those obtainable by the HCl transport; hence, alternate crystal growth method was sought. A method of some promise is solution growth from liquid tin, which has been developed to the point of yielding boules of polycrystalline Nb_3Sn weighing up to several hundred grams.

The feasibility of solution growth of Nb_3Sn is derived from the Nb-Sn phase diagram(ref. 83) which shows that Nb_3Sn is a peritectic compound with a peritectic temperature of 2130°C. Above 930°C it is the only compound in the system and it is in equilibrium with molten tin. The critical aspect for the feasibility of this method is considered to be the solubility of niobium in molten tin as well as variation of solubility with temperature. The solubility of Nb is very low at low temperatures and increases slowly with temperature. It reaches a value of about 10% at 1700°C and thereafter it increases rapidly so that at the peritectic temperature it is nearly equivalent to the composition of the compound. Hence the compound should be transportable from higher to lower temperatures in liquid tin.

The compound Nb_3Sn itself is not a line compound. It can dissolve in excess of 5% of niobium, but very little, if any, tin. In the temperature range between 1800°C and the peritectic temperature the compound is progressively more deficient in tin. Thus, since large solubility of Nb in tin is desired, the practical range of temperature for solution growth is 1700° to 1900°C.

A convenient apparatus arrangement evolved in this work is shown in Fig. I-1. A cylindrical graphite crucible is used in a growth technique in many respects similar to Bridgman growth. The choice of graphite as a crucible material follows from the observation that of the few available practical crucible materials at this temperature the refractory metals Mo and W as well as several refractory oxide crucible materials are excessively soluble in the Sn-Nb melt at this temperature*. Unfortunately, the graphite crucibles also present similar problems, hence, the possibility of using niobium as crucible material was also attempted as will be described.

The graphite crucibles ranged in inside diameter from about 2 to 5 cm and overall length from 30 to 45 cm; the height of sample metal ranged between 10 to 20 cm. The crucibles were wrapped in about six turns of .012-cm thick graphite sheet (Graphoil) which proved to be very effective as a radiation shield. A water-cooled fused silica tube was used as an outside enclosure. Low frequency (10 kHz) rf induction heating was used, since a large skin depth was desired. Since the vapor pressure of tin in the growth temperature range amounted to several Torr, an argon atmosphere was used instead of vacuum to prevent the formation of bubbles in the melt and in the solidified samples. The growth was carried out by passing the hot zone from the bottom to the top of the crucible at rates ranging from 0.63 to 0.08 cm/hr, until no significant changes in the microstructure of the sample occurred. Static transports were also performed which produced results similar to the slowest travel rate used. The starting materials were electron-beam melted niobium and zone-refined tin with purities better than 99.9 and 99.999%, respectively. Determination of temperature was usually done before each run by means of a pyrometer; temperature readings as a function of rf power were taken at the bottom of a graphite well submerged in liquid tin. The temperature gradient at the growth interface has not been determined.

---

* L. J. Vieland, private communication.

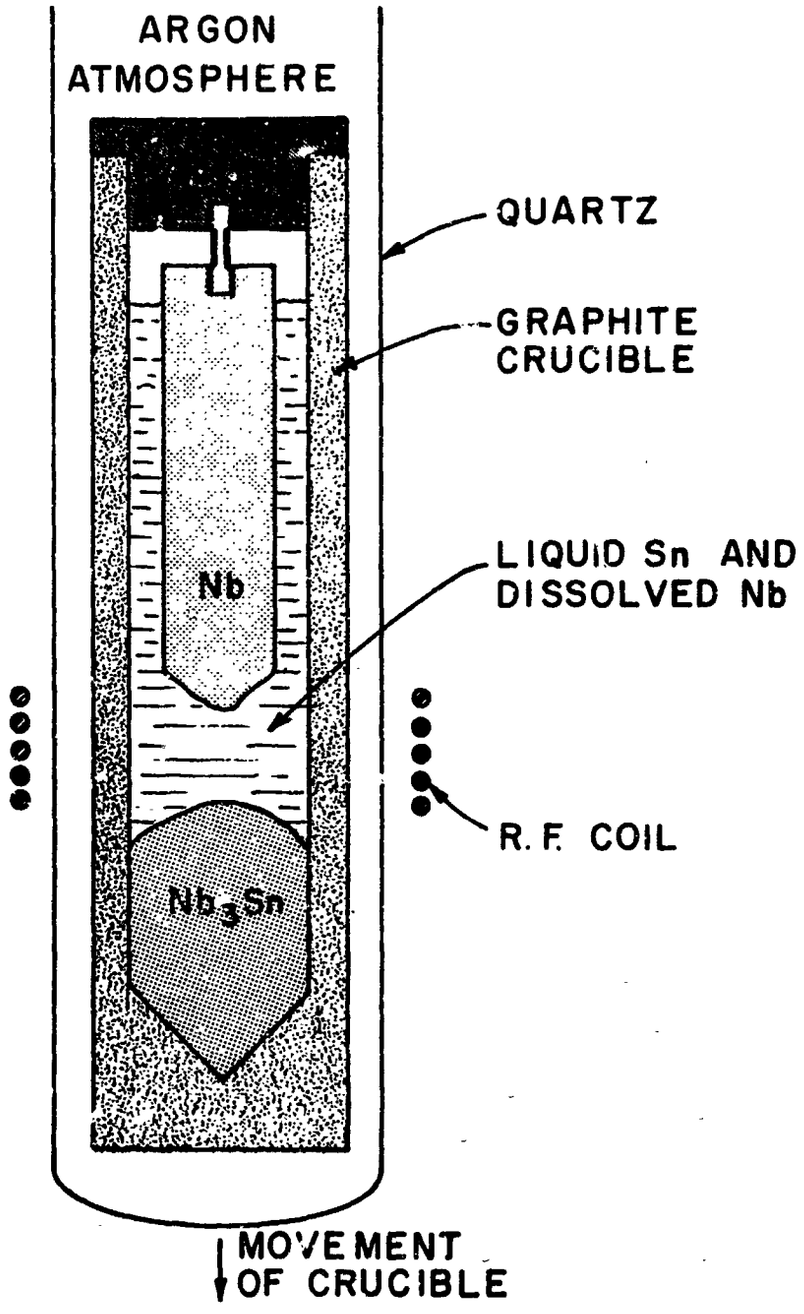

Figure I-1. Apparatus for growing Nb_3Sn from Liquid Tin.

B. RESULTS

The results of three runs made at different temperatures in graphite crucibles follow. The crucible inside diameter was 1.6 cm. In these runs the atomic percent of tin in the starting tin-niobium mixture was 40%. The rate of travel of the hot zone was 0.164 cm/hr.
In Figs. I-2, I-3, and I-4 are shown the cross sections of materials growth from the tin bath at 1715°, 1890°, and ∿ 2000°C, respectively. In all three of these specimens second phases are present. In Fig. I-2

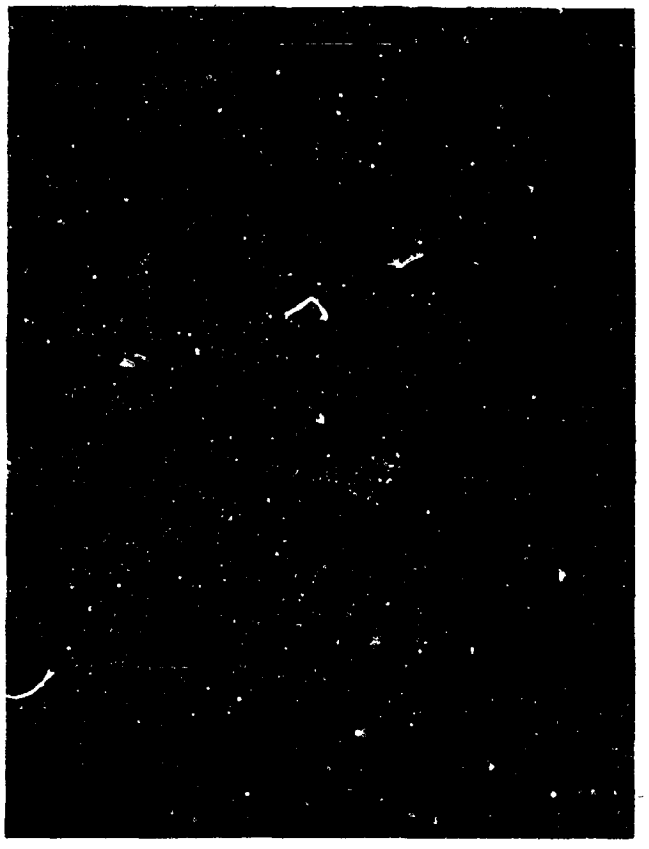

Figure I-2. Longitudinal cross-section of Nb_3Sn grown at 1715°C showing large islands of tin (dark areas), 240X.

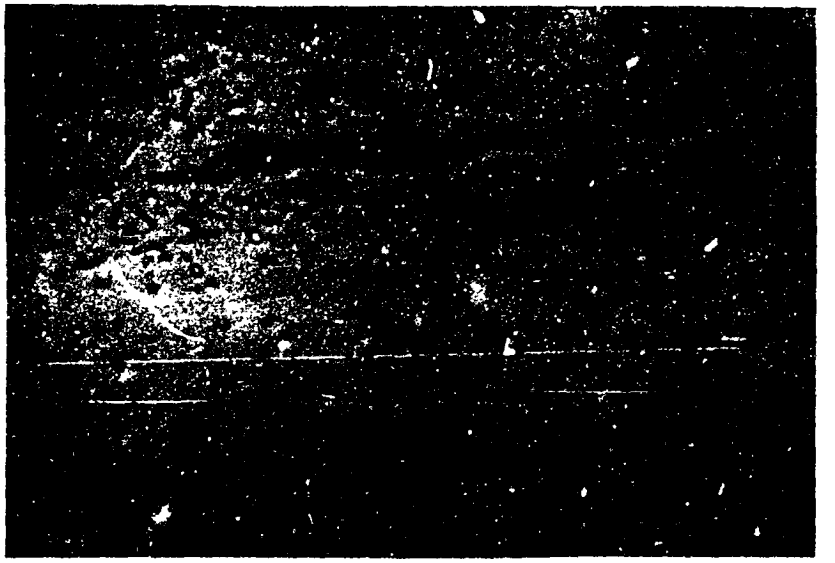

GROWTH DIRECTION

Fig. I-3. Longitudinal cross-section of Nb_3Sn grown at 1890°C, showing long islands of tin and small rods of NbC (240X).

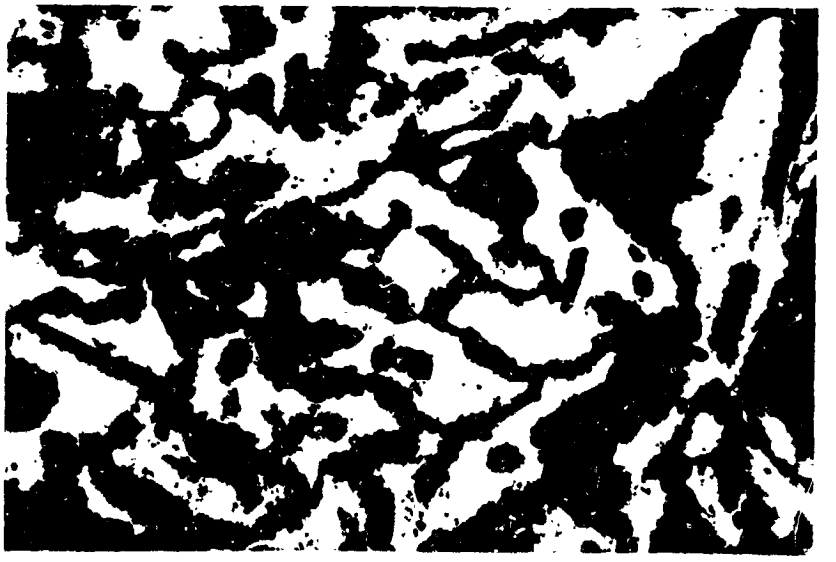

GROWTH DIRECTION

Fig. I-4. Longitudinal cross-section of Nb_3Sn grown at ~2000°C showing large areas of NbC (light) mixed with Nb_3Sn (dark), 120X.

large islands of free tin are evident; in Fig. I-3 islands of tin and finely dispersed rods of NbC appear; and, in Fig. I-4, the predominant phase is NbC with Nb_3Sn and Sn as additional phases. These results indicate that at the lowest temperature there is little if any graphite contamination, but a pronounced tin inclusion. As the temperature is increased, graphite contamination increases rapidly and the entrapment of tin is decreased. These effects can be explained on the basis of the variation of solubility of niobium in molten tin.

In Figs. I-5 and I-6 etched cross-sections of Nb_3Sn (Fig. I-8 above) are shown, taken in perpendicular and parallel directions to the growth axis, respectively. The grains were up to 1-mm in diameter and about 1-cm in length. The shape of the grains provides evidence of grain growth taking place in the direction of the moving zone. This suggests that the growth of large grains should be feasible, if the accompanying NbC and tin phases could be eliminated.

One approach at eliminating the tin phase was made by zone recrystallization of sample I above, which contained the largest amounts of tin and smallest amounts of NbC. The sample was placed in a tight-fitting Nb crucible and a heat treatment was made in the same manner as the growth run. The hot zone was passed from bottom to top twice at a rate of 0.164 cm/hr; first at a temperature of $\geq$ 1865°C and then at $\geq$ 1950°C. The recrystallization produced startling effects. The amount of free tin decreased from about 10% to less than 0.1% for the twice recrystallized material as estimated from the photomicrographs. Virtual elimination of horizontal-grain boundaries took place and a noticeable grain growth occurred up to about 3-mm diameter. The removal of tin was achieved by the same mechanism as that in the original solution growth. This can be seen in Fig. I-7 where moving islands of tin left trails in the Nb_3Sn (caused by minor differences in tin concentration in the Nb_3Sn). The trails fade out gradually, indicating concentration equilization by diffusion. Similar photomicrographs have shown that remaining horizontal grain boundaries also moved in the moving hot zone at about the same speed as the tin islands. Vertical-grain boundaries were present but fewer in number than in the as-grown material. Cross-sections transverse to the growth axis have shown that most of the residual NbC was collected at the vertical-grain boundaries. It is evident that the NbC impurity impedes the grain growth during recrystallization; clearly, this impurity must be eliminated in order to obtain extensive grain growth of Nb_3Sn.

Attempts to obtain pure Nb_3Sn were made by using thick-walled niobium crucibles, instead of the graphite, filled with liquid tin. This approach was similar to that used in growing polycrystalline Nb_3Sn by the so-called "dissolving crucible method" (ref. 84). Typically, these crucibles were 2.5 cm in O.D. and about 0.8 cm in I.D. In this procedure, a portion of the inner wall of the niobium crucible was

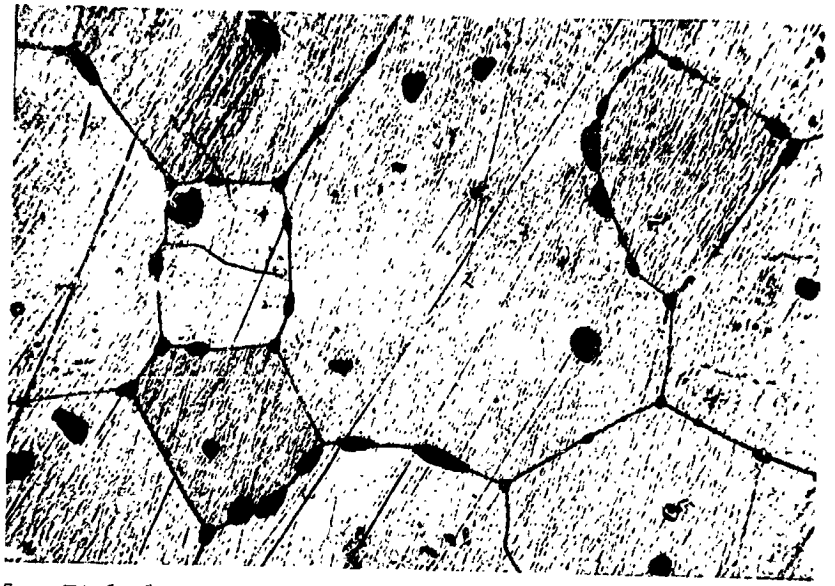

Fig. I-5. Etched cross-section of Nb_3Sn taken transversely to the growth axis showing polygonal grain structure (50X). Dark dots are free tin.

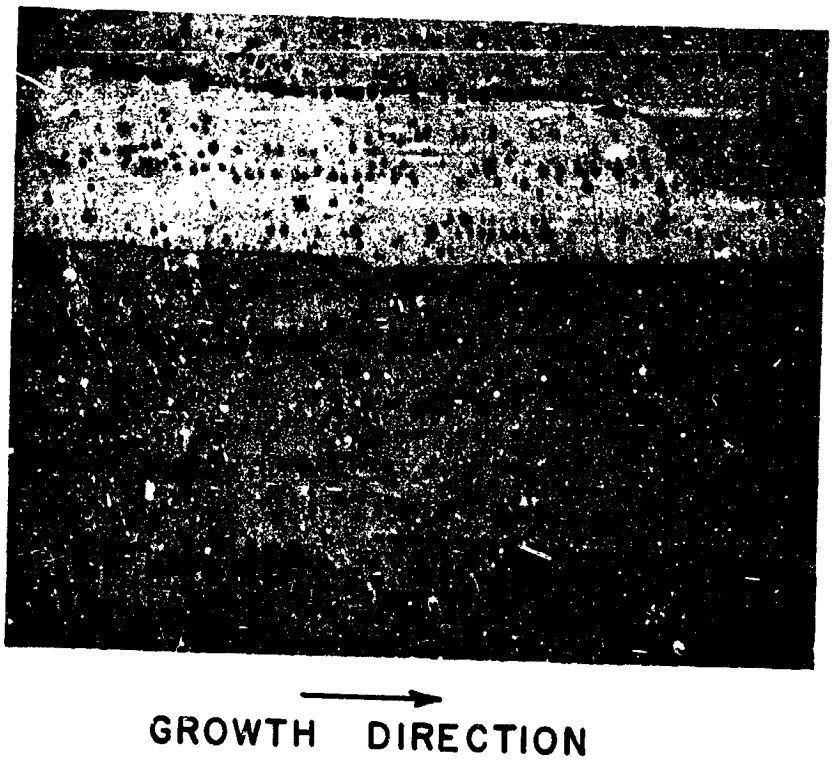

Fig. I-6. Etched cross-section of Nb_3Sn taken longitudinally to the growth axis showing grains growing in the direction of that axis (50X).

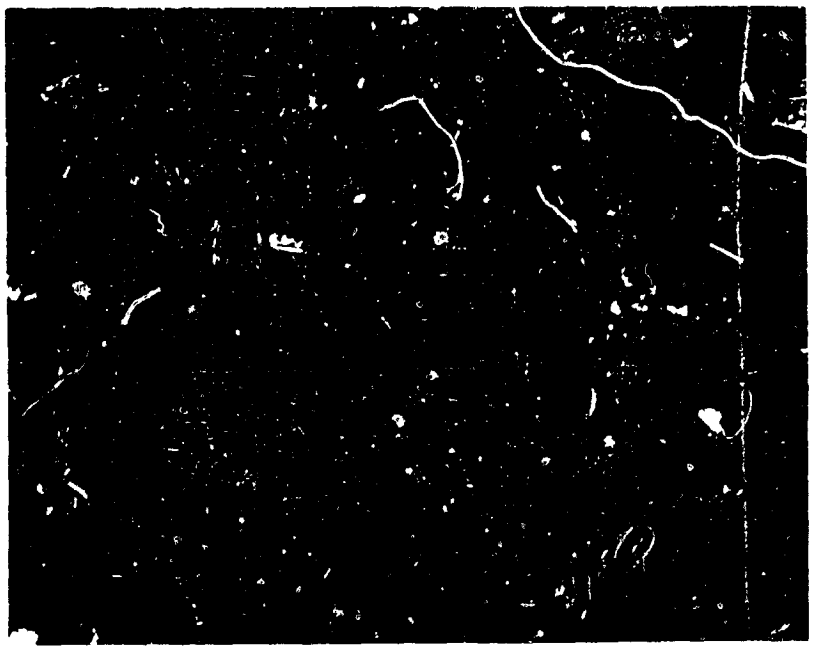

Fig. I-7. Longitudinal cross-section of zone-recrystallized Nb3Sn showing a concentration gradient trail left by a moving island of tin in the direction of grain growth (500X).

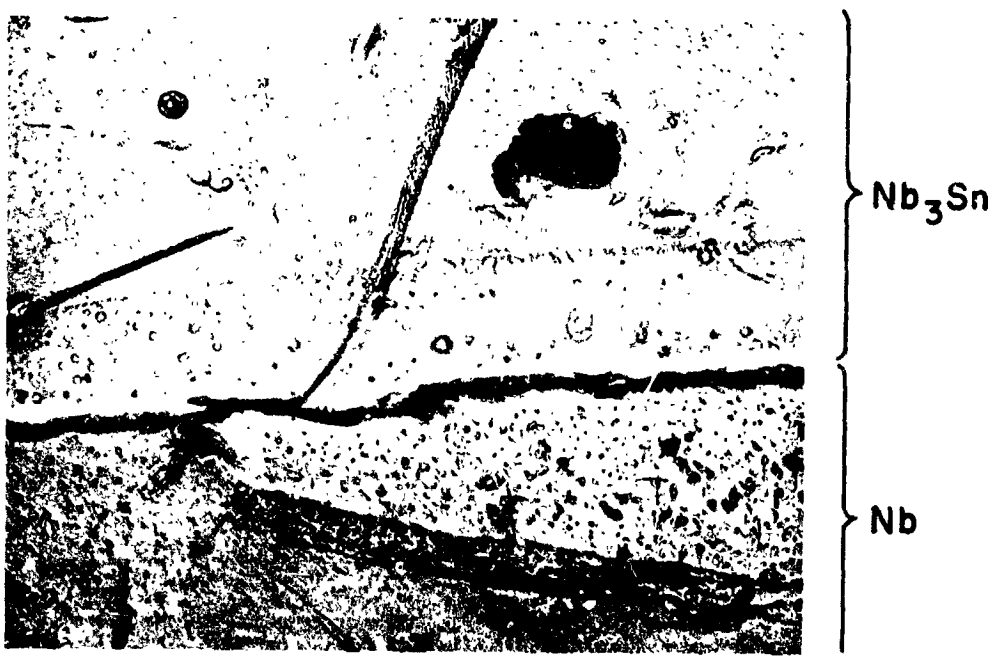

Fig. I-8. Etched cross-section of Nb-Nb3Sn interface showing a diffusion zone in Nb3Sn adjacent to niobium which is indicative of Nb_3Sn crystal growth by diffusion.

used up in the formation of Nb_3Sn and the excess niobium was the crucible for the Nb_3Sn. In each case, however, the crucible sprang a leak due to an unfavorable radial temperature profile and most of the material spilled out. Partially successful results were obtained by having the Nb crucibles placed in tight-fitting graphite crucibles. When several recrystallization passes were performed with such an arrangement, all free tin was found to be consumed by the excess niobium. This process was accompanied by the formation of numerous cavities which apparently resulted from the difference between the combined atomic volumes of elemental niobium and tin and the molar volume of Nb_3Sn. This difference is about 10%.

In addition to the growth mechanism described above, another possible growth mechanism has been observed, namely, one of diffusion. An example of this is shown in Fig. I-8, where an interface of Nb_3Sn-Nb is shown. A diffusion zone of regular width appears in the etched Nb_3Sn. Well-developed grain boundaries in the Nb_3Sn indicate that individual Nb_3Sn grains continue growing epitaxially on the existing grains at the expense of niobium. Tests designed to use this mechanism for the growth of sizeable Nb_3Sn crystals have shown it to be too slow to be practical.

Measured properties of Nb_3Sn formed by solution growth included the superconducting transition temperature (T_c) and the lattice constant, from which chemical composition can be estimated (ref. 81). These results are summarized for three such samples in Table I-I. The lattice constants and composition for as-grown specimens 1 and 2, in equilibrium with liquid, are in good agreement with previous results (refs. 81, 82, 83). The lower values of the lattice constant and composition of the recrystallized material is apparently due to its being in equilibrium with niobium which, again, in agreement with the phase diagrams, would reduce its tin content. The high T_c values of the specimens (with transition widths of about 0.1°K) reflect a good quality material. The measured density of the Nb_3Sn material was within 99% of the theoretical density for samples not containing noticeable amounts of free tin.

C. SUMMARY AND DISCUSSION

It has been shown in this work that the solution growth of Nb_3Sn from liquid tin takes place readily at high temperatures. The transport occurs from higher to lower temperatures. Three factors were found to be unfavorable to the growth of large gains; these were free entrapped tin,

Table I-I

Specimen No.	Growth(G) or Recrystallization(R) Temp. °C	Lattice Constant Å	Atomic Percent Tin	Transition Temperature °K
1	1715 (G)	5.2906	25.0	18.0
2	1890 (G)	5.2896	24.4	18.2
3	≥1875	5.2892	24.2	18.1
4	≥1950	5.2865	22.5	

crucible contaminant NbC, and cavities arising from the difference in molar volumes of the reacting elements Nb and Sn and the compound Nb_3Sn. It has been found that the free tin can be eliminated either by higher growth temperature or by repeated zone recrystallization; the same factors lead to the growth of larger Nb_3Sn grains. Increased temperature, however, favors contamination by the graphite crucible. The use of Nb crucible presents leakage problems as well as cavity formation.

Regarding the prospects of obtaining large-single crystals by this technique, the following observations can be made:

1. Large crystals could be indeed grown in a crucible that would not present contamination problems at about 1900°C. Whether such crucible material can be found is questionable. The grown crystal might be slightly deficient in tin, but it appears possible to correct the stoichiometry by tin diffusion.

2. Use of crucibleless methods such as arc melting might be the answer to the crucible problem, although the control of temperature and other growth conditions might be difficult.

3. Further work with zone recrystallization of large diameter Nb_3Sn samples might minimize the cavity problem and produce sizeable grains.

4. Recrystallization of Nb_3Sn under pressure may eliminate cavity formation and promote grain growth.

APPENDIX J

ELECTRICAL TRANSPORT PROPERTIES OF Nb_3Sn IN THE NORMAL STATE

G. Gunsalus

A. INTRODUCTION

Three samples are used in these measurements, a vapor-transported polycrystalline sample deposited on a steatite substrate and measuring 1.92 cm by 0.95 cm by 0028 cm., and two single-crystal samples each about 5 cm by 0.5 cm by 0.5 mm are randomly cut adjacent portions of a larger single crystal. One of these is unannealed while the other was annealed at 1000°C for 20 hr. under high vacuum. Rough x-ray orientation shows the rod axis to be 23° from the [110] direction with the faces being [110] planes.

Contacts for current, Hall leads, and thermocouples were nickel plated on the samples and leads attached with indium solder. A small bifilarly wound heater is soldered to one end of the sample for use in thermopower measurements, and the other end is thermally anchored to a controlled temperature base in a variable-temperature cryostat. The sample is enclosed in a vacuum chamber which can be flooded with He gas for isothermal resistivity and Hall measurements.

Current leads are 0.005 in. copper. Thermocouples are of 0.003 in. premium grade copper and constantan thermocouple wire. Copper thermocouple wire is also used for Hall leads.

B. MEASUREMENTS

For thermopower measurements the sample chamber is pumped to 10^{-5} mm Hg or better with an oil-diffusion pump. Power is supplied to the sample heater so as to maintain a 0.5 to 2.0°K temperature gradient. The ΔT is determined by measurement of the two Cu-Ct differential thermocouples referenced at the cryostat temperature. The thermoelectric voltage is measured between the copper legs of the two thermocouples and the thermopower calculated at the average sample temperature. All voltage measurements are made with a Keithley model 150B microvoltmeter to an accuracy of $\pm$ 1%.

For resisitivity measurements the sample is maintained in an isothermal environment by surrounding with He exchange gas at about 1 atm. A standard four-probe dc measurement is made. Current is supplied by a dc power-supply current regulated to $\pm$ 0.1%. The voltage is measured

between the copper legs of the thermocouples with the Keithley 150B. An independent check is made by measuring across the constantan legs. These voltages always agreed to ± 0.7%.

Hall measurements were made in the same isothermal environment and with the same current supply as in the resistivity measurements. The Hall voltage is determined by averaging the four voltages measured using the possible combinations of normal and reverse electric and magnetic fields, so as to eliminate thermal effects.

Sample dimensions are determined with a traveling microscope to an accuracy of ± 0.001 cm.

C. DATA

Figure J-1 shows the thermopower as a function of temperature as measured on all three samples. Above 50°K the indeterminate error is ± 2%. The experimental scatter is of this order in that region. Below 50°K the error becomes much larger starting at ± 2% at 50°K and increasing to ± 10% at about 20°K. This arises from the rapid temperature dependence of Q as well as from the rapid decrease in thermocouple sensitivity in this range. The thermopower is positive for all samples indicating a hole contribution to the thermopower. The local maximum at 60°K in the polycrystalline sample is characteristic of a phonon-drag contribution to the thermopower, although it is not clear why this appears only for this sample. Of special interest is the large change in slope occurring at 46 ± 1°K in the data for the annealed crystal. This corresponds to the known lattice transformation in the material reported to occur at 43°K. The unannealed crystal data exhibit no such behavior.

Figure J-2 shows resistivity data for the two single crystals over the temperature range 18° to 100°K. Indeterminate error is ± 4% arising primarily from the dimension measurements while the experimental scatter is less then 1%. The annealed crystal data shows a distinct change of slope at 46 ± 1°K as in the thermopower. In the region above 46°K the annealed crystal data can be fit to better than 1% using the functional temperature of Woodward and Cody (ref. 16) using a residual resistivity, ρ_o, of 1.00×10^{-5} ohm-cm.

Figure J-3 shows $(d\rho/dT)$ vs. T for the annealed sample as determined by graphical differentiation of Fig. J-2. For comparison calculated values using the Woodward and Cody (ref. 16) functional dependence are plotted.

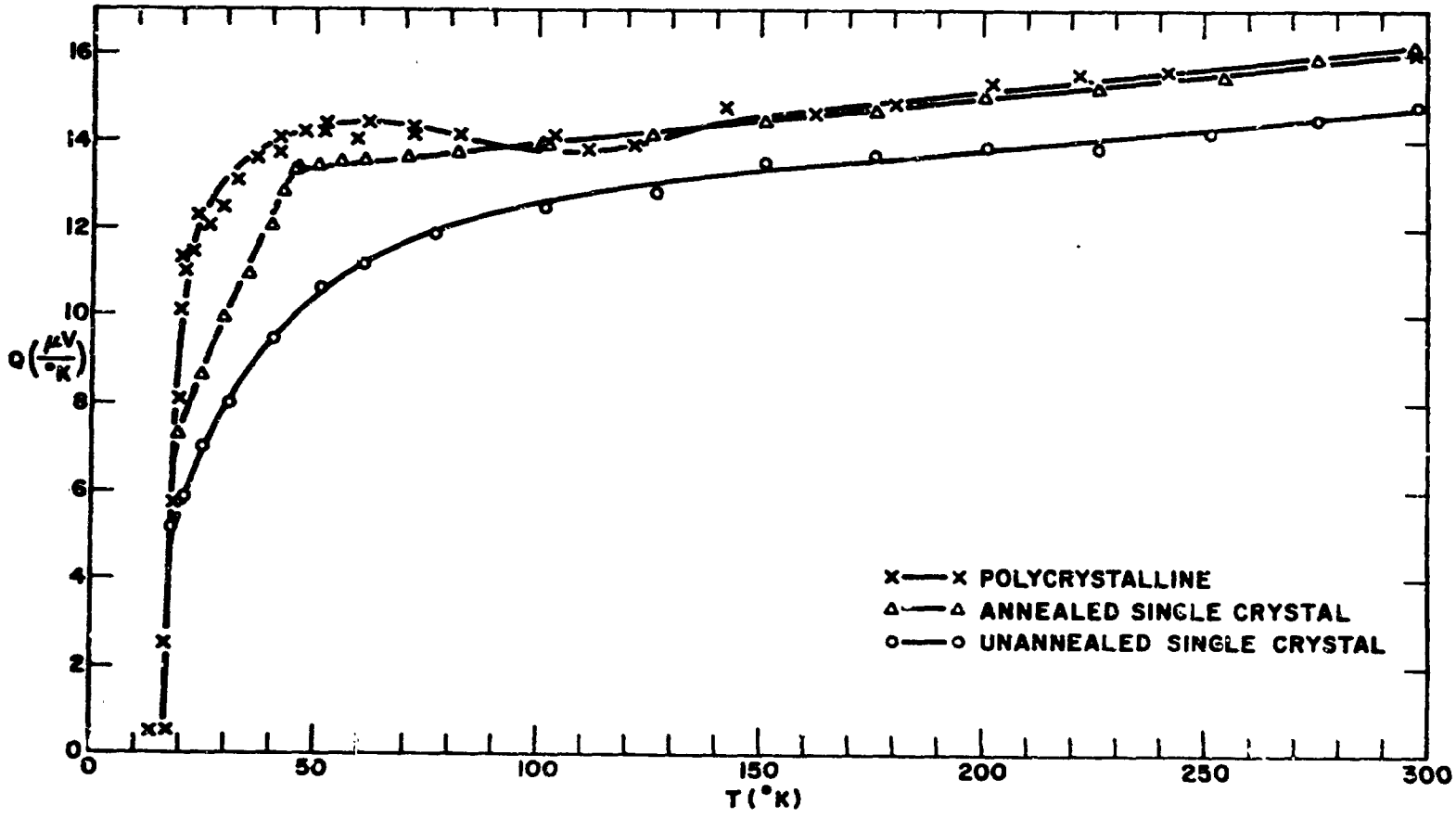

Figure J-1. Thermopower vs. T.

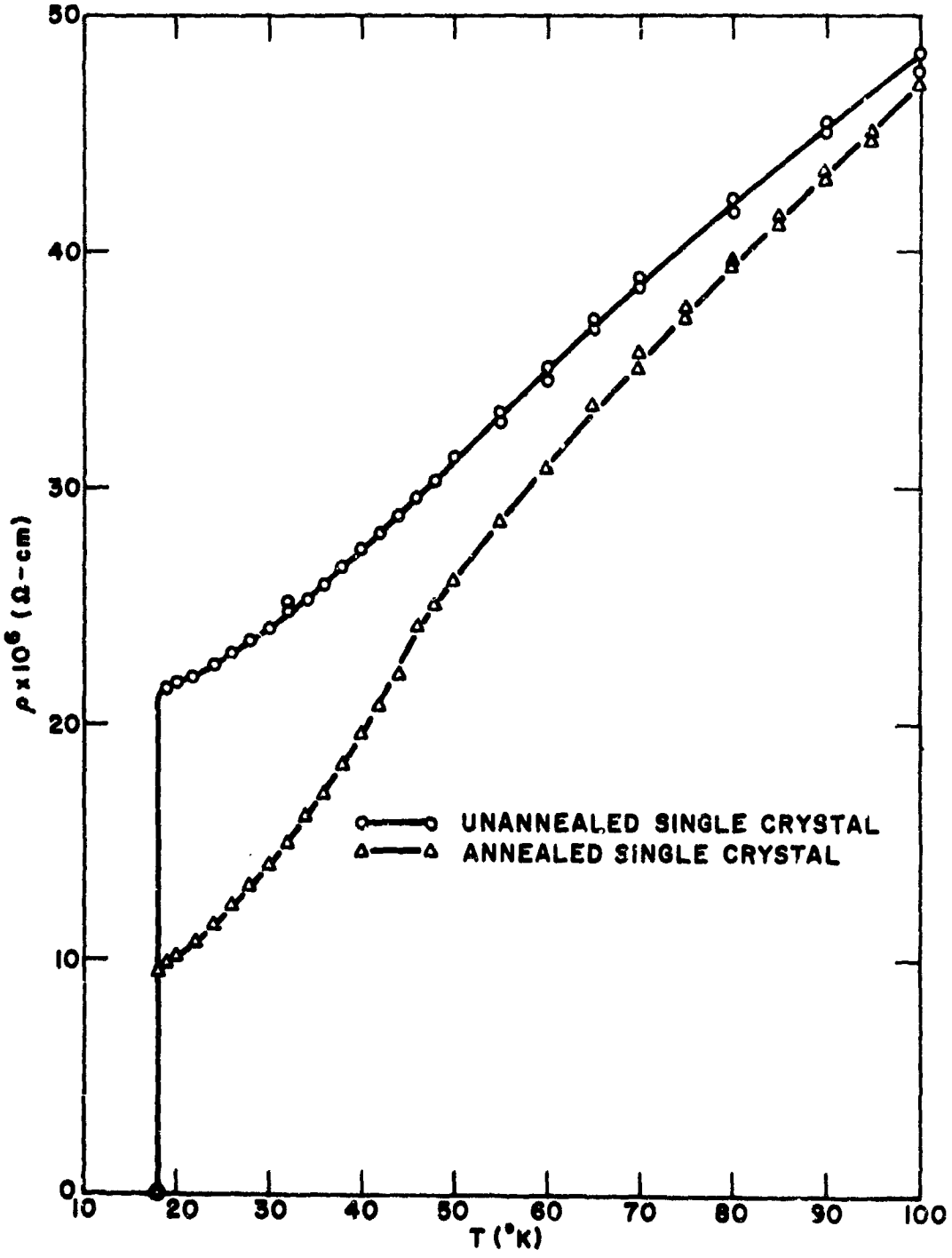

Figure J-2. Resistivity vs. T.

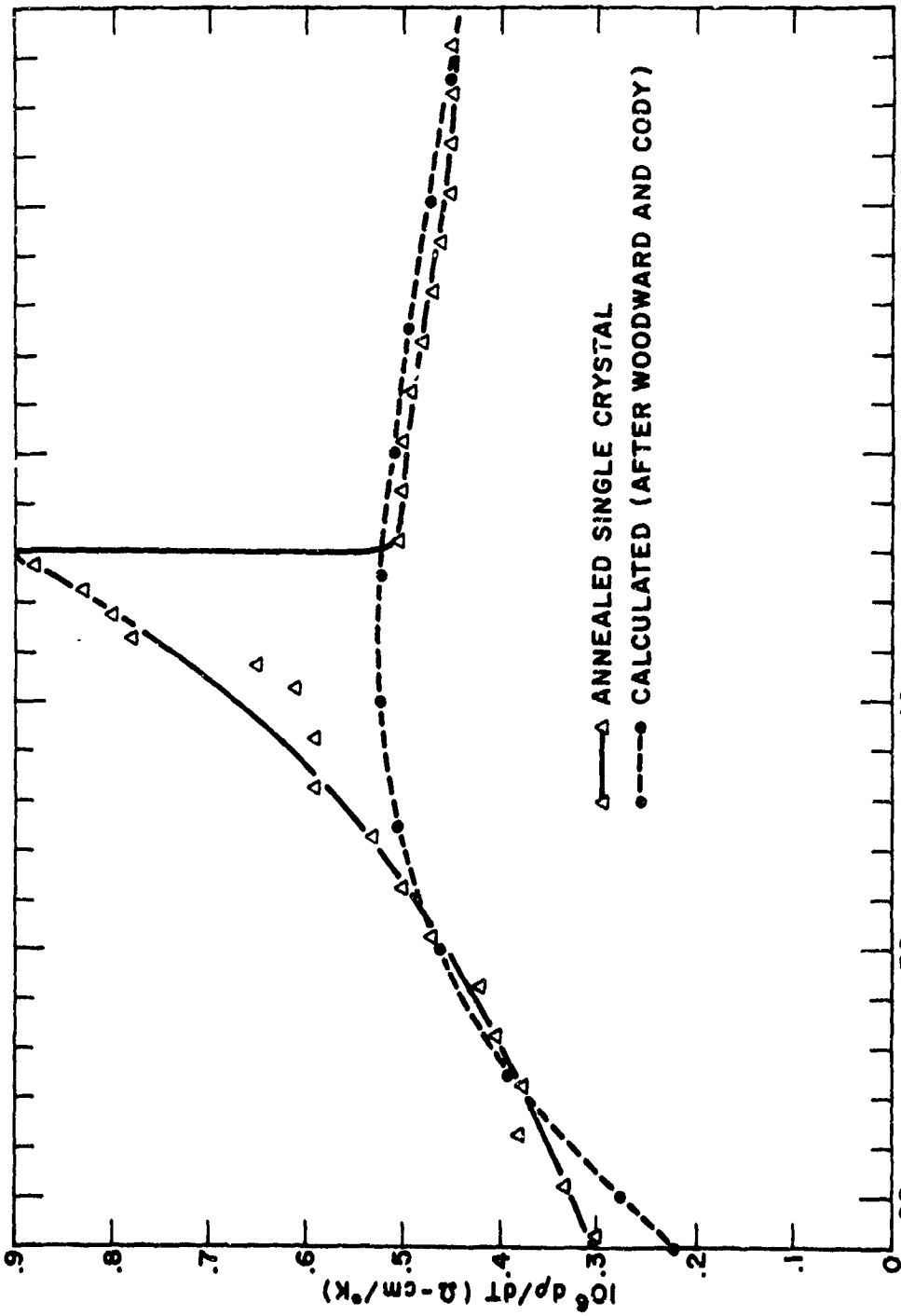

Figure J-3. Differential resistivity vs. T.

The Hall data indicate hole conduction in corroboration with the thermopower measurements. Carrier concentration as determined from the Hall data is plotted versus T in Fig. J-4. The polycrystalline data is corrected for shape and is in agreement with the data of (ref. 16) for the same material. There is a rise of 10% in the hole concentration from 20° to 300°K. The large thickness of the annealed sample yielded Hall voltages bordering on the sensitivity of the measuring equipment. Consequently, the indeterminate error is large. As can be seen from the experimental data, there is large scatter and this data should be used only for qualitative evaluation.

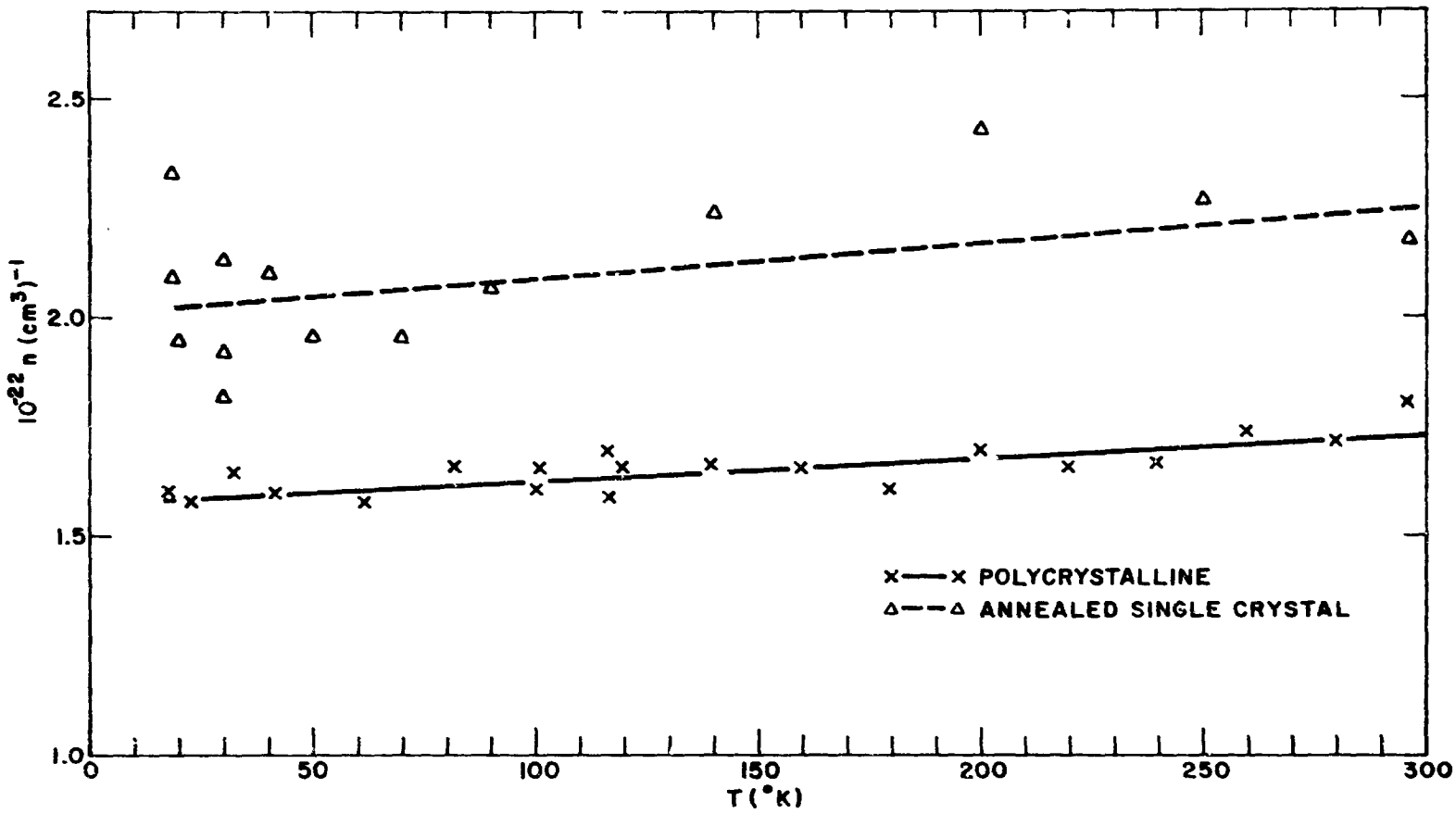

Figure J-4. Carrier concentration vs. T.

REFERENCES

1. R. Malfert, B. W. Batterman and J. J. Hanak, Physics Letters 24A, 315 (1967); R. Malfert, B. W. Batterman and J. J. Hanak, Phys. Status Solidi 32, K67 (1969).
2. J. J. Hanak and H. S. Berman, *Crystal Growth*, Supplement to J. Phys. Chem. Sol., Pergamon Press, N. Y. (1967), 249.
3. J. S. Shier and R. D. Taylor, Phys. Rev. 174, 346 (1968).
4. L. J. Vieland and A. N. Wicklund, Phys. Rev. 166, 424 (1968).
5. L. R. Testardi and T. B. Bateman, Phys. Rev. 154, 402 (1967).
6. K. Hechler, G. Horn, G. Otto, and E. Saur, J. Low Temp. Phys. 1, 29 (1969).
7. G. D. Cody, Tech. Rep. AFML-TR-65-169, 93 (1965).
8. K. Maki, Phys. Rev. 148, 362 (1966).
9. T. R. P. Gibb, Jr. and D. P. Schumacher, J. A. C. S. 64, 1407 (1968).
10. RCA Review 25, 333-624 (1964).
11. J. Labbe and J. Friedel, J. Phys. Radium 27, 153 and 303 (1966).
12. B. W. Batterman and C. S. Barrett, Phys. Rev. Letters 13, 390 (1964); Phys. Rev. 145, 296 (1966).
13. A. M. Clogston and V. Jaccarino, Phys. Rev. 121, 1357 (1961).
14. A. H. Wilson, Proc. Roy. Soc. A, 167, 580 (1938).
15. See for example J. M. Ziman, *Electrons and Phonons*, (Oxford University Press, London, 1962) p. 264-270.
16. D. W. Woodward and G. D. Cody, RCA Rev. 25, 393 (1964).
17. L. J. Vieland and A. Wicklund, to be published.
18. K. R. Keller and J. J. Hanak, Phys. Rev. 154, 628 (1967).
19. A. M. Clogston, A. C. Cossard, V. Gaccarino, and Y. Yafet, Phys. Rev. Letters 9, 262 (1962); Rev. Mod. Phys. 36, 170 (1964).
20. P. W. Anderson and E. I. Blount, Phys. Rev. Letters 14, 217 (1965).
21. J. L. Birman, Phys. Rev. Letters 17, 1216 (1966).
22. See for example L. D. Landau and E. M. Lifshitz, *Statistical Physics* (Pergamon Press Ltd., London, 1962) Chap. 14.
23. R. W. Cohen, G. D. Cody, and J. J. Halloran, Phys. Rev. Letters 19, 840 (1967).

24. W. Rehwald, Phys. Letters 27A, 287 (1968).

25. A. M. Clogston, Phys. Rev. 136, A8 (1964).

26. See for example. Landolt-Bornstein, Zahlenwerte und Funktionen aus Naturwissenschoft und Technik, Group III, Vol. 1, Elastic, Piezoelectric, Piezooptic, and Electrooptic Constants of Crystals, p. 16-39, Springer Verlag, Berlin, 1966.

27. L. R. Testardi, R. R. Soden, E. S. Griener, J. H. Wernick, and V. G. Chirba, Phys. Rev. 154, 399 (1967).

28. J. J. Hanak and H. S. Berman, Proc. International Conference on Crystal Growth, Boston, published in J. Phys. Chem. Solids, 28, 249 (1967).

29. R. L. Powell, M. D. Bunch, and R. J. Corruccini, Cryogenics 1, 139 (1967).

30. E. J. Woll and W. Kohn, Phys. Rev. 126, 1693 (1962).

31. G. D. Cody and J. J. Halloran, to be published.

32. See also: S. Barisic and J. Labbe, to be published in J. Phys. Chem. Solids.

33. L. F. Mattheiss, Phys. Rev. 38, A112 (1965).

34. L. Vieland and R. Cohen, to be published.

35. L. P. Kadanoff, W. Gotze, D. Hamblen, R. Hecht, E. A. S. Lewis, V. V. Palciauskas, M. Rayl, J. Swift, D. Aspnes, and J. Kane, Rev. Mod. Phys. 39, 395 (1967).

36. G. Liebfried, Mechanische und Thermische Eigenschaften der Kristalle; in Handbuch der Physik, edited by S. Flugge (Springer-Verlap, Berlin) Vol. VII/1, p. 252 (1955).

37. L. R. Testardi, T. B. Bateman. W. A. Reed, and V. G. Chirba, Phys. Rev. Letters 15, 250 (1965).

38. W. L. McMillan, to be published, Quoted in T. H. Geballe, B. T. Matthias, J. P. Remeika, A. M. Clogston, V. B. Compton, J. P. Maita and H. J. Williams, Physics 2, 243 (1966).

39. L. J. Vieland and A. W. Wicklund, Phys. Rev., to be published.

40. G. D. Cody, R. W. Cohen, and L. J. Vieland, *Proceedings of the Eleventh International Conference on Low-Temperature Physics*, 1009, (1968), St. Andrews, Scotland.

41. R. W. Cohen, to be published.

42. G. K. White, Cryogenics 2, 292 (1962).

43. M. Weger, B. G. Silvernagel and E. S. Greiner, Phys. Rev. Letters 13, 521 (1964).

44. A summary of extensive experimental work on Nb_3Sn can be found in F. D. Rose, editor, RCA Rev. 25, 333 (1964)(19 papers).

45. J. Labbe, S. Barisic, and J. Friedel, Phys. Rev. Letters 19, 1039 (1967).

46. See for example, P. B. Allen, M. L. Cohen, L. M. Falicov, and R. V. Kasowski, Phys. Rev. Letters 21, 1794 (1968).

47. Willens et.al., Sol. State Comm. 7, 837 (1969).

48. R. W. Cohen, G. D. Cody, L. J. Vieland, W. Rehwald, to be published.

49. A. B. Migdal, Sov. Phys. JETP 7, 505 (1968).

50. R. W. Cohen, thesis (unpublished).

51. G. D. Cody, RCA Rev. 25, 414 (1964).

52. Y. Nambu, Phys. Rev. 117, 648 (1960).

53. C. S. Koonce and M. L. Cohen, Phys. Rev. 177, 707 (1969).

54. P. Morel and B. W. Anderson, Phys. Rev. 125, 1263 (1962).

55. W. L. McMillan, Phys. Rev. 167, 351 (1968).

56. G. D. Cody, J. J. Hanak, G. L. McConville, and F. D. Rosi, RCA Rev. 25, 338 (1964).

57. J. J. Hopfield, Phys. Rev. (in press).

58. B. W. Batterman, presented at the Eighth General Assembly and International Congress of the International Union of Crystallography, University of New York (Stony Brook), August 1969.

59. J. P. McEvoy, presented at the International Conference on the Science of Superconductivity, Stanford University, August 1969, Conference Proceedings, Physica (to be published).

60. M. Weger, Rev. Mod. Phys. 36, 175 (1964).

61. T. B. Reed, H. C. Gatos, W. J. LaFleur, and J. T. Roddy, *Metallurgy of Advanced Electronic Materials*, Ed. G. E. Brock, Interscience, New York 71 (1963).

62. F. J. Bachner, J. B. Goodenough, and H. C. Gatos, J. Phys. Chem. Sol. 28, 889 (1967).

63. R. Hagner and E. Sauer, Nat. Wiss., 49, 444 (1962).

64. L. Pauling, in *Theory of Alloy Phases*, Trans. of ASM Vol. 48A, 220 (1956).

65. W. L. Picklesimer, Oak Ridge National Laboratory Report 2296, 1957.

66. H. W. King, F. H. Cocks, and J. T. A. Pollack, Phys. Lett. 26A, 77 (1967).

67. S. A. Medvedev, R. V. Kiseleva, and V. V. Mikhailov, Fiz. Tverdogo Tela, 10, 746 (1968) [transl. Sov. Phys. - Sol. St. 10, 584 (1968].

68. L. D. Landau and E. M. Lifshitz, *Statistical Physics*, Pergamon Press, New York, 1958, Chap. XVI.

69. L. J. Vieland and A. W. Wicklund, Sol. St. Comm., 7, 37 (1969).

70. B. T. Matthias, T. H. Geballe, R. H. Willens, E. Corenywit and G. W. Hull, Jr., Phys. Rev. 139, A1901 (1965).

71. B. T. Matthias, T. H. Geballe, L. D. Longinotti, E. Corenywit, G. W. Hull, R. H. Willens, and J. P. Maita, Science 156, 645 (1967).

72. H. C. Theurerer and J. J. Hauser, J. Appl. Phys. 35, 554 (1964).

73. J. J. Hauser, D. D. Bacon and W. H. Haemerle, Phys. Rev. 151, 296 (1966).

74. J. Edgecumbe, L. G. Rosner and D. E. Anderson, J. Appl. Phys. 35, 2198 (1964).

75. J. J. Hanak, J. I. Gittlemen, J. P. Pellicane and S. Bozowski, Phys. Letters 30A, 201 (1969).

76. J. J. Hanak, K. Strater, G. W. Cullen, RCA Review 25, 342 (1964).

77. B. W. Roberts, Prog. in Cryogenics (G.B.) 4, 159-231 (1964).

78. J. J. Hanak, J. J. Halloran, and G. D. Cody, "Magnetization Studies of Single Crystals of Nb_3Sn", in *Proceedings of the 10th International Conference on Low-Temperature Physics, Moscow, September 1966.*

79. G. D. Cody, R. W. Cohen, and L. J. Vieland, "Characteristic Parameters of B-W Superconductors", Presented at the International Conference on Low-Temeprature Physics, St. Andrews, Scotland, September 1968.

80. V. Hoffstein, W. R. Cohen, Phys. Letters, (in press).

81. L. J. Vieland, RCA Review 25, 379 (1964).

82. J. H. N. v.Vucht, D. J. vanQoijen, and H. A. C. M. Bruning, Phillips Res. Repts. 20, 131 (1965).

83. H. Pfister, Zeit. fur Naturforschung 20a, 1059 (1969).

84. S. A. Medvedev, K. V. Kiseleva, and V. A. Lykhin, Fix. metal metalloved., 24, 1050 (1967).